BEHIND-WALL TARGET DETECTION USING MICRO-DOPPLER EFFECTS

by

Patrick Kibambe Mashoko Nkwari

Submitted in partial fulfilment of the requirements for the degree

Doctor of Engineering (Electrical and Electronic Engineering)

in the

Department of Electrical and Electronic Engineering Science

Faculty of Engineering and Built Environment

UNIVERSITY OF JOHANNESBURG

October 2019

SUMMARY

BEHIND-WALL TARGET DETECTION USING MICRO-DOPPLER EFFECTS

by

Patrick Kibambe Mashoko Nkwari

Supervisor: Prof. Saurabh Sinha

Co-supervisor: Prof. Hendrik Christoffel Ferreira (late)

Department: Electrical and Electronic Engineering Science

University: University of Johannesburg

Degree: Doctor of Engineering (Electrical and Electronic Engineering)

Keywords: Synthetic aperture radar, frequency modulation, Doppler measurement, radar remote sensing.

During the last decade technology for seeing through walls and through dense vegetation has interested many researchers. This technology offers excellent opportunities for military and police applications, though applications are not limited to the military and police; they go beyond those applications to where detecting a target behind an obstacle is needed.

To be able to disclose the location and velocity of obscured targets, scientists' resort to electromagnetic wave propagation. Thus, through-the-wall radar (TWR) is technology used to propagate electromagnetic waves towards a target through a wall. Though TWR is a promising technology, it has been reported that TWR imaging (TWRI) poses a range of ambiguities in target characterisation and detection. These ambiguities are related to the thickness and electric properties of walls. It has been reported that the mechanical and electric properties of the wall defocus the target image rendered by the radar. The defocusing problem is the phenomenon of displacing the target away from its true location when the image is rendered. Thus, the operator of the TWR will have a wrong position, not the real position of the target. Defocusing is not the only problem observed while the signal is travelling through the wall. Target classification, wall modelling and others are areas that need investigation.

Consequently, many approaches are proposed in the literature to address these issues. This researcher proposes the use of micro-motion as source of the micro-Doppler effect to detect the presence of a target behind a wall.

In physics, a body in motion is a source of the Doppler effect when an electromagnetic wave impinges on the body. The Doppler effect is a physical phenomenon observed when an electromagnetic wave bounces off a moving target or when the radar is in motion and the target is stationary. It is used to determine the radial velocity of a moving target. However, there are many targets of interest that do not perform radial motion. This motion is often complex and is known as micro-motion. Motion such as the rotation of a rotor propeller, vibration of infrastructure and the movement of limbs, as well as the level of vibration of structures, is known as micro-motion.

Therefore, knowing the type of target under investigation yields vital information in advance. It is known that all living humans undergo micro-motion, even when stationary. Micro-motion is regarded as an important source of micro-Doppler effects. The heartbeat, chest movement due to breathing and the movement of limbs will be investigated as human micro-motion in this thesis. In many cases micro-Doppler is superimposed on the main Doppler induced by the translation motion of the target. Many research reports have been published on micro-Doppler and how to retrieve it. This work is devoted to investigating the retrieval of a human signature in the home environment.

In a home environment, the signal transmitted by radar has two possible patterns; the signal can travel from the radar to the target by passing through the wall only or it can be obstructed by other appliances and the wall as well. Consequently, the signal may undergo more disturbance while travelling through the wall and electronic appliances in various ways. An investigation involving detection of a human being in a home environment is undertaken in this thesis. A combination of micro-Doppler movement of the limbs, the heartbeat and chest movement in the presence of a wall and appliances can be used as a human signature. The human signature is mixed with many other return signals when collected at the radar receiver. Thus, one can separate the appliances' wall signal return from the overall signal returned to be able to detect human micro-motion.

To conduct the experiment, a frequency modulation wave radar is built. The radar system works as a synthetic aperture radar in the frequency range of 2315 - 2591 MHz. In addition, because of the limitation in terms of the frequency range of the radar that is built, a simulation is performed in MATLAB. The built radar uses the industrial, scientific and medical band, which is an unlicensed band. The simulation will run in a frequency range

other than the aforementioned range to study the behaviour of the radar in different frequency bands.

In this work, continuous wave frequency modulation radar is used to detect the micro-Doppler effect coming from a human body obstructed by a wall and appliances. This work is of great interest in many countries, where buildings and bridges occasionally collapse while under construction. In the mining sector, this will help in finding survivors in case of a landslide. The application of this work is not limited to the aforementioned cases. To fight rhinoceros poaching, the system can be mounted on a drone, then sent to survey a game reserve. In addition, the system can be used in law enforcement. In such a case, a police officer will be equipped with this radar to determine the number of human beings inside a building. This type of radar could be used as well to detect guns carried by people inside a building. Moreover, the radar can detect concealed objects inside a building, to give police prior knowledge before entering a building.

Various important results emanated from this research: (1) It demonstrated the fact that micro-Doppler frequency is an efficient way of extracting and classifying the micro-movement of a target. This allowed the researcher to achieve the primary scientific objective of detecting human activities behind a wall in the presence of appliances. The target was mobile and non-cooperative; micro-Doppler return was sensed with an FMCW radar. (2) In addition to that, this research achieved one more scientific objective by designing a low-cost FMCW radar to collect and analyse radar signatures with MATLAB software. (3) Furthermore, a detailed analysis of the classification of a target behind a wall was proposed. The researcher demonstrated a way to extract human micro-Doppler in the presence of a fan. This deals with the case when two micro-Doppler signals are overlapping. (4) Besides that, the antenna used in the experiment was made in the laboratory. (5) Furthermore, a printed circuit board was designed and tested for radar signal generation. (6) Research reported in the literature did not consider a small chest area when detecting human beings. The additional contribution of this thesis is that in the home environment people of different height may live together; therefore, assuming that the subject behind the wall will always be an adult might disregard some parameters necessary for the evaluation of the radar. Simulation involving human beings of different height has thus been presented.

ACKNOWLEDGEMENT

I am deeply indebted to my supervisor, Prof. Saurabh Sinha, and co-supervisor of this project, Prof. Hendrik Christopher Ferreira (late), for consistently providing me with the required guidance to enable the timely and successful completion of this research work. In spite of their extremely busy schedules in the department and faculty, they were always available to share with me their deep insight, wide knowledge and extensive experience.

My utmost appreciation and gratitude go to Prof. Sinha and the late Prof. Ferreira for their ability to secure funding for my study. This research was funded by Global Excellence and Stature (GES) Master's and Doctoral Scholarships. In addition, I am grateful to Prof. Sinha for guiding me to obtain funds from IEEE for my experiment through the EPICS-in-IEEE project.

I would like to thank all members of the wireless laboratory research group and all friends who contributed in one way or another for all the thoughtful and mind-stimulating discussions we had, which prompted me to think beyond the obvious (Dr Suvendi Rimer, Prof. Khmaies Ouahada and Dr Mahlaku Mareli). I have enjoyed their companionship immensely during my stay in the YLab, University of Johannesburg.

I would like to thank the institution and the entire Faculty of Engineering and the Built Environment, especially the members of the Department of Electrical and Electronic Engineering Science (EEES), for their help and guidance. They have been great sources of inspiration to me and I thank them from the bottom of my heart.

I would like to thank my wife, Francoise Kasongo Lwamba, and my kids, Light Musao, Lloyd Kibambe and Lacya Kalunga, for supporting me all the time I was studying. I thank my brothers and sister, Serge Mubembe, Differentiel Laura Mbuyu, Tenseur Nsapu, Jonathan Nkaa, Immacule Ndumba and Thierry Kuthsina, for their encouragement.

I would like to thank my friends for their continuous support. I appreciate the positive reinforcement and motivation, pushing me never to give up and always to do my best.

Last but not least, I would like to thank my parents, Joseph Kibambe Mubembe Mashoko and Georgette Musao Kasongo, for their continuous presence, encouragement and financial support to allow me to pursue my postgraduate studies.

LIST OF ABBREVIATIONS

2-D	Two-dimensional
3-D	Three-dimensional
ADC	Analog-to-digital
BS-FBTVAR	Block-sparse forward-backward time-varying autoregressive
Cm	centimetre
CWDR	Continuous wave Doppler radar
CWR	Continuous wave radar
DCNN	Deep convolutional neural network
E	Electric field
EEES	Electrical and electronic engineering science
E_i	Incident electric field
EM	Electromagnetic
EPICS	Engineering projects in community service
Er	Radiated electric field
FDTD	Finite-difference time domain
FMCW	Frequency modulation continuous wave
FOM	First-order multipath
GHz	Gigahertz
IEEE	Institute of Electrical and Electronic Engineering, Inc.
IT	Information-theoretic
Kg	Kilogram
LISP	Linear inverse scattering problem
LNA	Low noise amplifier
LS	Layer stripping

m	Metre
MATLAB	Matrix laboratory
MHz	Mega Hertz
MIMO	Multiple input multiple output
ML	Maximum likelihood
mm	millimetre
PA	Power amplifier
PCB	Printed circuit board
PD	Power divider
PRF	Pulse repetition frequency
PRI	Pulse repetition interval
RADAR	Radio detection and ranging
RCS	Radar cross-section
RF	Radio frequency
SAR	Synthetic aperture radar
SNR	Signal-to-noise ratio
STFT	Short-time Fourier transform
SVM	Support vector machine
TRI	Time reversal imaging
TWR	Through-the-wall radar
TWRI	Through-the-wall radar imaging
TWRS	Through-the-wall radar sensing
UCWR	Unmodulated CWR
UWBPD	Ultra-wideband pulse–Doppler
V	Volts
VCO	Voltage-controlled oscillator

W	Watt
WoS	Web of Science
YLab	Wireless laboratory

TABLE OF CONTENTS

LIST OF FIGURES

LIST OF TABLES

CHAPTER 1 INTRODUCTION

1.1 CHAPTER OVERVIEW

In this thesis, the researcher is investigating the possibility of using frequency modulation continuous wave (FMCW) radar to detect a human being in a home environment. The micro-Doppler data are extracted from the raw data collected with the FMCW radar. This chapter outlines the background of the research and formulates concrete research questions based on the possibility mentioned above. Justification for the importance of this research is presented and relevant objectives and goals are outlined to define and defend the contribution to the body of knowledge.

1.2 BACKGROUND TO THE RESEARCH

Knowledge of the unknown has been a subject of interest among humans from the beginning of their existence. This is no different in modern times; humans are still making concerted efforts to find answers to questions about the unknown. In this case, the researcher is investigating the possibility of seeing through a wall. Human eyes make use of light reflected from an object to see. The fact that human eyes can only see when light is reflected automatically limits the field of vision of a human to a certain spectrum. It is known that visible light has a very short frequency band spectrum. Furthermore, the frequencies of visible light allow transparency in few materials found on earth. Consequently, the researcher made use of electromagnetic (EM) waves with frequencies of a few gigahertz (GHz), which penetrate many building materials and vegetation [1].

Currently, there is a great deal of interest in the use of radar to detect concealed targets, using a system called through-the-wall radar imaging (TWRI) [2, 3]. The core aim of TWRI is to use EM waves to sense objects inside an enclosed building or obstructed by non-metallic material. The important objective in this case is to extract the physical characteristics of a scene under inspection. This type of radar opens doors to many applications, such as military and rescue security applications [4, 5] . Recently this type of radar has been used in Nepal, where four men trapped under debris were found and rescued [6]. For military applications, the objective is to detect concealed objects such as bombs or to distinguish terrorists from hostages in an urban environment. In hostage rescue, great care has to be taken to avoid collateral damage. Furthermore, this technology

can be applied in mines up to a certain depth when miners are trapped underground, as happened in 2016, when three miners were trapped and killed underground in Lily mine, South Africa [7]. In addition, in rescue applications, TWRI is used to detect survivors after a natural disaster such as an earthquake or tornado. Seeing through an opaque object could be helpful in hostage rescue missions as well, as mentioned earlier. TWRI offers a wide range of applications; among others it can reveal the presence of concealed objects and human bodies inside a building. TWRI can detect animate and inanimate targets, which is an advantage compared to the thermal camera.

It has been reported that by using TWRI, a target inside a building could be detected and distinguished [8, 9, 10]. However, although this technology is promising, it poses some challenges, such as signal fading and target defocusing, which both reduce human detectability in this type of application [11]. Wall modelling and target differentiation are further challenges.

Signal fading is significant because the signal travels through the wall twice before getting back to the radar receiver. This implies significant attenuation from the wall. This is the reason why most research undertaken in this area uses frequencies that can penetrate the wall easily. Furthermore, some work in the literature shows that a target could be displaced from its actual position while the scene is being imaged [8]. This problem is known as target defocusing. Thus, these issues are addressed differently in the literature [12, 13].

A great deal of work has addressed the attenuation caused by a wall. To mitigate the wall attenuation, researchers tend to build TWRI systems that work below 3 GHz frequency. Therefore, Table 1-1 presents a summary of different papers reporting on wall attenuation. The first column presents the reference of the paper in the bibliography, the second column presents the different waveforms used in different papers, the third column presents the frequency transmitter used for the radar and finally, the last column presents the processing method used in different papers to mitigate the wall effect. At the frequencies presented in column three, the wall attenuation is more reasonable than at higher frequencies. Another approach that has been proposed to mitigate wall clutter is based on background subtraction. This approach assumes that the wall characteristics are known, or the wall is modelled mathematically, prior to the radar imaging. The value of the wall electric characteristics is then subtracted from the raw data [12, 13]. This approach gives good results but is not realistic in practice because of the unknown electric characteristics of the wall. Moreover, knowing that the electric characteristics of the wall may vary as a function of the frequency and humidity makes background subtraction more complex.

Table 1-1: Frequency and type of radar used most in TWRI.

Ref.	Radar type and waveform used	Frequency	Processing method used
[5]	Synthetic aperture radar (SAR) based on stepped frequency	0.7-3.1 GHz	The authors compared the relative strength of the exterior wall returns to behind-wall targets using the singular value decomposition method.
[8]	SAR based on stepped frequency	1-3 GHz	The authors used a refocusing approach to remove the effect of the wall. They used the idea of match filtering to compensate for the effect of the wall and to reconstruct the point target response; this was possible if the wall parameters were known.
[9]	SAR based on pulse frequency	2 GHz	The authors used two different imaging schemes to mitigate the error due to the wall effect. The first one relied on forming target displacement trajectories from a different standoff distance, and assuming different values of wall thickness and dielectric constant. Then the second one, relying on an image sequence, was generated.
[10]	SAR based on pulse frequency	100, 300, 500, and 600 MHz	The authors developed a two-dimensional (2-D) contrast source inversion-based imaging technique for layered media and their application to through-the-wall imaging.
[13]	SAR based on stepped frequency	2 GHz	This work was an extended version of 2-D imaging done previously by the authors. They analysed three-dimensional (3-D) imaging via delay-and-sum beamforming in the presence of a single uniform wall.
[14]	SAR based on stepped frequency	1-3 GHz	In order to mitigate the spatial zero-frequency and low-frequency components significantly, corresponding to wall reflections, the authors used spatial filters across the antenna array.
[15]	SAR based on pulse frequency	2-6 GHz	The authors used a time-domain approach to optimise the detectability of the target and applied a back-projection microwave imaging algorithm for 3-D image recovery of radar objects.

Consequently, to deal with high wall reflection without relying on prior knowledge of the electric wall characteristics, some other approaches have been proposed [14, 16]. Such an approach uses the signal received to estimate and model the wall characteristics. This requires a strong algorithm to determine the characteristics of the wall, such as a singular value decomposition [5]. To solve the issues mentioned earlier without relying on background subtraction or the first backscattering signal, other authors proposed using an array of antennas that are spatially spread [17]. By using different positions of the antennas, one can extract the electric wall characteristics at different points. These collected characteristics are used to estimate the true electric wall parameters. This type of approach is well fitted to real-time applications, since one can extract the dielectric characteristics of the wall while sensing. The disadvantage of this type of radar is the number of antennas, which can be cumbersome. Thus, for applications where the weight has to be kept as low as possible for human portability, this approach may not be practical. The next subsection introduces the research problem and the hypothesis.

1.3 RESEARCH PROBLEM AND HYPOTHESIS

1.3.1 Research problem

To address the hypothesis, the following research questions have been formulated:

a) How does the medium through which the radar signal propagates affect the detectability of a human behind the wall?
b) How can one detect a physically weak victim after an earthquake while the person's breathing and heartbeat signal strength is weak?
c) How can one detect a target with a lower chest radar cross-section (RCS), such as a child?
d) How can the range ambiguity of a radar caused by different types of walls be reduced in order to determine the real position of the target?

One thus observes that the medium in which the signal is propagating affects the detectability of the target behind the wall. This thesis also proposes an approach to detect a weak victim, which involves cancelling the clutter around the target. This approach is taken because the target may be miss-imaged while the radar is scanning the area of interest. In addition, a lower chest size implies a lower RCS. A small chest size can be observed when children are taken as target. In this case, one may sample a weak return signal, which will require highly sensitive radar to detect the signal.

1.3.2 Hypothesis

Micro-motion has been used to detect, identify and classify targets of interest in radar system technology. However, the detection, identification, and classification can be misrepresented if a good algorithm is not used or if the target is obstructed. Much research found in the literature addresses the issue. To classify human limb movement, the authors in [18, 19, 20] demonstrate that one can classify movement of the feet, hands and chest. In [21], using a harmonic radar operating at 12 and 24 GHz frequencies, the authors were able to detect breathing and chest movement.

The research reported in the literature considers a target obstructed by single or multiple wall slabs. In a home environment, considering a wall slab as the only obstruction between the target and the radar can be misleading, since besides the wall, the scene may contain different home appliances. The research conducted in this area strives to determine the possibility of finding a target that lies behind a wall and a home appliance simultaneously. Therefore, experiments where the radar signal has to go through the wall and at least one home appliance such as a fridge, television or fan, will be conducted.

The following hypothesis has been formulated to summarise the aforementioned paragraphs:

If through-the-wall radar signal attenuation and human micro-motion are related to the media where the signal is propagating and to the micro-Doppler effect, then the presence of an appliance between a target and the radar may cause the non-detectability of the target, but it would still be possible to detect chest and limb movement using a micro-Doppler radar.

1.4 JUSTIFICATION FOR RESEARCH

1.4.1 Introduction

The FMCW radar is used for scanning an object behind one slab or multiple slabs of wall. To perform the imaging, an EM wave is transmitted via a transmitter antenna, goes through the wall, then reflects from objects behind the wall. After reflection, the signal travels back to the receiving antenna through the slab of wall. At a frequency of a few GHz and below, most construction materials let the EM wave pass with reasonable attenuation. However, the signal undergoes the following phenomena while passing through the wall: reflection, refraction, diffraction and absorption [2].

Therefore, the primary objective of this research is to understand how EM waves are used to rescue people in cases of natural disaster. Nowadays EM waves are used everywhere. While this may be helpful, for example in medicine for X-ray examinations or for telemedicine monitoring, it can also be harmful to a certain extent when the transmission power is not well managed. Therefore, many regulatory bodies limit the transmission power of EM waves. EM waves have been used in many applications, such as telecommunication, medical treatment (cancer treatment), etc.

Human beings being buried under rubble is a frequent problem in areas where natural disasters occur or wherever there is war. When buildings collapse, there are always human beings under the rubble who need to be evacuated as soon as possible. However, the methods used to rescue them usually require time.

It should be mentioned that the signal received by the radar is complex because of the reflection, refraction, diffraction and absorption. Noise and clutter are constituents of the received signal that make the interpretation of the signal difficult. Therefore, signal processing is required to display a human-interpretable image. Signal processing requires a performant algorithm to solve this complex problem, but since there is no exact method to achieve this, researchers and engineers in the radar area encounter challenges.

In this research, the researcher aims to detect humans who may be immobile or mobile under debris. The debris may constitute a wall-only or wall-appliance combination. After a natural disaster, human beings trapped inside a building or under a fallen wall may be conscious or unconscious. The researcher aims to detect the target in both situations. In addition, because the target may be an adult or a child, this research will extend its investigation to a reduced RCS, taking into account a child's chest size.

1.4.2 Research gap in through-the-wall radar imaging

Despite much research in TWRI, there are still unsolved problems, thus further research is required into the aspects discussed below.

1.4.2.1 Detectability of the human being

The micro-Doppler effect is the main phenomenon used to search for and rescue humans buried under rubble after a building has collapsed or an earthquake. To detect the presence of a target (human being), an EM wave is emitted in the direction of the area of interest. The EM wave illuminates the target, then the target scatters back a modulated wave in the direction of the radar. The movement of the breathing and heartbeat of the human target

modulates the backscattering wave. However, there are still questions that have not been addressed. One can consider that after an earthquake, human victims may be weak. Thus, the breathing and heartbeat signal strength of the trapped victim may be too weak to be detected by the radar. Highly sensitive TWR sensing (TWRS) systems are needed to solve this problem.

Much research done in this area considers the victims as adult human beings. However, after an earthquake or if a building collapses, children may be trapped under the rubble as well. The heartbeat rate can vary significantly with the age of a person [22]. Therefore, a radar may miss some targets owing to their heartbeat ratio. In addition, the RCS of a child's chest is lower than that of adult victims. This issue can be investigated. Besides that, the position in which the victim is found should be taken into consideration because it can vary the RCS.

In February 2016, three gold miners were trapped underground in South Africa [7]. Scientists can investigate the detectability of a human being who is buried alive. In this case one should consider that the soil contains some metal components in its natural state. Because of this, the dielectric properties may be close to a perfect conductor.

In addition to the above issues, the radar resolution should be investigated. It has been reported that it is difficult to detect human beings while they are standing against a wall. This is due to the radar range resolution. One can investigate the possibility of distinguishing the target and the wall as distinct objects.

1.4.2.2 Wall modelling

The lack of a well-designed wall model remains a huge challenge in this area. Research has considered knowledge of the wall parameters or the first return signal coming from the wall. An effective wall model should take into consideration the state of the wall. Since humidity and the frequency band used can have a significant influence on the transmitted signal, one should take into consideration the time of year in which this system can be used effectively. Researchers could consider investigating humid and dynamic conditions as well, rather than only dry walls.

1.4.2.3 Target differentiation

TWRI has been used successfully to detect human beings inside buildings. However, a new technique should be investigated when the scene of interest contains more than one target. In a scenario where there are hostages and terrorists in the same building, rescuers

need to be able to distinguish effectively between the two targets. Thus, new techniques should be applied to differentiate between the activities of hostages and terrorists.

The next section is devoted to the research methodology. To determine the hypothesis of this work, the study followed a course of steps to identify open issues in the body of knowledge.

1.5 RESEARCH METHODOLOGY

The research methodology used in this study is illustrated in Figure 1.1.

1.6 DELIMITATIONS OF RESEARCH

It has to be mentioned that radar technology is a vast area of research. Radars can be found in civil aviation, military aviation and in meteorology etc. Therefore, delimiting the research subject in this thesis is very important. Knowing the application for which the radar has to be used is one among many elements that can make radar work better in one application than in another.

Furthermore, what may be a target in one application might be clutter for another application. This last statement can be seen in weather radar, of which the target may be rainfall and the development of cloud. On the other hand, cloud and rain are seen as clutter in air traffic control.

For the sake of this investigation, the researcher is working on TWR. TWR is a low-transmission power radar compared to radar used for air traffic. The transmission power has to be kept low because the signal has to travel through human tissue, which cannot be exposed to higher RF energy.

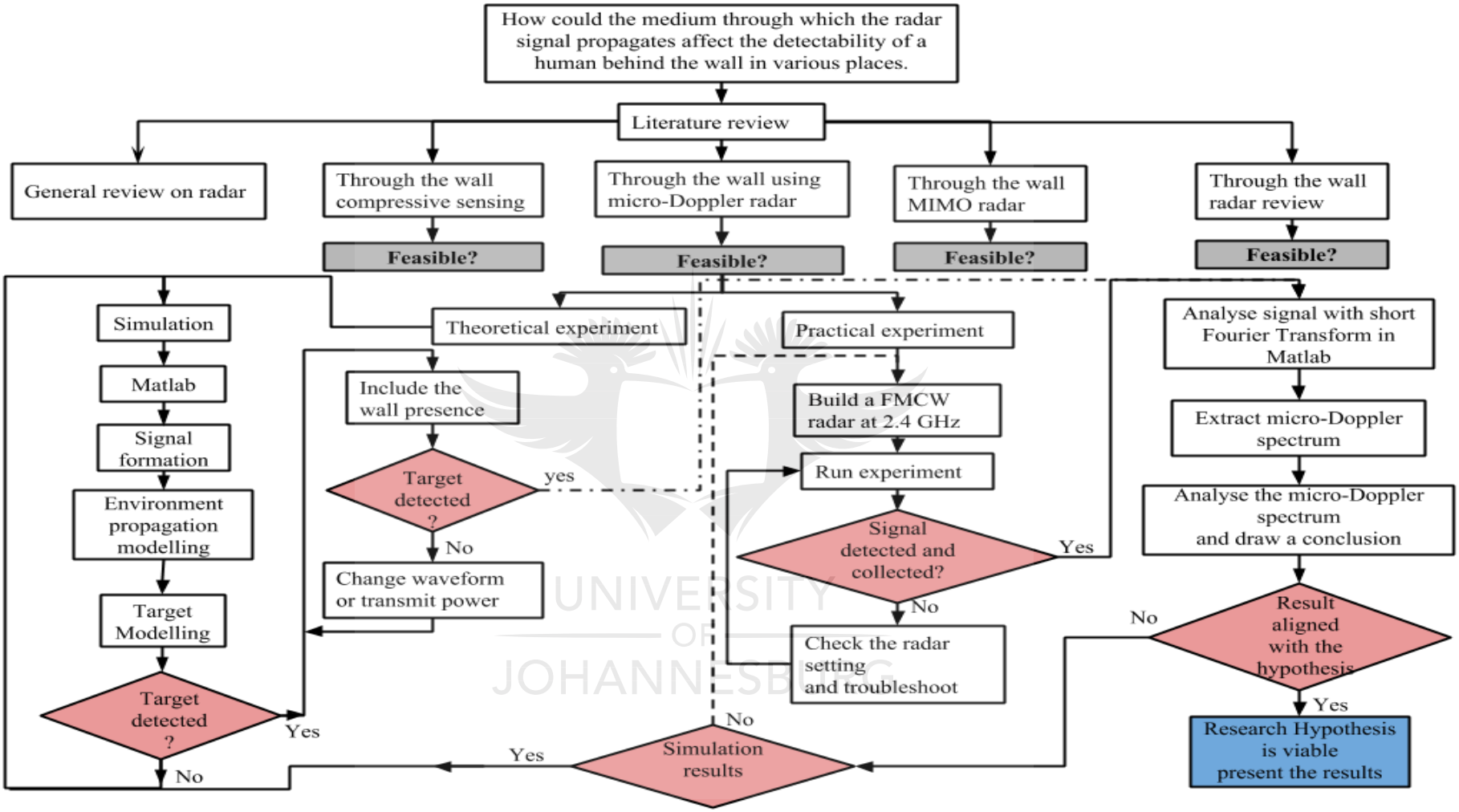

Figure 1.1: Research methodology followed for the proposed research.

Thus, taking into consideration the power transmission, a practical choice has been made of the FMCW radar as sensor with a lower RF power amplifier (PA) wattage. In addition to power transmission, FMCW is cost-effective compared to pulse radar, which requires a high wattage PA. FMCW radar is used as sensor to detect human activities inside a room.

Most research conducted in the TWR considers that the human behind the wall is an adult man or woman whose height is above a certain limit. To the best of the author's knowledge, no research reported in literature has considered different heights of targets behind the wall. The lower height is considered in this thesis as children. Thus, this research devoted effort to investigating the return signal from children to adults in the simulation environment.

All experiments were done in a laboratory environment at the University of Johannesburg and the author's residence, both in South Africa. Because the study used micro-Doppler frequency to detect a subject behind the wall, mobile appliances were considered. Therefore, a fan was carefully considered as the main source of continuous mobility in a warm region, particularly in the home environment. Fans considered were ceiling and mobile fans used daily in the home environment. In addition, this application considered hot regions of the globe where the use of fans is necessary.

1.7 RESEARCH CONTRIBUTION

This thesis has made the following contribution:

Collection, signal processing and analysis of data collected with FMCW radar for different targets

Using FMCW radar, a target signature was collected, and the signal was processed. The data were collected in a laboratory environment and in a house where appliances were distributed normally. The targets comprised of human with different height and the fan. The target was walking toward the radar; the target direction line formed an angle different from the direction of the radar.

FMCW radar hardware design

To perform data collection, this thesis contributed by designing a cost-effective FMCW and high-performance radar. The hardware radar can be used in many scenarios to collect micro-Doppler data.

Target micro-Doppler signature

The investigation identified movement coming from the chest and limbs. With this type of radar, one is able to detect weak signals coming from a human target.

1.8 PUBLICATION FROM THIS RESEARCH

The following paper resulted from the research carried out during this work:

P. K. M. Nkwari, S. Sinha and H. C. Ferreira, "Through-the-wall radar imaging: A review," *IETE Technical Review,* vol. 35, no.6, pp. 631-639, September 2017 [23].

The IETE Technical Review is indexed by the Web of Science (WoS).

The following article by the author has also been submitted and is under review:

P. K. M. Nkwari and S. Sinha, "Frequency Modulation Continuous Wave Radar through the Wall Using Micro-Doppler," submitted to a journal indexed by WoS.

1.9 OVERVIEW OF STUDY

The rest of this thesis is structured in the following manner:

Chapter 2 is devoted to a literature review of relevant topics in TWRI to investigate the research hypothesis. Different techniques encountered in TWRI are reviewed in this chapter. While reviewing TWRI, attention is focused on reviewing the detectability of vital signs in the presence and absence of a wall. The chapter highlights the gaps remaining in this area of research as well.

Chapter 3 presents a systematic discussion of the methodology used to complete the research, from the hypothesis phase to the measurement and conclusion phase. The methodology used here is the micro-Doppler, thus different micro-Doppler techniques are reviewed, and the relevance of the micro-Doppler used in this research is shown.

Chapter 4 presents the radar built to collect the data. The data are collected with an FMCW radar. The setup and the connection of different modules are presented. Chapter 3 and Chapter 4 constitute a tool to test the researcher's hypothesis throughout the experiment and the simulation.

Chapter 5 focuses on the results of the study and experiments conducted. The chapter is divided into two main sections, the simulation run in MATLAB software and the experimental section. Simulation was used in this thesis because of lack of material that has to work at certain frequencies. Thus, simulations were performed at other frequencies to indicate how the radar should behave at those frequencies.

The second section related to the experiment describes the experiment undertaken with an FMCW radar built to function at 2.4 GHz, with two antennas. In this section, the researcher discussed the results obtained in the simulation and real experiment. The relevancy of this work depends on those results.

Chapter 6 concludes this thesis and draws relationships between the simulation and the actual experiment. This chapter determines the possibility for future research by taking into account all the results obtained in this thesis.

1.10 CONCLUDING REMARKS

The introduction to this chapter revealed a gap in the current body of knowledge. To confirm this, the background and context of the problem were reviewed, leading to the formulation of the research hypothesis. It was shown how the research hypothesis was justified by the research methodology. The next chapter undertakes a literature review on radar in general and on TWR in particular.

CHAPTER 2 LITERATURE REVIEW

2.1 CHAPTER OBJECTIVES

The chapter is divided into five sections: general background on the radar system, radar used in a through-the-wall system, interior structure reconstruction, the research gap in TWR imaging and the conclusion.

To get an overview of radar, a general background on radar is given as an introduction to the chapter in section 2.2. Thereafter, in section 2.3, an introduction to different types of radar used in the TWR is presented. After reviewing the different types of radar used in TWRI and the different approaches used to mitigate radar clutter in section 2.3, section 2.4 is dedicated to interior structure reconstruction. Interior structure reconstruction is another interesting area of research for TWRI. Using a TWR allows a structure to be imaged without the necessity to enter it. One can ascertain the layout of a building or structure while using this radar. In section 2.5, different gaps remaining in the body of knowledge are presented. Thus, to identify a gap in the body of knowledge that this work sought to fill, a section devoted to the research gap in TWR imaging has been introduced. In this section, the researcher focuses on the gap remaining in this area of research. Finally, concluding remarks are presented.

2.2 GENERAL BACKGROUND ON RADAR SYSTEM

2.2.1 Radar system

Radar is an acronym for “radio detection and ranging” [24]. Radar uses EM waves to reconstitute the image of a target in the area of investigation. To illustrate the radar system, Figure 2.1 has been introduced. Figure 2.1 shows a block diagram with the different blocks that a radar system contains. These different blocks are necessary to enable collection of the echoes of the signal sent by the radar.

To be able to detect any target in the vicinity of the radar, a wave is generated in the form of an electric signal at frequency, f_1. The wave can take different waveforms, including the form of a pulse. The signal at frequency f_1 is carried by another signal at a different frequency from f_1. The second signal has a frequency of f_2. The two signals generated are

then combined inside the transmitter. The process of combining the two frequencies is called modulation. Afterwards $f_1 + f_2$ are passed through a switch and radiated in the free space via an antenna. The radar pulse is transmitted in free space as an EM wave. The EM wave will bounce off any obstacle or object found in its way. After the bouncing, a small portion of that wave returns to the receiver antenna, called the echo. In radar technology, the bouncing is known as the scattering phenomenon. A small amount of the scattering signal returns to the same antenna used for the receiver in a monostatic radar or to the receiver antenna in the bistatic configuration. This small return is fed to the receiver antenna. The incoming signal will pass through a switch and then go to the receiver for signal conditioning and amplification. From the receiver it proceeds to the data recorder, then the processor, ending in the display. At the display, one can see the shape of the object off which the EM wave bounced, depending of the nature of the target. Figure 2.1 represents a radar system with its different main blocks.

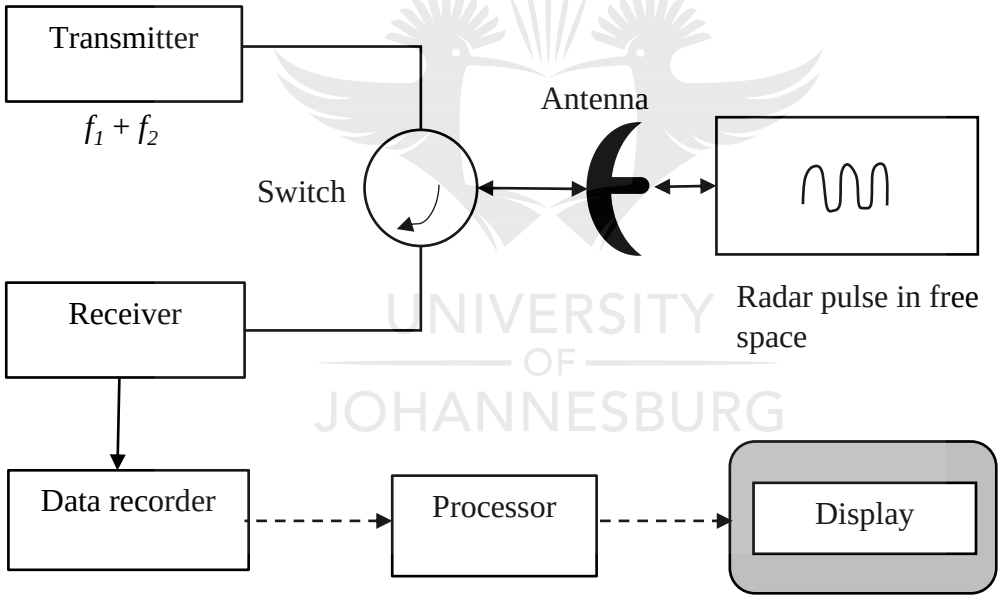

Figure 2.1: Radar system with different blocks.

In Figure 2.1, it is shown that using an EM wave is very useful, as it offers the possibility of detecting the presence of an object. While a camera will necessitate the presence of light to produce an image, radar can work even in darkness. Besides that, radar has the advantage of seeing through opaque objects, which the camera cannot do. Taking into account the advantages of radar over its counterpart, the camera, radar will fit well in the application of this work.

While the radar is emitting its signal in the air, any object found in the way of the signal propagation will induce a signal bounce. The signal bounce may come from many objects. The object that one needs to detect is known as a target, while the rest of the return signal is known as clutter. Therefore, what can be considered as clutter for one application can be considered as target for another. This can be seen in aviation; the airplane is a target to be detected. The signal has to pass through fog to reach the airplane. The fog and rain are clutter, because they decrease the signal strength. On the other hand, the weather radar sees rain and fog as target in order to process weather forecasting. Thus, calling an object a target is a function of the application of the radar.

To detect a target under investigation, the wave form and the frequency of transmission are of great interest and have to be chosen meticulously. A waveform is chosen according to the function of an application, because some waveforms fit better into an application than others.

Radar has been used in different applications to solve different problems encountered. Thus, radar can be classified in terms of its operating frequency, waveform and the place where the radar will operate [25].

2.2.2 Radar ranging

Radar can reveal the range of a target and the type of target by processing the return signal from the target.

To illustrate the signal propagation, a case of a pulse radar has been introduced in Figure 2.2. In this figure transmitted and received signals are shown. In Figure 2.2, the top signal represents the transmitted train of pulse. The bottom signal represents a received train of pulse.

Consider that at time $t = 0 = t_0$ a pulse 1 is sent from the radar antenna. By assuming that the radar was transmitting pulses before time t, pulse 2 can be considered to have been sent at time $t_2 = t - PRI$ and pulse 3 at time $t_3 = t - 2 \cdot PRI$. Here PRI is known as the pulse repetition interval. As illustrated, the train pulse has three pulses, which are transmitted through the air via the antenna. This train returns in the form of echoes when it reflects from any object. As transmitted, the echoes train constitutes three echoes, which are respectively for pulses 1, 2 and 3. While the echoes train is returning, a time difference from the moment the train pulse has been transmitted and the train echo has been received

is observed. This time difference is illustrated in Figure 2.2 and represented by Δt. Δt can be translated in terms of distance, as the velocity of the wave is known. Thus: $R = \frac{C \cdot \Delta t}{2}$.

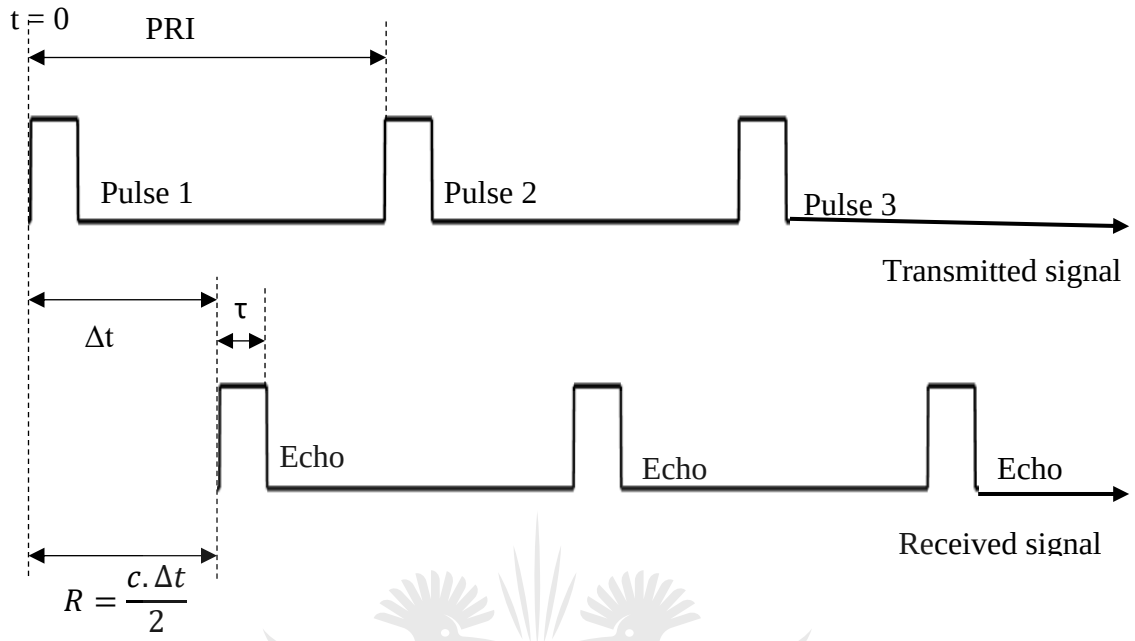

Figure 2.2: Transmitted and received train of pulses.

To reveal the range, a train of pulses is sent to the target, as illustrated in Figure 2.2. The pulses have the same width, denoted τ, and are transmitted at regular intervals. The interval from the starting point of pulse 1 to the starting point of pulse 2 is known as the PRI. The PRI is also called the inter-pulse period, as it constitutes the period of the signal, which can be represented as T as well. In terms of frequency, the PRI is interconnected with a pulse repetition frequency (PRF). The PRF is the inverse of the PRI. Let f_r denote the PRI, which can be calculated as follows:

$$f_r = \frac{1}{PRI} = \frac{1}{T}. \tag{2.1}$$

From Figure 2.2, one can see that the radar only transmits a signal for τ time. For the rest of the period, the signal is low. The radar listens for any return signal in the interval when it is not transmitting a signal. The listening interval allows a radar to detect far-away targets present in the vicinity. This listening interval is proportional in a certain way to the range that one would like radar to have. Beyond that time the radar will expect to receive an echo of pulse 2. Thus, the time interval is related to a range called the unambiguous range. The next sub-section is devoted to the unambiguous range.

2.2.2.1 Unambiguous range

For echo 1 to reach the radar receiver, the signal will have to travel two ways after a time delay T. The two-way distance travelled by the radar is known as the radar unambiguous range, R_u [26]. According to Figure 2.2, echo 1 is regarded as the return signal from a target at range R_1 due to pulse 1. Furthermore, echo 2 can be regarded as the return signal from a target at range R_1 owing to pulse 2, or on the other hand as the return signal from a target far away at range R_2 owing to pulse 1. Therefore, the ranges can be calculated as follows:

$$R_1 = \frac{C.\Delta t}{2} \tag{2.2}$$

and

$$R_2 = \frac{c.\Delta t}{2} \tag{2.3}$$

or

$$R_2 = \frac{c(T + \Delta t)}{2}. \tag{2.4}$$

Thus, using echo 2 brings about a certain ambiguity in the calculation of the range. To overcome the status of unambiguity, the radar has to wait a sufficient amount of time before sending another signal, once the preceding pulse has been sent. The amount of time has to be sufficient to allow the echo of the far-away target to reach the radar receiver. Thus, the maximum unambiguous range must be half of the PRI:

$$R_u = \frac{cT}{2} = \frac{c}{2.f_r}. \tag{2.5}$$

2.2.2.2 Range resolution

Range resolution is the ability of a radar to distinguish between two different targets at the closest range. This is one of the main metrics in the radar system, because it will help greatly in different applications.

To explain the range resolution, Figure 2.3 introduced the concept. In this figure the radar is placed at this position while transmitting a signal in the air. Three cases have been shown in Figure 2.3. The first one involves two humans who are in the same bin but separated in the cross-range, the second two humans in two different bins, but in the same cross-range, and the last one two humans in different bins and different cross-ranges.

Normally, radar operates between a minimum and a maximum range, R_{min} and R_{max} respectively. The distance between the R_{min} and R_{max} is divided into bins of equal width, ΔR. ΔR is the range resolution and if one considers that the distance between R_{min} and R_{max} is divided into N range bins, ΔR can be calculated as follows:

$$\Delta R = \frac{R_{max} - R_{min}}{N}. \tag{2.6}$$

Figure 2.3 is an illustration of different scenarios in which human beings may find themselves in relation to the radar and each other.

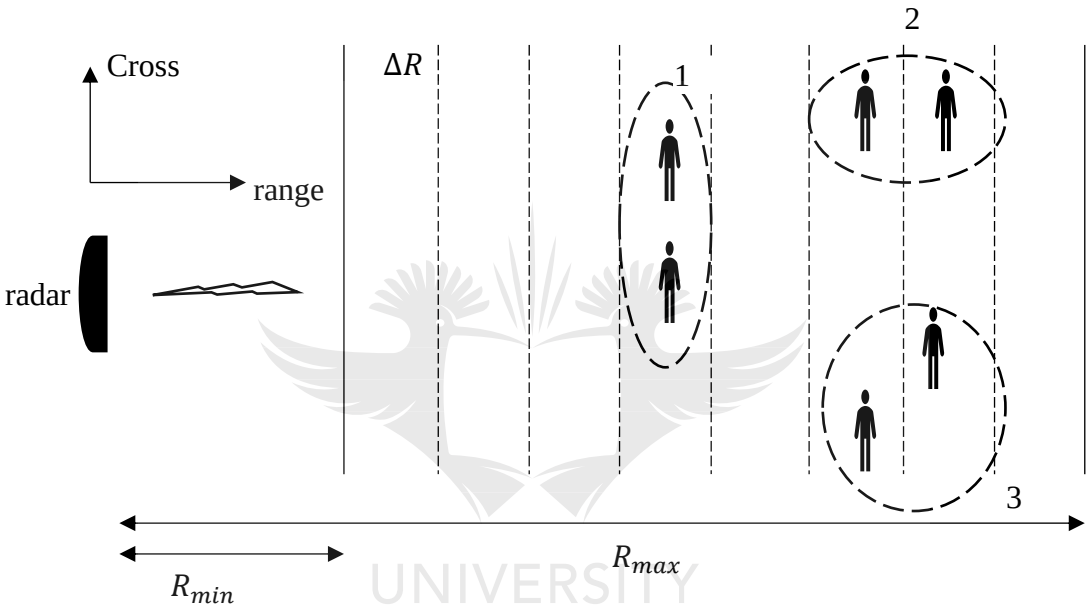

Figure 2.3: Range resolution.

In Figure 2.3, consider the humans found in the same range bin ΔR, in situation 1. For the radar to be able to distinguish between the two targets, image processing is necessary in the cross-range. In situation 2 the two targets can be distinguished in range. Finally, in situation 3 the target can be distinguished in range and cross-range. The range resolution ΔR is determined as greater than or equal to $\frac{c\tau}{2}$ in order to distinguish between two different targets.

$$\Delta R = \frac{c\tau}{2} = \frac{c}{2.B} \tag{2.7}$$

with the radar bandwidth

$$B = \frac{1}{\tau}. \tag{2.8}$$

Thus, to achieve a fine range resolution radar, one has to build a radar with greater bandwidth. From (2.8), one can see that in order to get greater bandwidth, the pulse width has to be reduced. This has the undesirable effect of reducing the maximum range of the radar by influencing the average transmit power.

2.2.3 Doppler frequency

The Doppler frequency is a notion that is necessary to this research, as it is the method chosen to detect the target. To illustrate the notion of Doppler frequency, Figure 2.4 has been presented. In this figure a radar is transmitting a signal while a human is walking. The radar sends an EM wave to the target, then receives the return signal. Using the delay of the received wave, the radar will detect the range at which the target is. This delay is translated in terms of the frequency, known as frequency shift. A frequency shift from the transmitted wave will be observed if the EM wave bounces off a moving target. This frequency shift is known as the Doppler effect [27]. This phenomenon finds many applications in physics and engineering. In Figure 2.4 a human being is moving towards the radar and another one is moving away from the radar.

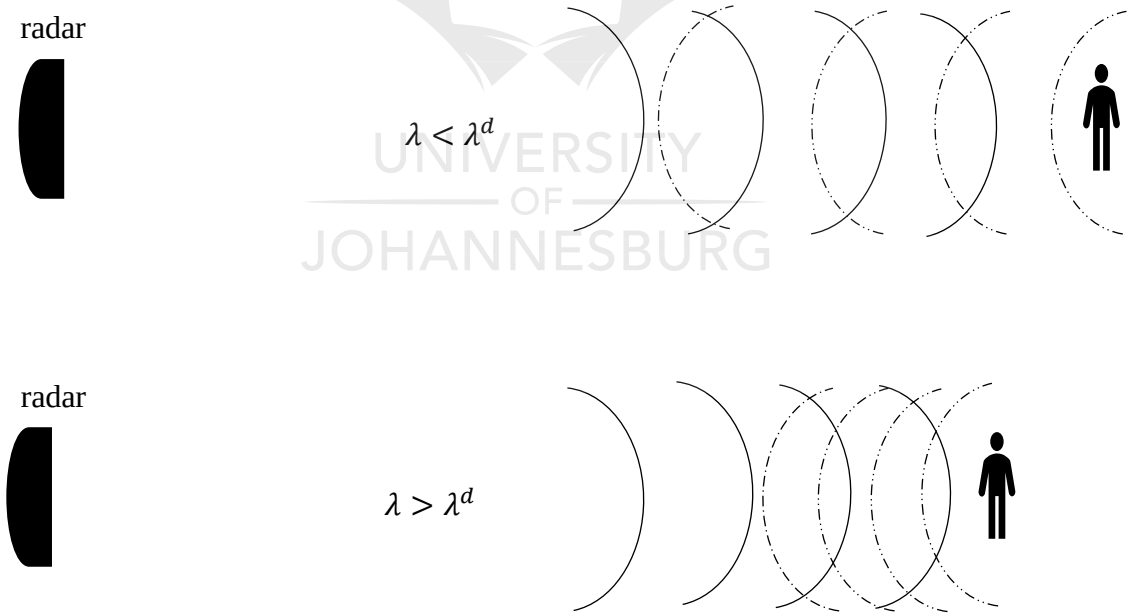

Figure 2.4: Doppler effect for moving target.

Based on Figure 2.4, consider a human being moving towards the radar at velocity v and the pulse of width τ impinging on the target. Also, consider d as the distance the target covers in the pulse width elapse of time Δt.

The distance can be calculated as follows:

$$d = \Delta t.v. \tag{2.9}$$

It is known that the radar wave moves at the speed of light. Then the trailing edge covers the distance of $c.\tau - d$. To find the time spent by the pulse to cover that distance, one can calculate it as follows:

$$\Delta t = \frac{c.\tau - d}{c}. \tag{2.10}$$

Incorporating (2.10) into (2.9) yields this formula after rearrangement:

$$d = \frac{\tau.v.c}{c + v}. \tag{2.11}$$

In Figure 2.5 the Doppler effect is illustrated, but this time in terms of the velocity time and distance. In Figure 2.5, the top part of the figure represents a radar that has a velocity of v_r and a human at position A moving towards the radar at a velocity v at time t_0. The bottom part of the figure represents the same scenario, but this time the human is at position B after Δt time.

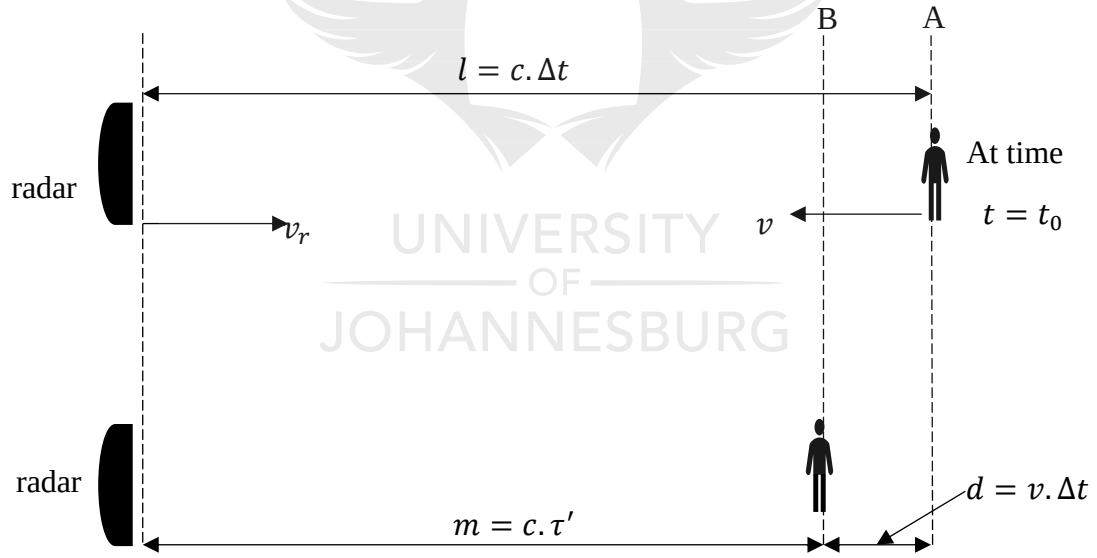

Figure 2.5: Doppler effect demonstration on human being.

Therefore, as illustrated in Figure 2.5, when the target moves from point A to point B it will cover a distance d, which has been deduced in (2.11). Then the entire distance remaining from the target to the radar is:

$$m = c.\tau'. \tag{2.12}$$

That distance can be rewritten as follows:

$$m = c.\tau' = l - d. \tag{2.13}$$

Initially, the distance between the radar and the target is from point AA to point B in Figure 2.5, which is the distance:

$$l = c.\Delta t. \tag{2.14}$$

Substituting (2.11) and (2.14) into (2.13) will yield:

$$m = c.\Delta t - \frac{\tau v c}{v + c}. \tag{2.15}$$

Substituting (2.10) into (2.15) will yield:

$$c.\tau' = \frac{c^2.\tau}{v + c} - \frac{v.c.\tau}{v + c} = \frac{\tau(c^2 - v.c)}{v + c}. \tag{2.16}$$

$$\tau' = \frac{\tau(c - v)}{c + v}. \tag{2.17}$$

Equation (2.17) is for a close target, meaning the distance between the target and the radar is decreasing. On the other hand, the opening target equation is for a target that is moving away from the radar. The opening target is computed with the following formula:

$$\tau' = \frac{\tau(c + v)}{c - v}. \tag{2.18}$$

Equations (2.17) and (2.18) are known as the time dilation factor.

In all logic the number of pulses transmitted by the radar is equal to the number of pulses that will strike the target. Thus, the frequency can be calculated as follows:

$$f_t.\tau' = f_r.\tau. \tag{2.19}$$

Substituting (2.18) into (2.19) yields:

$$f_t = f_r.\left(\frac{c - v}{c + v}\right). \tag{2.20}$$

The Doppler frequency is the difference between the radar radial velocity and the target radial velocity:

$$f_d = f_t - f_r = \frac{v - v_r}{c} f_r. \tag{2.21}$$

2.2.1 Radar classifications

In the classification of radar, one finds ground-based, airborne, space-borne and ship-based radar systems [25]. Simply knowing where the radar is to be installed enables one to classify it. For instance, the radar is called ground-based when installed on ground to monitor the vicinity. The place of installation is not the only parameter that guides the classification of radar. Radar can also be classified based on the frequency band, antenna type, waveform and functionality [25]. In this work, the researcher will focus on waveform classification, namely continuous wave radar (CWR) and pulse radar. In CWR there are

subsets of radar called modulated CWR and unmodulated CWR (UCWR). Pulse radar includes a moving target indicator and pulse Doppler radar. The choice of radar signal is related to the application.

2.2.1.1 Continuous wave radar

CWR is a type of radar that finds utility in many applications. Recently, CWR has been used to estimate cuffless blood pressure. To acquire the arterial pulsation at the aortic arch, the authors placed a transmitter and receiver antenna at the sternum [28]. CWR is finding increasing application in biomedical engineering [28, 29]. In [29] the authors used a CWR to detect inmates' vital signs. In the case of TWRI, the CWR is used to detect activities inside a building [30]. Thus, two main subsets of CWR, known as unmodulated and modulated CWR, were identified.

a. Unmodulated continuous wave radar

As its name implies, UCWR is radar used in applications where cost is a constraint and where one is interested in the speed of a moving target. To detect the speed of a target, an unmodulated wave is transmitted towards a target. The backscattering signal is fed into a receiver antenna. The radar will detect a Doppler shift of the signal if the target is moving. On the other hand, if the target is stationary, the UCWR will be unable to detect it.

b. Modulated continuous wave radar

In this system, the radar sends a continuous wave to the target and then receives the echoes. The EM wave is modulated by the movement of the target, which induces echoes. A major problem with this type of radar is inability to measure the range of the target. UCWR can only measure speed by employing the Doppler effect. Therefore, once ranging information is required, the transmitted wave is modulated. The modulation used most often is frequency modulation or phase shift keying modulation.

Figure 2.6 illustrates an FMCW signal transmitted and received by the radar. The dotted line is the transmitted signal, while the solid line is the received signal. The Y-axis represents the frequency of transmission and reception, while the X-axis represents the time. As time passes, the frequency increases up to the maximum frequency before falling sharply to the minimum frequency.

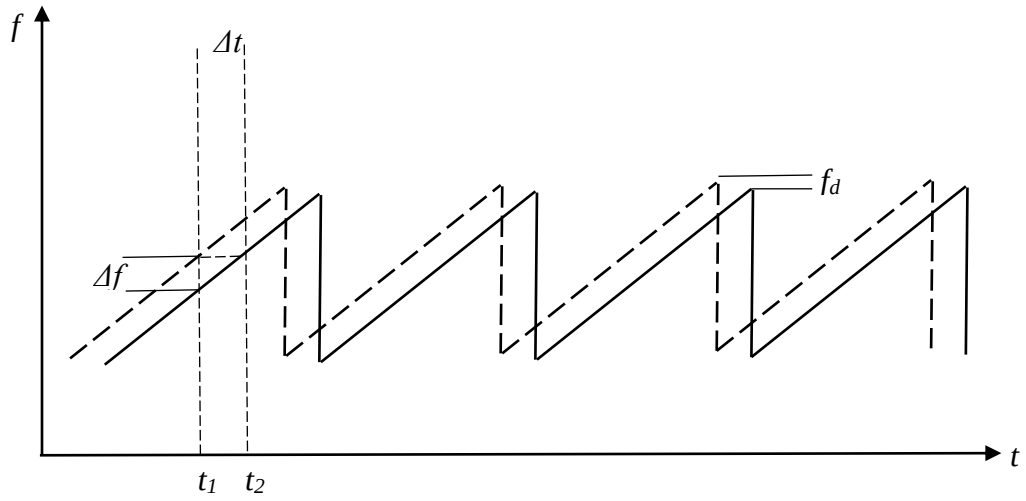

Figure 2.6: Frequency modulated continuous wave.

Because the signal is periodic, this cycle will start over time. Furthermore, the received signal is collected with a certain delay, Δt, which is attributed to the travelling time of the signal from the radar to the target and back. If the target is moving, a Doppler shift frequency will be observed in the return signal. The shift frequency is represented by f_d in Figure 2.6.

Because in TWRI ranging is imperative, there is a high preference for using a modulated transmitted signal rather than an unmodulated one. The modulated signal is more prominent than the unmodulated signal because the modulated signal can detect the Doppler shift and the range of the target. Many researchers have used an FMCW in the area of TWRI to advantage. In an FMCW radar system, a signal varies its operating frequency. The variable frequency is transmitted toward the target, as illustrated in Figure 2.6. Afterwards the signal is reflected from the target; the radar receives a fraction of the signal coming from the target. Equation (2.22) is used to determine the range in FMCW,

$$R = \frac{c.\Delta t}{2} = \frac{c.\Delta t}{2.\frac{df}{dt}} \tag{2.22}$$

where c is the speed of light, Δt is the delay time, Δf is the measured frequency difference, $\frac{df}{dt}$ is the frequency shift per unit of time, R is the distance between the target and the radar; then factor 2 represents the round trip that the signal is taking to travel from the antenna to the target. Figure 2.6 illustrates a linear frequency modulation signal, which is transmitted, and the receiving signal.

The different patterns of the transmitted waves differentiate the type of modulation. Thus, one finds saw-tooth modulation and stepped modulation. To the best of the researcher's knowledge, the most frequently used modulation in TWRI is stepped frequency modulation.

a. **Stepped frequency modulation**

This type of modulation changes the wave signal frequency in the form of stairs. It has the advantage of resonating with different targets at different frequencies. One can see this type of radar as a special case of an FMCW.

b. Sawtooth frequency modulation

Sawtooth frequency modulation is another modulation found in FMCW radar. It is a common form of modulation found in many applications. The kind of modulation is used for its ability to cover a relatively large range.

c. Triangular frequency modulation

Triangular frequency modulation is also a modulation found in FMCW radar. It has the advantage of detecting a target when the frequency is downward.

d. Rectangular frequency modulation

Rectangular frequency modulation is found in FMCW radar. Rectangular frequency modulation is known as square frequency modulation as well, because of the form of the signal pattern.

2.2.1.2 Pulse radar

In pulse radar, as its name implies, a high-transmission power signal is transmitted towards the target for a short period. The radar has a listening period when it is expecting any echo from a target or obstacle. This type of radar has the advantage of measuring the range and Doppler effect from the target. In order to distinguish the two closest objects, the radar must be a high-resolution range. The range resolution is determined as in (2.8).

Thus, to obtain a high-resolution range, one can attempt to create a short-period pulse. Unfortunately, it is difficult to have high-power energy in a short-period signal. A pulse compression technique has therefore been introduced to overcome this problem.

***Pulse compression**:* This technique uses a pulse modulated in frequency or phase. This modulation allows the radar to transmit enough energy for target detection. It has the advantage of increasing the range resolution. Where a high-resolution range is needed, this type of modulation can be used.

2.3 RADAR USED IN THROUGH-THE-WALL SYSTEM

2.3.1 Vital body sign detection

Important research done in TWRI is aimed at detecting vital signs behind a wall. Heartbeat, chest movement and limb movement are used to detect the presence of a human being inside a building. This section will review the different approaches used in radar technology for vital sign detection. While the first subsection will be devoted to different methods used to detect vital signs in the absence of any obstruction between the radar and the human being, the second subsection will be devoted to detecting vital signs in the presence of a wall.

2.3.1.1 Vital body sign detection without obstruction

Remote sensing for vital sign detection where there is no obstruction is an application mainly used in biomedical systems for non-invasive monitoring of patients. In this kind of application, the elements used to monitor the patient are heartbeat and breathing. Researchers have shown great interest in this application [21] [31, 32, 33].

While many researchers are trying to extract vital signal signatures [21], [31], there are others who are extracting human signatures from body movements [34]. The authors in [34] found that the Doppler spectra of the limbs could be used to distinguish a walking human being sufficiently from a stationary one and other moving objects. In addition, the Doppler spectra could be used to determine the size, gender and posture of the human being. In order to enhance target detection, the authors decomposed the overall backscatter into components associated with the limbs and torso. Moreover, the authors used radar polarimetry with a view to detect concealed objects on the human body.

2.3.1.2 Vital sign detection in opaque media

Detection of human beings using a TWRI system is mainly based on detection of heartbeat [15], respiration [15] and movement [3]. Research done in this area has demonstrated that seeing through an opaque object is possible. At a lower frequency, the wall attenuation of an EM wave is low as well [8]. This property is used to reveal a target inside a building.

2.3.2 Through-the-wall radar imaging

A radar system works by making use of EM wave propagation in a medium to image a scene [30]. In the case of a through-the-wall system, the media are air and wall. The

properties of the medium determine two fundamental constraints affecting the design of any radar system: the power and the bandwidth constraint. Knowledge of the properties of the medium is therefore imperative. While the air's electric characteristics are known, this is not always the case with the wall. It has to be mentioned that electric wall characteristics may vary significantly with the frequency, the humidity and the material used in construction. Thus, EM waves experience important power attenuation while going through a wall. It is for this reason that the next section is devoted to mitigation techniques and revision of how researchers attempt to mitigate these constraints and which type of radar is used.

2.3.2.1 Through-the-wall system scenario

The scenario of a TWRS is presented in Figure 2.7. In this figure, a radar is placed far from the wall. The distance from the radar to the wall is such that the wave hitting the wall is a plane wave. Beyond the first wall lies a human being at a random distance from the first wall. Behind the human is another wall. There are two more walls at the side of the human, which are not represented in the figure.

Figure 2.7: Behind-wall scene.

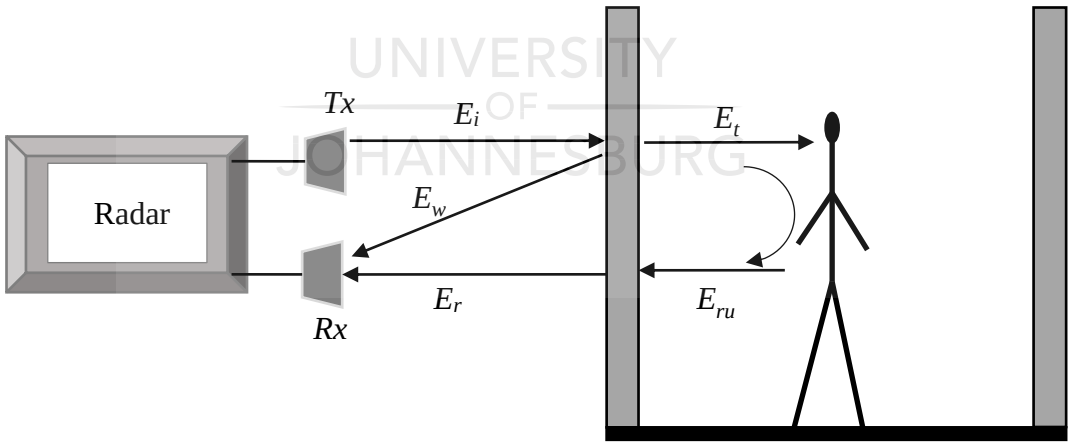

In Figure 2.7, the radar is a monostatic radar transmitting a signal to the wall. A portion of the signal goes through the wall while the rest disperses on the wall surface. Some of the dispersed wave returns to the radar. This is considered the first return of the signal. In some cases, the first return signal can be used to detect the wall when the wall properties are unknown. On the other side of the wall the other portion of the signal travels to the human inside the building. After bouncing off the human and other objects inside the room, the signal returns to the wall first, then the radar. At that moment the returned signal

can be processed. Researchers investigate the dispersion properties of an incident EM wave E_i on a wall to extract useful information from the reflected wave E_r and the transmitted wave E_t [4], [35].

A wall behaves as dielectric material when a wave E_i passes through it. Therefore, three phenomena are observed when an EM wave is in the presence of a dielectric material, namely reflection, absorption and transmission. The first and third phenomena are imperative in radar applications because of the information contained in them. In the present case these are referred to as E_r and E_t. Reflection is important in order to detect the object in front of the radar. Although this phenomenon is necessary, it is harmful to a certain extent when the target is obstructed. One can see that E_{ru} will have a stronger return than E_r because of the delay related to the distance and the dispersion of the wave on the wall. The reflected signal from a target E_{ru} is important to allow the radar to detect the target. If the wall reflection is significant, the return target signal beyond the wall may be difficult to recover. Thus, this phenomenon requires proper control or needs to be understood well in order to mitigate its effect. The transmission from the wall is most desirable in the current case, because the stronger the signal is beyond the wall, the better chance one has of detecting a target behind the wall.

When the incident wave

$$E_i(t) = A_i.\cos(2\pi f_i t) \tag{2.24}$$

impinges on a wall, there is a reflected wave

$$E_w = A_w.\cos(2\pi f_i \tau_w) \tag{2.25}$$

$$\tau_w = t - t_w$$

and a re-emitted wave

$$E_t = A_t.\cos(2\pi f_i \tau_i), \tag{2.26}$$

$$\tau_t = t - t_t \tag{2.27}$$

that emanates from the wall. E_t is emitted up to the target, then a small portion of the wave is backscattered to the radar through the wall. The return signal could be expressed as

$$E_r(t) = A_r.cos\left[2\pi f_i\left(t - 2\frac{R(t)}{c}\right)\right] \tag{2.28}$$

where t_w is delay due to free space return propagation from the wall, t_t is delay due to through-the-wall propagation, t_r is delay due to free space, through-the-wall and free space propagation from the target to the radar. E_i is the incident wave, A_i is the amplitude of the incident wave E_i, f_i is the carrier frequency, E_w is the wave reflected from the wall, A_w is the amplitude of the reflected wave E_w, τ_w is the time the signal took to make a

round trip from the antenna to the wall, E_t is the reemitted wave from the wall to the target, A_t is the amplitude wave of the reemitted wave, τ_t is the time the signal took to travel through the wall up to the target, E_r is the reflected wave from the target to the receiving antenna, A_r is the amplitude of the $E_r(t)$ wave, $R(t)$ is the distance from the target to the radar, and c is the speed of light. Factor 2 is a round trip from the radar to the target. One can see that $E_r(t)$, the signal coming back from the target, contains the dielectric properties of the wall and the target. To find the attenuation incurred by the wall, A_w has to be computed. A_w contains the reflection coefficient of the wall and the target.

By comparing the signal E_w and E_r, one can observe that E_r is less than E_w because E_r undergoes attenuation via the wall. Thus, E_w tends to suppress the signal E_r. Then in practice the strong backscattering from the wall tends to dissimulate the target backscattering, such as a human being or furniture inside a building, of which the RCS is relatively small. Therefore, detecting a target behind a wall becomes more challenging and the challenges increase when the target is stationary. Furthermore, the target signal strength weakens when the target is closer to the wall. When the target is closer to the wall, the radar tends to see the target and the wall as a whole. In this scenario, a high-resolution radar system will be required, otherwise targets behind a wall will be obscured and sometimes totally invisible in the image formed.

In radar technology, the backscattering signal from an unwanted object is regarded as clutter [30], [36]. Therefore, a wall backscattering signal is regarded as clutter in the case of TWRI. Knowledge of this clutter is crucial because one wants to know how much a signal has to be attenuated while travelling through the wall. Thus, prior to applying the image formation method, wall reflections should be suppressed or considerably mitigated.

The surface and the composition of the wall can thus significantly influence the way the wave propagates in the TWRS system. It has been demonstrated that using different types of radar could mitigate the effects of the wall [13, 14], [37, 38]. The next section will review the different approaches used to mitigate wall interference.

2.3.3 Wall clutter mitigation

In this section, a review of frequently used approaches of mitigation found in the literature is introduced.

2.3.3.1 Linear inverse scattering algorithms in TWRI

The linear inverse scattering problem (LISP) is used in optic and radar systems to find the scatter electric properties from the backscattering EM wave.

Consider the backscattering EM wave $\beta(\omega)$, which is collected by the radar. In contrast, $k(\omega)$, the electric properties of the wall, are unknown. Both terms are dependent on frequency ω and position; the position has been omitted to simplify (2.29). The LISP has the objective to approximate the model that maps $\beta(\omega)$ to the $k(\omega)$ and to find the electric properties of the wall in the case of TWRI. In the form of an equation the problem is formulated as:

$$\beta(\omega) = G(\omega)k(\omega) + n \tag{2.29}$$

where $G(\omega)$ is a matrix that represents the model mapping the backscattering to the electric properties of the wall. n is the additive noise present in the system. Because the LISP infers the value of $k(\omega)$ from the knowledge of $\beta(\omega)$, this problem is known as an inverse problem. Thus, the LISP has been used in TWRI.

In TWRI, the LISP is used to find the wall characteristics while detecting a target behind the wall. To address the issue in real situations where the parameters of the wall are either unknown or known with some level of uncertainty, several approaches have been reported in [39], [30]. Though LISP can be used in TWRI with great accuracy, nonlinearity of the wall increases the data acquisition time [40], [35]. Therefore, a proposed linear inverse scattering algorithm based on the Born approximation [35] is used to mitigate the wall effect. In [40], to perform fast data acquisition, the authors proposed an efficient data acquisition and processing scheme based on 3-D TWRI.

In [36], a 2-D EM imaging technique for urban areas in multipath propagation was proposed. To mitigate the multipath effect in the TWRI, a linear inverse scattering approach based on the Kirchhoff approximation was combined with the finite-difference time domain (FDTD) method. To solve the Green's function and the incident field involved in the kernel of the linear integral equation, the authors applied the FDTD technique [36].

2.3.3.2 Diffraction tomographic algorithms for TWRI

Tomography is also an inverse scattering algorithm, which is used to characterise the media electric property for a wall in case of TWRI and for the ground in case of ground-

penetrating radar. Using the tomographic algorithms, the author distinguished between adults and children, seated and standing human beings [41].

In [41], a 3-D diffraction tomographic algorithm for real-time TWRI was proposed. This method was successful in detecting the presence of a target behind a wall.

On the other hand, [42] proposed to image buried targets under multi-layered media with a multi-frequency multi-monostatic measurement configuration. The author used the Born approximation to linearise the backscattering wave, then the Green's function and the Fourier transform to image the scene of interest. To increase the data processing time, the author in [42] proposed two techniques: (1) Coherent summation over all receiver locations in the linear inverse scattering algorithms, which offered simplicity over a non-linear solution, and (2) The reconstruction of all the pixels in the transverse plane at each down-range pixel with 2-D inverse fast Fourier transform using the diffraction tomography algorithm.

2.3.3.3 3-D TWRI

Though LISP is a successful imaging method, it is mainly applied in two dimensions. In addition, most of these algorithms deal with a single-layer homogeneous wall [43]. Under different wall-target scenarios it has been shown numerically that a 3-D or adaptive beam former can provide high-quality focused images [43].

In [43], using a SAR, the authors represent the backscattering signal from the scanning region as follows:

$$E_s(r_{rm}, r_{tm}, k_n) = \int G(r_{rm}, r, k_n)\, G(r, r_{tm}, k_n)\sigma(r)dr. \qquad (2.30)$$

The backscattering signal is represented by $E_s(r_{rm}, r_{tm}, k_n)$ received by the receiver at the $m-th$ position; the signal has been engendered by the transmitter at the $m-th$ position. $k_n$is the free space wavenumber of the $n-th$ operating frequency in the range of f_{min} to f_{max} having a frequency step of Δf. $G(r, r_{tm}, k_n)$ and $G(r_{rm}, r, k_n)$ are layered medium Green's functions, which model the wave propagation process from the transmitter to the target and from the target to the receiver. The model takes into consideration the presence of the wall. The entire model will not be complete without consideration of the target and range. Therefore $\sigma(r)$ is the reflectivity of the target; on the other hand, r with their respective indices are position vectors of the $m-th$ transmitter, receiver and target. The indices t and r represent the transmitter or the receiver.

Therefore, to solve (2.30), the Green's function is approximated. This is another inverse scattering algorithm.

It should be mentioned that though the 3-D TWRI has advantages over the LISP, it has been realised that the 3-D system requires much acquisition data time while using the SAR. Therefore, a 3-D image algorithm with a multiple input multiple output (MIMO) radar was proposed in [44, 45]. This technique is of importance, as it can be used in a real-time application. In [44], to compensate for the wall effect, Green's function was integrated into the MIMO through-the-wall beam former.

2.3.3.4 TWRI with unknown wall parameters

Efforts have been made to detect a target through the wall without knowledge of the electric parameters of the wall. If the wall effect is not taken into account, blurred images and ghost targets are obtained [46], [47], [48]. To address the issue of a target beyond an unknown wall or a wall with uncertain parameters, a two-step imaging procedure was proposed in [39]. The authors considered the backscattering field as a totally scattered field reflected by the wall and the obscured objects. In addition, in [39] LISP was used to estimate the thickness and the dielectric permittivity of the wall. To infer wall and target information from the knowledge of a far field incident wave, LISP was the preferred method. Therefore, using LISP, the entire problem was solved by means of a truncated singular value decomposition algorithm. The problem with this method is the assumption that the wall is homogeneous, while this is not a physical reality. Thus, further studies should be undertaken to consider more complex scenarios.

Therefore, an algorithm using a spectrum Green's function was proposed to autofocus the target behind an ambiguous wall [49]. After using the spectrum Green's function, a fast Fourier transform was used to reconstruct the image in a short computation time. In [49], the authors used time reversal imaging (TRI). The target displacement was explained, as the focusing time was unsuitably selected using TRI. To solve that issue, a time factor was added to the imaging formulation to deal with the difference in time arrival. Using this method, the authors could detect a target behind multiple walls in the right position.

The authors in [50] developed a matrix formulation so that they could investigate the diffuse scattering from a rough surface and inhomogeneous volume. They stated that the surface roughness caused an increase in diffuse scattering around the specular direction, even for cross-polarisation.

In addition, they found that the surface roughness caused a peak to appear in both the like and cross-scattering coefficients at near vertical incidence, as well as a decrease in these coefficients at large incidence angles, which occur in backscattering.

2.3.3.5 Compressive sensing for TWRI

Compressive sensing is a signal-processing method used to reconstruct a signal with less measurement or signal sample. Therefore, when this method is used in a radar system, the current consumption and the sampling time are less than when ordinary radar is used. Consequently, there is a trend among researchers to use this method in TWRI to increase the time acquisition.

Consider an ordinary radar collecting data. The data are in the form of an analogue signal. This analogue signal can be represented by a function $f(x)$. The signal $f(x)$ has to be digitised before further processing by the processor. Thus N is the number of samples to be used so that the signal $f(x)$ is digitised. It is known that a high value of N requires more processing memory and storage memory, therefore a large data pipe [51]. To diminish this complexity, a compressive sensing method was proposed in [52, 53, 54]. By using a compressive sensing method, one will be able to sample the same signal $f(x)$ with k number of samples, as in (2.31). While using $k \ll N$, care must be taken not to deteriorate the information in the signal.

$$N \gg k. \tag{2.31}$$

$$k.\emptyset = N. \tag{2.32}$$

To reconstruct the signal, k is multiplied by a random matrix $\emptyset$ as in (2.32). $\emptyset$ was chosen in accordance with the data that had to be collected.

TWRI, like most sensing systems, requires a tremendous amount of sampling, therefore a long data acquisition time. Using the sparsity method, one can sample the space of interest in the case of TWRI.

In order to circumvent the large amount of sampling and the long data acquisition time associated with TWRI, some authors proposed a compressive sensing method [51] - [53].

2.3.3.6 Layer stripping

The layer stripping (LS) method has been used extensively for years for media characterisation [55], [56], [57].

LS is a nonlinear method based on a scattering wave from the media. The dielectric media are reconstructed recursively in determining the dielectric properties of one layer at a time,

then removing the previously reconstructed layer to reconstruct the following one [58]. This method is very effective and finds application in TWRI and ground-penetrating radar systems [55] - [57].

The LS method is not limited to TWRI; it can also be applied to liquid-level measurement in tanks to evaluate the liquid permittivity and to estimate the liquid height of multiple layers of liquids inside the tank [59].

2.3.3.7 MIMO radar through-the-wall imaging

MIMO uses multiple wireless channels with a spatially distributed transmitter and receiver to send and receive a signal. MIMO increases signal reliability and increases the RCS owing to diversity on the angle of observation of the target.

In TWRI, because of the presence of the wall, clutter is experienced. To remove the clutter, different approaches have been proposed, based on human features characterised by the motion of heartbeat, breathing, etc. While observing a human behind a wall, a shadow effect of a human target, known as a ghost target, has been reported [60]. To overcome the ghost target effect, some authors have proposed MIMO [61], [62].

In [62] the author analysed the difference between targets and the shadow ghost using MIMO TWRI. The authors combined the coherent factor and non-causal coherent or non-coherent change detection to surmount the limitation of the change detection.

In [62], the author identified the first-order multipath (FOM) "ghosts" as the most effective interference sources, because they were lying inside the room being investigated. Because the FOM ghosts were in the same vicinity as the target, the power level of the FOM ghosts tended to be close to that of the target. A phase coherence factor technique was used to suppress the ghost target with MIMO.

Also, as explained in the 3-D TWRI subsection, when using an SAR, the time taken to acquire data is long [4]. Therefore, to decrease the acquisition time and cancel the smearing effect, an author proposed using MIMO [44]. By using MIMO radar, the author was able to detect the target behind multiple walls by using an algorithm based on Green's function.

In addition, the authors in [63] proposed three techniques for fast data acquisition and real-time processing through the wall. To decrease the acquisition time, their first technique was based on compressive sensing with a layered media Green's function incorporated. Besides short time acquisition, this technique offers the possibility to detect a target behind multiple walls. The second technique was a beamforming algorithm for through-the-wall

imaging using real-time data collection MIMO. The third one was a real-time processing algorithm for single and multiple walls.

The researcher reviewed different techniques and radar used in TWR in the above sections. In many cases, authors intend to detect human beings behind the wall, thus the next section is devoted to the detection of vital signs using radar.

2.4 INTERIOR STRUCTURE RECONSTRUCTION

A radar signal has the advantage of penetrating building material. For this reason, researchers use radar to reconstruct the interior of a structure. This has the objective of finding the wall layout by removing an obstruction while one does not have access to the building.

In [64], the authors presented an approach that can be used to estimate the backscattering of the dihedral and trihedral formed by the floor-wall and the ceiling-wall-floor respectively. To retrieve the dihedral and trihedral backscattering the paper also uses, as in [37], [39] and [34], the decomposition method. The decomposition method expresses the overall backscattering return in singular components.

The authors in [65] simulate a building using the floor-wall and floor-wall-ceiling as simple scattering mechanisms. They make the same assumption as in [64], that a building is commonly formed of a dihedral and trihedral. Here the authors also use the decomposition algorithm. The authors consider that the data collected are represented as:

$$s(k,\theta,\emptyset) = \sum_{n} s_n g_n(k,\theta,\emptyset). \tag{2.33}$$

with

$$s_n = \iint s(k,\emptyset) g_n(k,\emptyset) df\ d\theta\ d\emptyset. \tag{2.34}$$

$s(k,\theta,\emptyset)$ being the backscattering signal; it is frequency- and angle-dependent. $g_n(k,\theta,\emptyset)$ is an element of the scattering basis set. It is known that buildings generally have canonical shapes as corners (floor-wall and ceiling-wall-floor). These corners exhibit a high backscattering signal. The high backscattering signal is then used as main signal return while decomposing the received signal. In the signal decomposition algorithm, an assumption was made in accordance with the backscattering signal strength. Thus, while imaging the building, all high backscattering signals were assumed to be coming from the building corner. Knowing that, the authors could reconstruct the image of the building.

2.5 RESEARCH GAP IN THROUGH-THE-WALL RADAR IMAGING

Despite much research in the area of TWRI, there are still unsolved problems, thus further research is required into the following aspects:

2.5.1 Detectability of the human being

The micro-Doppler effect is the main phenomenon used to search for and rescue humans buried under rubble after a building has collapsed or an earthquake. To detect the presence of a target (human being), an EM wave is emitted in the direction of interest. The target is illuminated by the EM wave, then the target scatters back a modulated wave in the direction of the radar. The movement of the breathing and heartbeat of the human target modulate the backscattering wave. However, there are still questions that have not been addressed. One can consider that after an earthquake, a human victim may be weak. Thus, the breathing and heartbeat signals of the trapped victim may be too weak to be detected by the radar. One approach might be taking recourse to highly sensitive TWRS systems. Highly sensitive TWRS systems allow the detection of a weak response from the target.

After reviewing the body of knowledge, one notices that most of the research done in this area regards victims as adult human beings, which is not always true in case of disaster. This can be observed after an earthquake or if a building collapses; people of different ages may be trapped under the rubble, including children. Research has demonstrated that there is significant variation in the heartbeat, depending on the age of a person [66]. In addition, the RCS of a child's chest is lower than that of an adult victim. This can influence the return signal in certain ways.

As mentioned in Chapter 1, in South Africa three gold miners were trapped and died underground. The detectability of a human being who is buried alive is an important research area. In this case one has to consider that the soil contains some metal in its primitive state. Because of this, the dielectric properties may be close to a perfect conductor. This is one of the gaps in the body of knowledge requiring further research.

In addition to the above issues, radar resolution requires more study in order to have high-resolution radar. It has been reported that it is difficult to detect human beings while they are standing against a wall. This is due to the radar range resolution.

2.5.2 Wall modelling

The lack of a well-designed wall model remains a huge challenge in this area. Researchers have considered knowledge of the wall parameters or the first return signal coming from the wall. An effective wall model has to take into consideration the state of the wall. Since humidity and the frequency band used can have a significant influence on the transmitted signal, one should take into consideration the time of the year in which this system can be used effectively. Researchers could consider investigating humid and dynamic conditions as well, rather than only dry walls.

2.5.3 Target differentiation

TWRI has been used successfully to detect human beings inside buildings. However, a new technique has to be investigated when the scene of interest contains more than one target. In a scenario where there are hostages and terrorists in the same building, rescuers need to be able to distinguish effectively between the two targets. Thus, new techniques have to be applied to the activities of hostages and terrorists.

2.5.4 Summary of literature related to this research

To summarise the research conducted in TWRI, two tables have been presented. The first one summarises the research conducted in through-the-wall imaging in general without considering any aspect of the method used to collect data and the type of target; this is presented in Table A-1 in appendix A. The second table presents TWRI of previous work that used the micro-Doppler technique. These tables give a concise idea of the state of the knowledge in the area where the current research is performed. The first column contains the references to the papers that have been summarised in the table. The second column presents the journal name in which the paper has been published. The third column presents the journal impact factor at the time of referencing the work. The fourth column presents the frequency band of interest, namely the frequency used by the authors to run their experiment or their simulation. Finally, the last column summarises the contribution to the body of knowledge of each paper.

Table A-2 in appendix A presents a narrowed summary of research on TWRI using the micro-Doppler technique to detect activity inside a room. From the first column to the third column present the same items as in Table A-1. The fourth column presents the algorithm used in different papers to detect mobile objects. Then finally, each paper is summarised.

2.6 CONCLUDING REMARKS

TWRI is an essential area of research that helps rescuers, police and the military in their daily tasks. To date many sensing approaches have been adopted to image the scene of interest, assuming that the dielectric characteristics of the wall are known. This is impractical because rescuers or police do not know the type and state of the wall that they will find in the field. This presents researchers with opportunities to examine the forming of images through the dispersive medium of walls. Thus, without knowledge of the properties of the wall, some other approaches have been reviewed in this thesis. There is an urgent need to model walls in TWRI systems while decreasing the acquisition time to remove the uncertainty of unknown wall dielectric parameters.

TWRI systems require further study to bridge the gap in knowledge about the detectability of a target lying against a wall. This is very important in the rescue and police scenario. In the case of a rescue operation, when a building collapses, a human being could be lying against a wall. In a police scenario, a terrorist could be hiding against a wall. In both scenarios failure to sense the human being could cost lives.

An accurate algorithm is needed to eliminate or mitigate ghost target issues. Miss-imaging a target location affects both rescue and police applications. While in a rescue operation one might dig where there are no victims, in police intervention a terrorist could be confused with a hostage. Care must be taken to mitigate this effect.

In this research, the detection of humans with different chest RCSs is investigated. Because the researcher was unable to change the chest RCS in practice, a simulation was introduced in which the height of the human was changed. To simulate from a large chest RCS to a lower one, a simulation of human beings from a height considered normal for an adult down to one considered normal for a child of two years old was performed in MATLAB to study the difference in RCS. In addition, the signal was propagated through different home appliances to determine how it was affected by appliances.

CHAPTER 3 RESEARCH METHODOLOGY

3.1 CHAPTER OVERVIEW

Chapter 2 presented an in-depth review of TWR, starting with a general review on radar. It was discussed in connection with vital detection of a human being. A review was done of detecting a human being without obstruction and through an opaque medium. Thereafter, different methods of clutter mitigation were reviewed. The main methods to mitigate clutter are linear inverse scattering algorithms in TWRI, diffraction tomographic algorithms for TWRI, 3-D TWRI, TWRI with unknown wall parameters, compressive sensing for TWR, LS and MIMO radar TWI. These different methods all have pros and cons. Finally, different gaps persisting in the body of knowledge were mentioned.

In section 1.5 an outline of the proposed research hypothesis is given with reference to Figure 1.1. This chapter is intended to expand the research methodology to be followed in this thesis.

The process that was selected entails simulation. Through the simulation the researcher conducted experiments that were impossible to conduct with the radar that was built. In the simulation the experiment is conducted in the frequency band from 500 MHz up to 10 GHz. The frequency band to be used has been justified by the limitation of the hardware frequency band. The radar that was built covers the frequency from 2257.4 to 2591.8 Hz, which is an unlicensed frequency band. In the literature, it has been mentioned that the frequency below 3 GHz is preferred in this type of application. To avoid using licensed frequency and to explore the availability of different components, the frequency band of 2257.4 to 2591.8 Hz was chosen for the radar that was built. As the researcher wished to investigate the behaviour of the radar at different frequencies, it was decided to start from a frequency as low as 5000 MHz to 25 GHz. Therefore, the behaviour of the radar in the zone with less attenuation and with high attenuation was investigated.

3.2 JUSTIFICATION OF THE RESEARCH METHODOLOGY

To conduct this work, a literature review was undertaken in Chapter 2. In this chapter approaches taken by different researchers are presented. General knowledge on radar is reviewed.

Three main methods have been studied, namely through-the-wall compressive sensing, through-the-wall sensing using micro-Doppler radar and finally through-the-wall sensing using MIMO radar.

Using a compressive sensing method in the present case can be of benefit to this research in terms of acquisition time. However, as the method requires some knowledge of the signal that has to be processed, it proved inadequate for the current research. When using the compressive sensing method, one will need to have a priori knowledge of the human being behind the wall. If a supplementary tool is not used, a strong algorithm based on the actual application has to be used. Because of lack of adequate tools to indicate the position of the human being behind the wall, the method has been classified as non-feasible.

On the other hand, MIMO radar is a method that makes use of multiple receivers and transmitters. This method fits well in a system where the dielectric properties of the wall are unknown and have to be characterised, but because of the budget at the researcher's disposal, the method was classified as non-feasible.

Lastly, through-the-wall sensing using micro-Doppler radar has been chosen for use in this research. It is a monostatic radar, which is cost-effective to build compared to MIMO radar and radar using compressive sensing signal processing. Because the radar is mobile, one can detect the target without knowing the wall properties. This is one of the advantages of this method. Besides that, the research was aimed at detecting a target that has less mobility or emits weak vibration.

Thus, the rest of this chapter is devoted to the Doppler effect in general, but more specifically to the micro-Doppler effect in radar sensing.

3.3 DESCRIPTION OF METHODS OF ANALYSIS

To conduct this research, different simulations have been run, taking into consideration different human heights. The simulations were conducted with transmit radar frequencies of 2.4 GHz and 15 GHz as centre frequency. The transmit frequency was kept at 2.4 GHz, then 15 GHz, while varying the height of the human and the velocity. The velocities used for this simulation were from 0.5 to 3 m/sec, with a step of 0.5 m/sec each time. The maximum speed of 3 m/sec was justified by the fact that the possibility of finding a human running in the building was very low. On the other hand, the height varied because the researcher considered that people of different ages might be found inside a building.

Considering that a human being with a height of 1 m can walk, 1 m was chosen as the starting height because below that height a human being may not be able to walk [102]. From an initial height of 1 m the researcher considered an additional 30 cm as reasonable to give the difference in the spectrum return signal. Therefore, 1 m, 1.3 m, 1.6 m and 1.9 m were retained as simulation test height; 1.9 m was taken as the upper limit, because it is rare to find people taller than 1.9 m. Finally, the radar is located at position (X=10 m, Y=0 m, Z=2 m) in a 3-D system, while the human is located at the origin of the body fixed system (X=0 m, Y=0 m, Z=0 m) for the simulation.

In addition to the simulation, a radar was built with the following module:

a. A ramp generator
b. A voltage-controlled oscillator (VCO)
c. An attenuator
d. A PA
e. A power divider (PD)
f. A transmit antenna.

The receiving branch is constituted of:

a. A receiving antenna
b. A mixer
c. A low-noise amplifier (LNA)
d. A filter
e. An analogue-to-digital converter (ADC).

3.4 DELIMITATIONS OF RESEARCH

Radar technology is a vast area of research, therefore delimitation of the research subject is necessary. A few areas where radars are used are civil aviation, military aviation and meteorology. The target under investigation in this thesis was human limb movement in the through-the-wall the scenario. Thus, knowing the application for which the radar has to be used is one among many elements that can make radar work better in one application than in another. In addition, knowledge of the target predetermined the type of radar and the power transmission that can be used for this application.

Furthermore, what may be a target in one application might be clutter in another application in radar application. For this application, the objective was to detect the human rate of limb change. The rest of the return signal was considered noise. This implies that in

the home environment the clutter is the wall, appliances and different objects that may be found in the house.

For the sake of this investigation, the researcher investigated the through-the-wall environment. TWR is a low-transmission power radar compared to radar used for air traffic. The transmission power has to be kept low because the signal has to travel through human tissue, which cannot be exposed to higher RF energy. Thus, taking into consideration the power transmission, a practical choice has been made of the FMCW radar as sensor with a lower RF PA wattage of 13 dBm. In addition to power transmission, FMCW is cost-effective compared to pulse radar, which requires a high wattage PA. FMCW radar is used as sensor to detect human activities inside a room in the simulation.

Most research conducted in the TWR considers that the target behind the wall is an adult man or woman whose height is above a certain limit. To the best of the author's knowledge, no research reported in literature has considered different heights of targets behind the wall. This research has been performed in MATLAB with different targets having different heights. The lower height is considered in this thesis as children, while the higher height is considered as adults. Thus, this research devoted effort to investigating the return signal ranging from children to adults in the simulation environment.

Practical experiments have been conducted in a laboratory environment at the University of Johannesburg and the author's residence, both in South Africa. In addition to the clutter, a fan was carefully considered as the main source of continuous mobility in a warm region, particularly in the home environment. Therefore, a fan has been modelled in MATLAB to analyse the return signal embedded with micro-Doppler.

The next section demonstrates how the data were analysed.

3.5 INTRODUCTION TO MICRO-DOPPLER

Christian Doppler was an Austrian mathematician and physicist. In 1842, he published a paper on the phenomenon of the coloured light effect of stars through the Royal Bohemian Society of the Sciences in Prague [88]. This phenomenon later became known as the Doppler effect or Doppler shift. The paper demonstrated that when observing the frequency of a sound or light wave, this is dependent on the speed of the wave's source relative to the observer. Thus, one can determine the speed of an object by analysing the return wave that illuminates the object. In this thesis, detecting a target behind a wall using the Doppler effect is the objective. Therefore, this chapter is devoted to the micro-Doppler effect generated by micro-motion.

3.6 THE MICRO-DOPPLER SIGNATURE

In a radar system, a target signature comprises the kinematic properties that differentiate a target from other targets. The target signature helps to differentiate targets in an environment where there are many targets. To be able to differentiate between two signatures, the micro-Doppler effect can be used. By using a Doppler radar, a small variation in the frequency induced by motion can be detected. Studies have shown that by using radar, one can differentiate between animals and human beings [89].

3.6.1 Micro-motion

Using the Doppler effect, one can detect the target only if it is in motion. It has to be specified that when a target is in motion and some part of the target is vibrating or moving, this will cause a frequency shift about the main Doppler frequency shift. Such a frequency shift is known as a micro-Doppler frequency. Micro-motion is a source of micro-Doppler frequency. Thus, analysis of micro-motion is necessary in order to infer the micro-Doppler frequency.

3.6.2 Rigid body motion

In studying body motion, it is important to know the type of body in motion, which could be non-rigid or rigid. A non-rigid body is deformable. The distance between two particles in a non-rigid body can vary when the body is in motion. On the other hand, a rigid body is a non-deformable body with a finite size [90]. In the rigid body the distance between two particles does not change when the body is in motion. A rigid body is a body of mass M constituted from the sum of particles of mass m_i. Thus, a rigid body can be defined as follows: $M = \sum m_i$.

In Figure 3.1, a descriptive illustration of the two coordinate systems and the body in motion is presented. To represent a body in motion in space, two coordinate systems are usually used, as in Figure 3.1.

The first coordinate is known as the global or space-fixed system (X, Y, Z). The second coordinate is known as the local or body-fixed system (x, y, z). The radar is placed at the origin of the global system, while the cylinder is placed at the origin of the local system. On the cylinder, a point P is placed in order to illustrate the motion of the body.

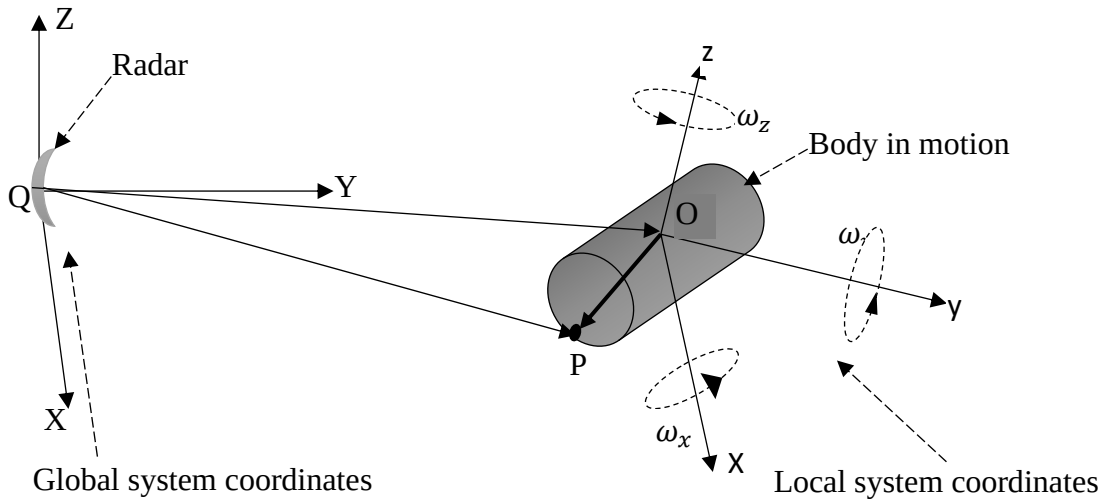

Figure 3.1: Global and local system coordinates with a body in motion.

In Figure 3.1, the first global coordinate is fixed to the space, meaning it does not change in relation to the space of observation. On the other hand, the local system changes in relation to space when there is motion, but not in regard to the body in motion. Therefore, a radar is placed at the origin of the global system coordinate. The body is placed at the origin of the local system. The body is fixed to the same coordinate. The local system coordinate is considered the centre of mass of the body. If the axis of the local system is not parallel to the axis of the global system, three independent angles can be introduced relative to the global system.

Consider a particle *P* at position *P* in the local system, belonging to the body in motion. To localise the same point in the global system, a vectoral sum is used as follows:

$$\overrightarrow{QP} = \overrightarrow{QO} + \overrightarrow{OP}. \tag{3.1}$$

Consider $\overrightarrow{QP} = r_{QP}$, $\overrightarrow{QO} = r_{QO}$ and $\overrightarrow{OP} = r_{OP}$ for easy reading of reference.

It is known that the velocity is the rate of change of a position with respect to time. Thus, the following equation determines the velocity:

$$\frac{d(r_{QP})}{dt} = \frac{d(r_{QO})}{dt} + \frac{d(r_{OP})}{dt}. \tag{3.2}$$

Equation (3.2) can be rewritten as follows:

$$v = V + \Omega \times r_{OP}. \tag{3.3}$$

V is considered the translation velocity of the centre of mass of the body, while Ω is the angular velocity of the body rotation. Therefore, it has been demonstrated that the body motion is a combination of translation and rotation movement.

To be able to represent the orientation of any object in space, quaternions, Euler angles and rotation matrices are frequently used.

3.6.2.1 Euler angles

Leonhard Euler introduced three angles known as Euler angles to describe a general rotation in space. The Euler angles describe an orientation of a rigid body with reference to fixed system coordinates.

Figure 3.2 represents three different steps that an object realises when in motion. Figure 3.2 a represents the initial position of the coordinate, progressing to Figure 3.2 b and finally Figure 3.2 c. The dashed axes are obtained after rotation about the z-axis. The dashed-dot axes are obtained after rotation about the new x-axis in the dashed line. The bold axes are obtained after the rotation of axes about the new z-axis in the dashed-dot line.

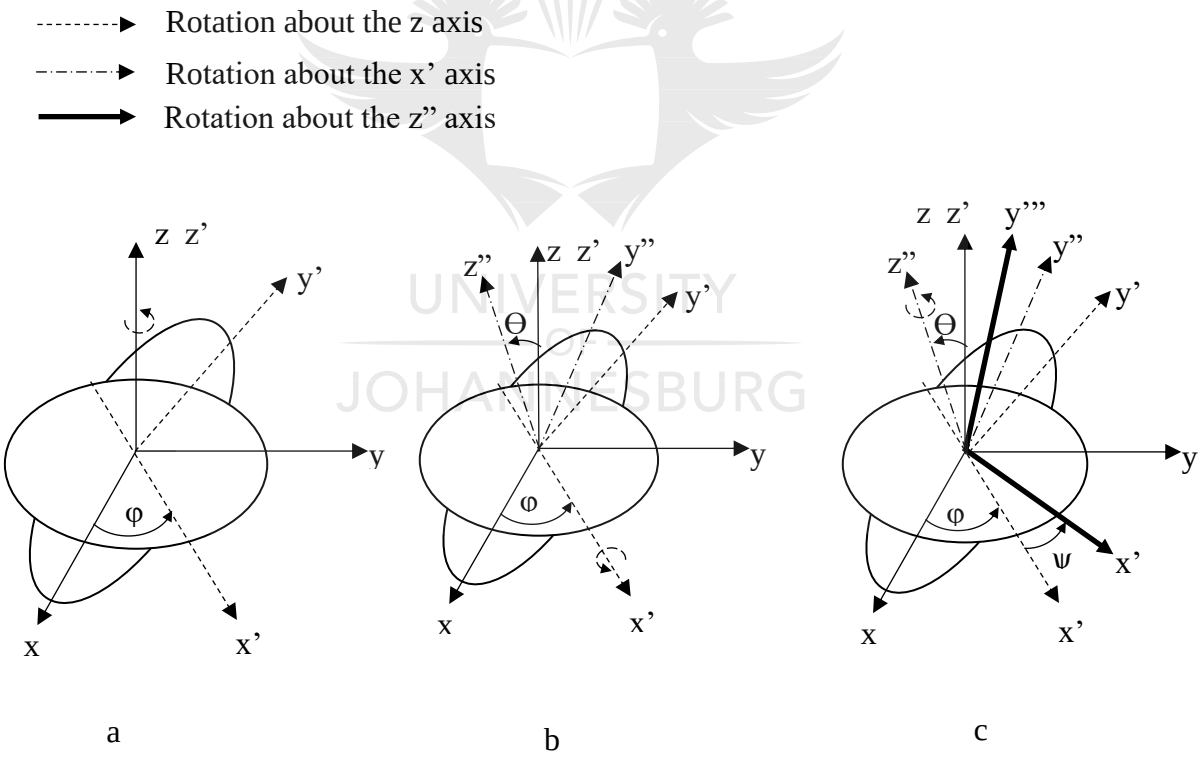

Figure 3.2: Euler angles.

In Figure 3.2 three successive rotations have been depicted to illustrate how an Euler angle works. The first rotation is about the *z-axis*, which yields an angle φ. This is depicted by the dashed axis in the figure. The second rotation is about the *x-axis*, yielding an angle of

θ. This is depicted by the dashed-dot axis in Figure 3.2.b. The last rotation about the new z'' yields an angle of φ. This is depicted by the bold axis in Figure 3.2.c. The aforementioned angles (φ, θ, ψ) are known as Euler angles. The rotations are counter-clockwise. The sequence of rotation has to be followed, as the matrix multiplication is not commutative.

Thus, there are 12 different sequences to represent an orientation while using Euler angles. The following are the sequences: $x-y-z$, $x-z-y$, $x-y-x$, $x-z-x$, $y-x-z$, $y-z-x$, $y-x-y$, $y-z-y$, $z-x-y$, $z-y-x$, $z-x-z$ and finally, $z-y-z$. For the case presented in Figure 3.2, one can see that the sequence $z-x-z$ is used.

Sometimes these rotations are specified in terms of roll-pitch-yaw as an $x-y-z$ sequence and in terms of the angles $(\psi-\phi-\varphi)$. Therefore, the rotation matrix is an important tool for computing rigid body rotation. Three elementary rotation angles are sufficient to find the orientation and the rotation of any rigid body. To rotate a rigid body using the roll-pitch-yaw, one has to rotate the body about the x axis as $x = [1 \quad 0 \quad 0]^T$ by an angle ψ, which is defined by the elementary rotation matrix:

$$\mathcal{R}_x = \begin{bmatrix} 1 & 0 & 0 \\ 0 & cos\psi & sin\psi \\ 0 & -sin\psi & cos\psi \end{bmatrix}. \tag{3.4}$$

A new y axis is yielded after the rotation $\mathcal{R}_x$. The rotation will be effectuated about this new axis $y = [0 \quad cos\psi \quad sin\psi]^T$ by an angle θ, which is defined by the elementary rotation matrix:

$$\mathcal{R}_y = \begin{bmatrix} cos\theta & 0 & -sin\theta \\ 0 & 1 & 0 \\ sin\theta & 0 & cos\theta \end{bmatrix}. \tag{3.5}$$

A new z axis is yielded after the rotation $\mathcal{R}_y$. The rotation will be effectuated about this new axis $z = [-sin\theta \quad cos\theta sin\psi \quad cos\theta cos\psi]^T$ by an angle of φ, which is defined by the elementary rotation matrix:

$$\mathcal{R}_z = \begin{bmatrix} cos\varphi & sin\varphi & 0 \\ -sin\varphi & cos\varphi & 0 \\ 0 & 0 & 1 \end{bmatrix}. \tag{3.6}$$

Therefore, the rotation matrix of the roll-pitch-yaw sequence is represented as follows:

$$\mathcal{R}_{x-y-z} = \mathcal{R}_z \cdot \mathcal{R}_y \cdot \mathcal{R}_x = \begin{bmatrix} r_{11} & r_{12} & r_{13} \\ r_{21} & r_{22} & r_{23} \\ r_{31} & r_{32} & r_{33} \end{bmatrix}. \tag{3.7}$$

The components of the rotation matrix are as follows:

$$r_{11} = \cos\theta \cos\varphi, \tag{3.8}$$

$$r_{12} = \sin\psi \sin\theta \cos\varphi + \cos\psi \sin\varphi, \tag{3.9}$$

$$r_{13} = -\cos\psi \sin\theta \cos\varphi + \sin\psi \sin\varphi, \tag{3.10}$$

$$r_{21} = -\cos\theta \sin\varphi, \tag{3.11}$$

$$r_{22} = -\sin\psi \sin\theta \sin\varphi + \cos\psi \cos\varphi, \tag{3.12}$$

$$r_{23} = \cos\psi \sin\theta \sin\varphi + \sin\psi \cos\varphi, \tag{3.13}$$

$$r_{31} = \sin\theta, \tag{3.14}$$

$$r_{32} = -\sin\psi \cos\theta, \tag{3.15}$$

and

$$r_{33} = \cos\psi \cos\theta. \tag{3.16}$$

Thus, for any sequence rotation matrix one can find the general rotation matrix derived from the elementary rotation matrix.

Though the Euler angles can represent any type of orientation of a rigid body, the main related issue is known as a gimbal lock. The gimbal lock is a situation when two axes are in the same plane. In this case one cannot perform any rotation about the axis in the same plane. To eliminate the gimbal lock, using quaternion algebra instead of Euler angles, rotation matrices is a solution. The quaternion is introduced in the next section to overcome the gimbal lock problem.

3.6.2.2 Quaternion

In 1843, while looking for a way to construct a theory of triplets that would be relevant to the study of 3-D geometry, William Rowan Hamilton discovered quaternions [91]. He was trying to find an analogy with the couplets of a complex number.

Quaternions, as per their prefix, quarter meaning four, comprise a system having four-dimensional vectors in the set, $\mathbb{R}^4$. The four-dimensional vectors are the following: α is the scalar and first element in the coordinate, then x, y and z are coordinates as imaginary parts. The four-dimensional vectors are used to represent a 3-D orientation. Therefore in 3-D, a vector can be represented as (α, x, y, z) from the origin of the axis. A point P having (x, y, z) coordinates is represented as follows: $P = x \cdot i + y \cdot j + z \cdot k$ in 3-D, if P is rotating through an angle α about a unit vector $s = a \cdot i + b \cdot j + c \cdot k$. The unit vector has the following components: (a, b, c). The rotation yields another point, which is found from the following transformation formula:

$$P' = qPq^{-1}, \tag{3.17}$$

with $q = e^{\frac{\alpha}{2}(ai+aj+ck)} = cos\frac{\alpha}{2} + (ai + bj + ck)sin\frac{\alpha}{2}$. q is the quaternion vector representing the unit vector s and q^{-1} is the conjugate of q. Thus, the translation can be represented by (3.18):

$$P' = q + P\ . \tag{3.18}$$

One can see that the case presented above is a special case of quaternion because the real part is considered equal to zero. Therefore, the quaternion represents a point in 3-D. Quaternion vectors are not communicative in multiplication. The order of multiplication must be maintained.

Thus, using the quaternion method is very useful to determine the orientation of an object in space. In this thesis, as one is dealing with a human body moving behind a wall, introducing such a concept is crucial for the simulation.

3.6.3 Non-rigid body

In contrast to a rigid body, a non-rigid body is deformable. The distance between two particles inside the body can vary when a force is acting on it. Modelling a non-rigid body is a complex exercise, which requires a high level of computation [85]. For that reason, a non-rigid body is modelled as a combination of rigid body segments connected through joints. Therefore, a body as a walking man is modelled as a rigid body connected through joints. In the rest of this work a human being will be modelled as several rigid bodies connected through joints. The rigid body motion is treated as a segment of the non-rigid body. This type of non-rigid body is known as a multibody system in mechanics.

3.6.4 Backscattering electromagnetics from body in motion

For several years it has been known that when an EM wave impinges on an object, this reradiates the EM wave in all directions. The reradiation is known as an RCS when calculated at a specific angle. The reradiated field of the object is computed with the assumption that the target is immobile. However, in the real world, immobile bodies are rarely found. Thus, all moving or oscillating objects will yield different reradiation. In other words, a moving target produces different scattering and RCS.

Finding the scattering EM wave from a moving target is a subject of great interest among scientist. It has been studied theoretically and practically [92, 93, 94, 95, 96]. Sideband

frequencies about the Doppler frequency induced by the translation are observed when the target oscillates linearly and periodically together with the translation movement.

One can derive a far field of a moving target by using the following equation [97]:

$$E_T(r) = exp\{j\ k\ r_i\ \cdot (u_k - u_r)\}E(r)\ . \qquad (3.19)$$

$k = 2\pi/\lambda$ is the wave number, with the unit vector of the incident wave as u_k, the direction of the observation unit vector as u_r, and $E(r)$ as the far electric field incident on the target before moving.

Figure 3.3 depicts a human being moving from an initial point to a final point in space. The radar is placed at the origin of the global coordinate observing the human motion. The distance between the radar and the human is regarded as r before the motion starts and r_f when the final position is reached. The path that the human goes through has a distance r_i. The local coordinate is considered fixed in reference to the human being.

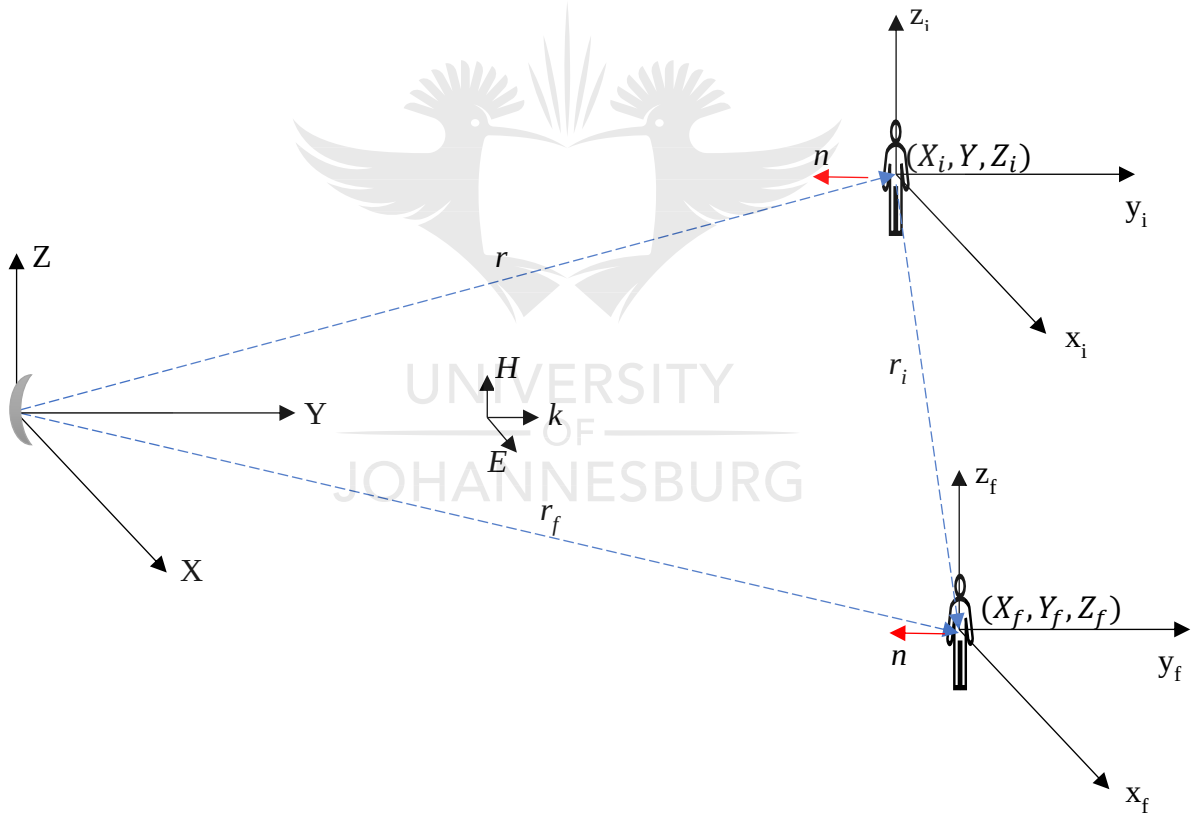

Figure 3.3: Translation movement.

In Figure 3.3, consider a human being standing at position $r = (X_i, Y_i, Z_i)$ in the space-fixed coordinates (X, Y, Z). If one considers the human as one body moving from (X_i, Y_i, Z_i) to a final position (X_f, Y_f, Z_f) in the space-fixed coordinates (X, Y, Z), this movement is a translation because the human is moving from one point to another. The translation vector is found with the following equation: $r_i = r + r_f$. Here r is the distance

vector from the radar to the human before moving. Furthermore, r_f is the final position of the human after translation.

Observing Figure 3.3 while applying (3.9), one can see that the only parameter that will change is the phase term $exp\{j\,k\,r_0\cdot(u_k-u_r)\}$. Because there is movement, the translation is a function of time. Thus, $r_i = r_i(t) = r_i(t)u_T$, having u_T as a unit vector of the translation. After translation, (3.19) becomes:

$$E_T(r) = exp\{j\,k\,r_i(t)u_T\cdot(u_k-u_r)\}E(r). \tag{3.20}$$

In the current case the radar that is used is based on monostatic radar. This set-up influences (3.20), where $u_k = u_r$, thus the phase factor is:

$$exp\{j\varphi(t)\} = exp\{j\,k\,r_i(t)u_T\cdot u_k)\}. \tag{3.21}$$

Thus, when the radar is transmitting an EM wave at frequency f_0, the received signal is expressed as follows:

$$s(t) = exp\{j\,k\,r_i(t)\cdot(u_k-u_r) - j2\pi f_0 t\}|E(r)|. \tag{3.22}$$

The phase factor of (3.22) represents the modulation of the micro-Doppler effect induced by the time-varying motion $r_i(t)$. This phase factor is important for this study, as it is the main factor that will have to be extracted in this thesis. This factor is a function of movement. If the target is vibrating, one can represent the signal as sinusoidal in the form of $r_i(t) = A_i\cos\omega t$ with A_i the reflective coefficient of the target and ω the angular frequency.

3.7 MATHEMATICAL CALCULATION OF THE MICRO-DOPPLER EFFECT

To be able to analyse the micro-Doppler spectrogram, mathematical expressions are necessary to clarify the phenomenon. Mechanical vibration or rotation of structures in a target analysis has been introduced in a detailed manner in [98]. In a radar area, a target is very often represented as a set of point scatterers [99]. Using point scatterers is a way to model a target in a simulation environment; it does not have any impact on the micro-Doppler spectrograms of the target.

Figure 3.4 is introduced in this subsection to explain the micro-Doppler effect. In this figure, a cylinder translating and rotating is observed. The radar is placed at the origin of the global system, while the antennas point towards the cylinder. From $t = 0$ to $t = 1$ the cylinder performs translation and rotation. The translation and rotation are studied to explain the micro-Doppler effect in a body in motion.

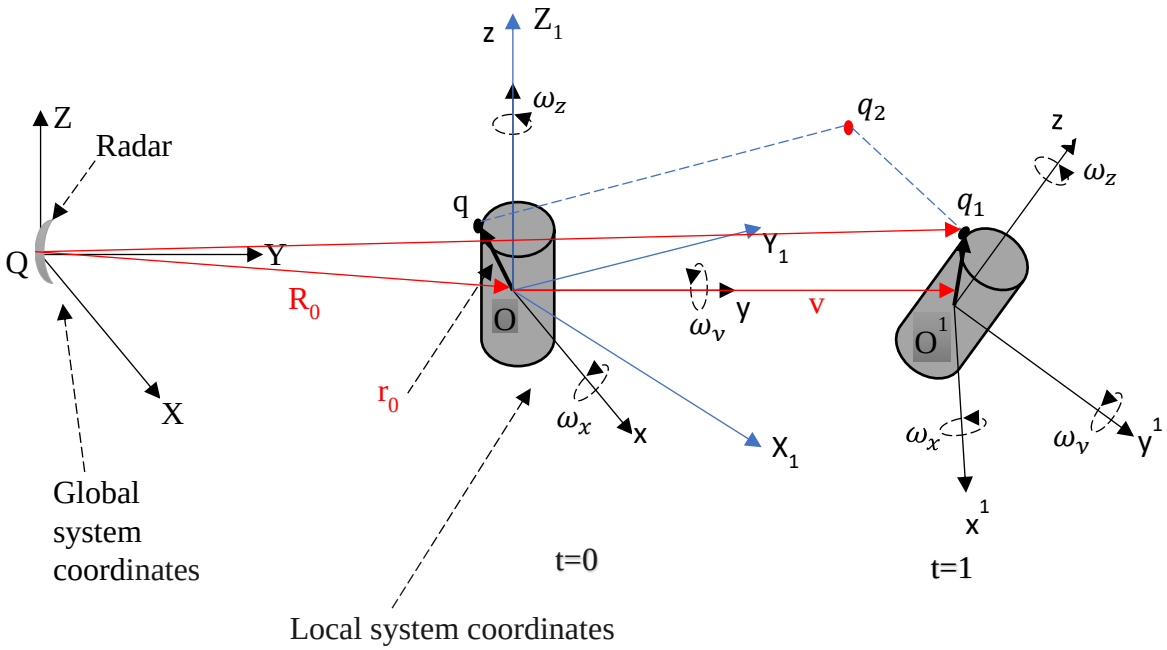

Figure 3.4: Rotation motion.

In Figure 3.4, a target in a local system coordinate (x, y, z) attached to the same target is illustrated. The radar is situated in the global system coordinate (X, Y, Z) and at the origin Q of the same coordinate. It is considered that the radar is stationary at origin Q. The target has a translation and rotation movement with respect to the global system coordinate. Another reference system coordinate (X_1, Y_1, Z_1) is introduced to observe the rotation of the target. The reference coordinate has the same origin as the local system coordinate and has the same translation as the target, but not the same rotation in respect of the global system coordinate. The distance from the origin of the reference system to the radar is R_0. The next subsection will introduce the extraction of a micro-Doppler induced by a target.

3.7.1 MICRO-DOPPLER EXTRACTION

As shown in Figure 3.4, the target has a translation with a velocity v with respect to the radar system coordinate. In addition, the target has a rotation velocity ω, which is dependent on the individual axis coordinate velocity $(\omega_x, \omega_y, \omega_z)$ in the target coordinate. The rotation velocity can be represented in the reference system coordinate as $\omega = (\omega_{X_1}, \omega_{X_1}, \omega_{X_1})^T$ or in the target system coordinate as $\omega = (\omega_x, \omega_y, \omega_z)^T$. A point scatterer q on the target at the time $t = 0$ translates from q to q_2 with a velocity v. The translation space covered by the target after the time t is found to be

$$OO^1 = vt. \tag{3.23}$$

Thereafter, the same point scatterer moves from point q_2 to q_1. The movement from point q_2 to q_1 is a rotary movement with an angular velocity ω. Observing the movement of the point q in the reference system coordinate, q is located at $r_0 = (X_0, Y_0, Z_0)^T$, then the rotation from q_2 to q_1 is described by a rotation matrix $\mathcal{R}_t$. Thus, the point scatterer will find itself at position:

$$r = O^1 q_1 = \mathcal{R}_t(O^1 q_2) = \mathcal{R}_t r_0. \tag{3.24}$$

From Q to q_1 is the final range in which the radar will observe the scatterer point after translation and rotation. This can be found vectorially as follows:

$$Qq_1 = QO + OO^1 + O^1 q_1. \tag{3.25}$$

It is known that

$$R_0 = QO\,. \tag{3.26}$$

By substituting (3.13), (3.16) and (3.14) into (3.15), the following equation will be obtained:

$$Qq_1 = R_0 + vt + \mathcal{R}_t r_0. \tag{3.27}$$

Then finally the range becomes:

$$r(t) = \|R_0 + vt + \mathcal{R}_t r_0\| \tag{3.28}$$

where $\|\cdot\|$ represents the Euclidean norm.

Suppose that the radar transmits a sinusoidal waveform having a carrier frequency f; the signal return from the point scatterer as a baseband becomes a function of $r(t)$. This signal is represented as follows [98]:

$$s(t) = \rho(x,y,z)exp\left[j2\pi f\,\frac{2r(t)}{c}\right] = \rho(x,y,z)exp\{j\Phi[r(t)]\}\,, \tag{3.29}$$

where $\rho(x,y,z)$ is the reflectivity of the point scatterer q, which is a function of the target system coordinates (x,y,z).

Here c is the speed of the EM wave that the radar transmits, and $\Phi(r)$ is the phase of the baseband of the receiving signal,

$$\Phi(r) = 2\pi f\,\frac{2r(t)}{c}. \tag{3.30}$$

To obtain the instantaneous frequency, one has to find the derivative of the phase of the baseband signal. The instantaneous frequency will reveal the Doppler frequency shift induced by the target's motion:

$$f_d = \frac{1}{2\pi}\,\frac{d\Phi(t)}{dt}\,. \tag{3.31}$$

Then substituting (3.30) in (3.31) yields:

$$f_d = \frac{2f}{c}\,\frac{dr(t)}{dt}\,. \tag{3.32}$$

Substituting (3.18) in (3.22) yields:

$$f_d = \frac{2f}{c}\,\frac{1}{2r(t)}\,\frac{d[(R_0 + vt + \mathcal{R}_t r_0\,)^T(R_0 + vt + \mathcal{R}_t r_0\,)]}{dt}, \tag{3.33}$$

$$f_d = \frac{2f}{c}\left[v + \frac{d(\mathcal{R}_t r_0)}{dt}\right]^T n\,, \tag{3.34}$$

with:

$$n = \frac{R_0 + vt + \mathcal{R}_t r_0}{\|R_0 + vt + \mathcal{R}_t r_0\|}, \tag{3.35}$$

as the unit vector of Qq_1.

Equation (3.8) can be written as (3.37), considering that the angular velocity vector is described as $\omega = (\omega_{X_1}, \omega_{Y_1}, \omega_{Z_1})^T$ in the reference coordinate Figure 3.4. The time interval may be considered infinitesimal when a high PRF and a low angular velocity are used. Consider

$$\mathcal{R}_t = exp(\widehat{\omega}t), \tag{3.36}$$

where $\widehat{\omega}$ is the skew symmetric matrix, which is associated with ω. Therefore (3.34) can be written as:

$$f_d = \frac{2f}{c}\left[v + \frac{d(e^{\widehat{\omega}t} r_0)}{dt}\right]^T n\,. \tag{3.37}$$

After computing the derivation inside (3.28):

$$f_d = \frac{2f}{c}\,(v + \widehat{\omega} e^{\widehat{\omega}t} r_0)^T n, \tag{3.38}$$

$$f_d = \frac{2f}{c}\,(v + \widehat{\omega}\boldsymbol{r})^T n = \frac{2f}{c}\,(v + \boldsymbol{\omega} \times \boldsymbol{r})^T n, \tag{3.39}$$

and n can be approximated as $\frac{R_0}{\|R_0\|}$ when $\|R_0\| \gg \|vt + \mathcal{R}_t r\|$. R_0 is the line of sight of the radar to the target. The approximation of the Doppler frequency shift is [98]:

$$f_d = \frac{2f}{c}\,(v + \boldsymbol{\omega} \times \boldsymbol{r}) \cdot n\,. \tag{3.40}$$

The first term in (3.40) is the Doppler shift induced by the translation, while the second term is the micro-Doppler induced by the rotation.

For time-varying rotation, the micro-Doppler term can be written as follows:

$$f_d = \frac{2f}{c}\,[\Omega(t) \times \boldsymbol{r}] \cdot n\,. \tag{3.41}$$

It has to be mentioned that the angular rotation velocity is a function of time, which can be expressed as follows [98]:

$$\Omega(t) = \Omega_0 + \Omega_1 t^1 + \Omega_2 t^2 + \cdots\ . \tag{3.42}$$

3.8 CONCLUDING REMARKS

To be able to run the simulation, some notions have to be introduced. This is the case with the micro-Doppler signature of the target, mathematically speaking. Other relevant notions are the rigid body motion in the three-dimensional space, the Euler angle, the quaternion and the backscattering of the EM wave from a body in motion. These are required to run the simulation, as the radar and the target have to be modelled in the MATLAB environment.

Simulation has been introduced in this research work to demonstrate the use of the radar system beyond the frequency of the built radar. In addition, this chapter gives deep understanding of the mathematical expression underlying the physical phenomenon. The next chapter will introduce the radar that was built and the setup of the experiment.

CHAPTER 4 FREQUENCY MODULATED CONTINUOUS WAVE

4.1 CHAPTER OVERVIEW

The radar that was built works at a frequency of 2.4 GHz as a centre frequency. Because of the limitation of the available hardware in terms of the frequency, in addition to the experiment, some simulations were set up at different frequencies in a band of 2.5 GHz to 20 GHz. The simulation setup was presented in Chapter 3 and in more detail in Chapter 5. Figure 4.1 represents a human walking towards the radar placed 10 m from where the human is starting his course. The radar is placed at a height of 2 m while transmitting its signal to the walking human. Figure 4.1 illustrates the setup of the simulations.

As specified in Chapter 2, section 2.2.11, an FMCW radar is of more advantage in this specific application. This chapter presents the setup of the radar and justifies the choice of this radar.

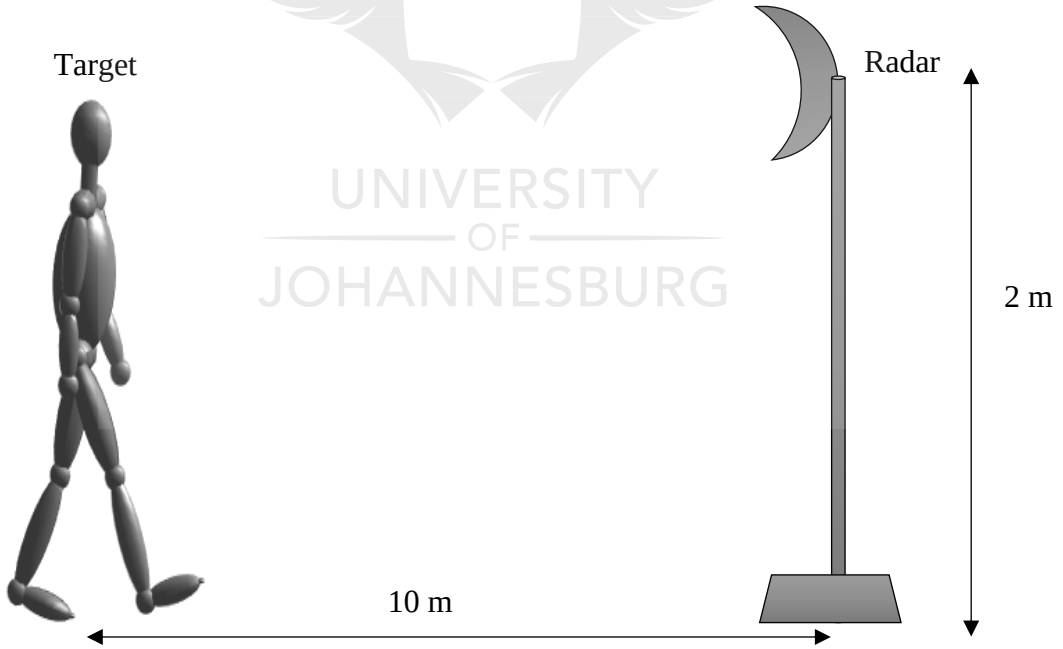

Figure 4.1: Setup of the simulation.

4.2 RADAR SETUP

The analysis conducted in this thesis is of data that have been collected with a radar built in the Centre for Telecommunication laboratory at the University of Johannesburg. The

radar used for the experiment was inspired by the Massachusetts Institute of Technology radar based on a coffee can [100]. The next subsection presents the radar used in detail, then the human and wall modelling.

4.2.1 Radar design

Figure 4.2 represents different components used to build the radar in the laboratory where the author did the research. The system comprises the following components:

a. The transmission branch is constituted of:
    a. A ramp generator
    b. A VCO
    c. An attenuator
    d. A PA
    e. A PD
    f. A transmit antenna.
b. The receiving branch is constituted of:
    a. A receive antenna
    b. A mixer
    c. An LNA
    d. A filter
    e. An ADC.

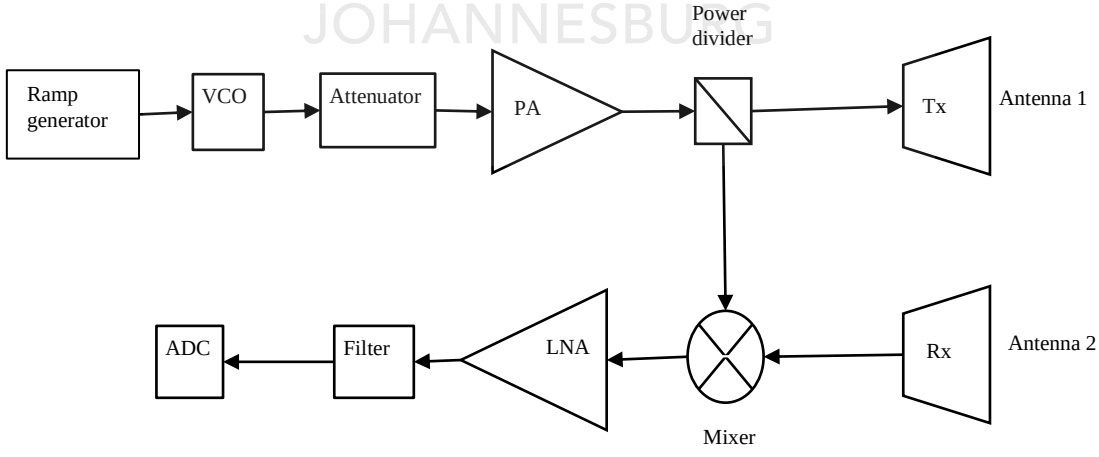

Figure 4.2: Radar built with different components for the experiment described in this thesis.

As one can see in Figure 4.2, the radar used in the experiment is an FMCW. The radar is input with a ramp signal generated by a signal generator or signal coming from the printed

circuit board. More details are given in Appendix A. The ramp signal voltage varies from 0 to 5 volts in a $20\,msec$ period. The VCO receives the signal coming from the signal generator and in turn generates frequencies in the range of 2257.4 to 2591.8 MHz, which are proportional to the input voltage. The VCO power output varies between 5.14 and 6.17 dBm, while the voltage varies between 0 and 5 volts. The signal coming from the VCO is fed to an attenuator and from the attenuator to a PA. The signal is sent to a PD from the PA. Thus, the PD splits the signal in half. The first half is transmitted to an antenna, Tx, while the other half is sent to a mixer for frequency synthesis. Once the signal has been sent to the antenna, this will transmit an EM wave, which will bounce from any object in the direction of the Tx radiation pattern. A small portion of the bounced EM wave will be collected by a receiver antenna Rx. The signal coming from the Rx will be demodulated with a mixer (Mx) by multiplying the half signal coming from the splitter and the signal coming from the Rx. The signal coming from the mixer is a beat frequency (BF), which is a baseband signal. Because the BF is a weak signal, it is thereafter sent to an LNA for amplification. A further process is undertaken from the LNA to detect any object in the scanning area. After the LNA the BT is filtered out for clutter removal. Then the signal goes from the filter to an ADC. In the present case the ADC is the audio card of a laptop. For signal processing, MATLAB and a DELL laptop are used. The antennas are designed using fundamental principles of electromagnetics. More details are given in Appendix B. The frequency band of 2.4 GHz has been chosen because it is an unlicensed band and is suitable for experimental purposes.

A small calculation yields a bandwidth of

$$B = 2591.8 - 2257.4 = 334.4\,MHz\,. \tag{4.1}$$

Then, using the following formula, the range resolution will be equal to 0.44 m. Thus, a range resolution of 0.44 m is a greater indication of limbs movement performed by a human being. For the actual study this range resolution is reasonable.

$$\Delta r = \frac{C}{2B} \tag{4.2}$$

In addition, using the sweep time $T_s = 20\,mSec$, the beat frequency is determined at $1114.6\,Hz \Longrightarrow 1.1$ kHz using the following formula:

$$f_{beat} = \frac{2B \cdot r}{C \cdot T_m}\,. \tag{4.3}$$

According to Shannon's theory, an analogue signal can be sampled at more than or equal to twice its frequency to be properly represented digitally. One can see that at this frequency an audio ADC can sample this signal.

To elaborate on all the modules used for the radar used in this study, Table 4-1 gives the part number of each component used. The first column presents the functionality of each part used for the radar, the second column presents the manufacture of the components, then the last column the part number of the components used.

Table 4-1: Modules used for the radar system

Module	**Manufacturer**	**Part Number**
VCO	Mini-Circuits	Zx95-2536c+
Attenuator	Mini-Circuits	VAT-3+
PA	Mini-Circuits	ZX60-272LN+
PD	Mini-Circuits	ZX10-2-42+
Mixer	Mini-Circuits	ZX05-43MH+
LNA	Mini-Circuits	ZX60-272LN+
Antenna	Homemade	Homemade

Figure 4.3 illustrates the radar built. The white antenna is the transmit antenna and the yellowish antenna is the receive antenna. In front of the antennas is the radar built with different modules, as presented in Table 4-1.

Figure 4.3: Radar built.

In Figure 4.3 one can see the entire radar and its different components; the radar is on a bench test floor and the antennas next to it.

Figure 4.4 represents the radar with different modules of the radar with the focus on the transceiver. From the bottom, the first module is the VCO. Thereafter comes the attenuator and then the PA. The component on top of the PA is the PD, dividing the signal in two. On the left hand the signal goes to feed the transmit antenna while on the right the signal goes to the mixer. On the far right-hand the cable coming from the mixer serves to receive the signal coming from the receive antenna. The signals coming from the PD and the antenna are input to the mixer, then sent to the LNA at the bottom of the mixer. The ADC module used for this experiment is the sound card of the computer.

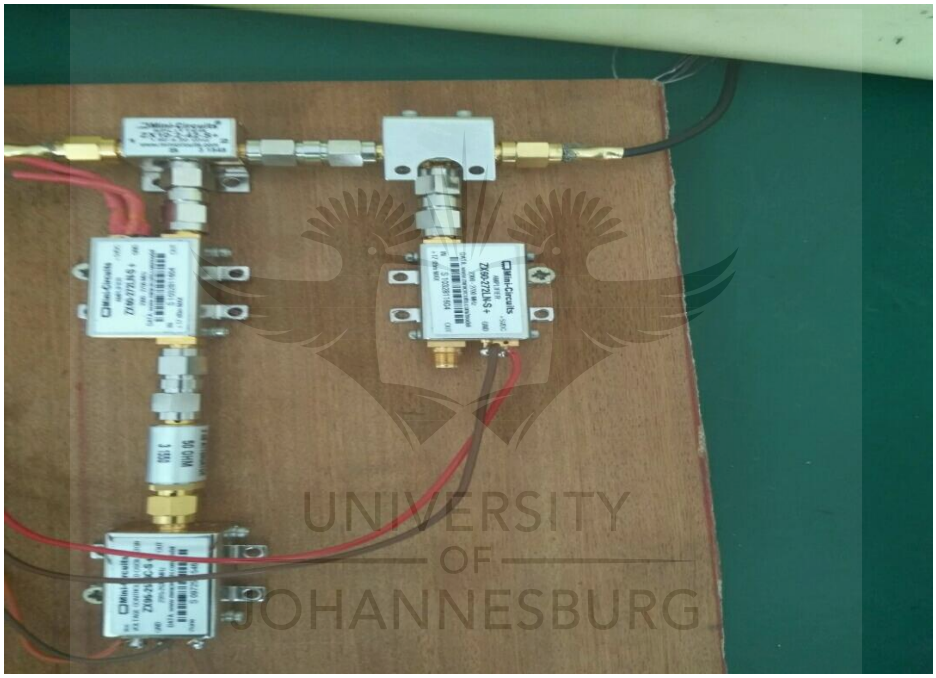

Figure 4.4: Modules of the radar.

In Figure 4.4, the radar that has been built with module components for noise immunity is illustrated. The VCO receives the signal coming from the signal generator, then in turn creates a frequency that is proportional to the voltage applied to it. The attenuator afterwards conditions the generated frequency (signal) in the range of power that is admissible to the PA. The PA amplifies the signal, then transmits it to the PD. The PD divides the signal into two, where one portion is transmitted via the antenna and the other portion of the signal is transmitted to the mixer. The mixer will demodulate the signal coming from the receiving antenna by mixing it with the signal coming from the PD. From the mixer the signal is passed through the LNA before going to the computer for further processing.

4.2.2 Human and wall model

Human signatures are introduced in this subsection because the target under investigation is a human being. Because the signal should travel twice through a wall before going back to the radar, wall modelling in TWR is discussed as well in this subsection.

4.2.2.1 Signal propagation in the absence of a wall (dielectric)

In this section, the researcher studies how a radar signal impinging on a human body behaves. The radar used in this experiment is monostatic.

Figure 4.5 presents a radar scene where a radar is placed at a point P at a distance r from a human being at point Q. The human and the radar are placed on the X-Z plane, while the Y-axis separates the radar from the human being. The radar is on a line of sight with the target under investigation.

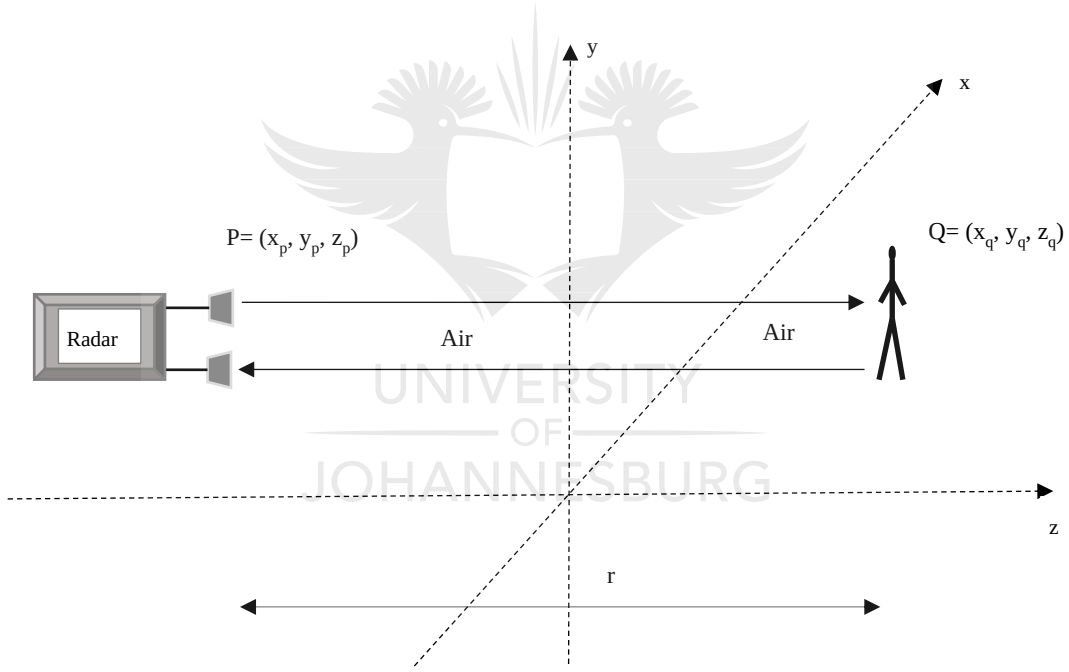

Figure 4.5: Signal propagating to the target without obstruction.

In Figure 4.5, a radar transmits a signal towards a human in the first case; then afterwards the signal bounces off the human to return to the radar. The radar is placed at a certain distance from the human being, in such a way that the wave reaching the human is a plane wave. The backscattering signal is a function of many radar parameters and the dynamic behaviour of the target. Consider a transmitter Tx and receiver Rx (radar) collocated at point $P = (x_p, y_p, z_p)$, where the distance between them is negligible. On the other side a

target (human being) is located at point $Q = (x_q, y_q, z_q)$. Let a signal, $s(t)$, be transmitted, propagating in the air while travelling from point P to Q.

Because the EM wave is propagating in the air, the velocity of the EM wave is regarded as equal to the velocity of light, c. The distance between the radar and the target r is such that the EM reaches the target at the far field.

In a Cartesian system the distance between the radar and the target can be written as follows:

$$r(P,Q) = \sqrt{(x_q - x_p)^2 + (y_q - y_p)^2 + (z_q - z_p)^2}. \quad (4.4)$$

The transmitted signal is represented mathematically as follows:

$$E_t(r,\omega) = e^{-jkr}E(0,\omega). \quad (4.5)$$

It is transmitted towards the scene of interest. The medium is a homogeneous isotropic and non-magnetic medium $\mu = \mu_0$ with a permittivity of $\varepsilon = \varepsilon_0$. k is the wave number of the signal. Note that k is a frequency-dependent factor and has the following value: $k(\omega) = \omega\sqrt{\epsilon(\omega)\mu_0}$.

Figure 4.6 presents the signal transmitted against the one received. In this figure the dashed line is the transmitted signal while the solid line is the received signal. The x axis represent the time that elapses when the signal is changing its value. On the other hand, the y axis represents the frequency.

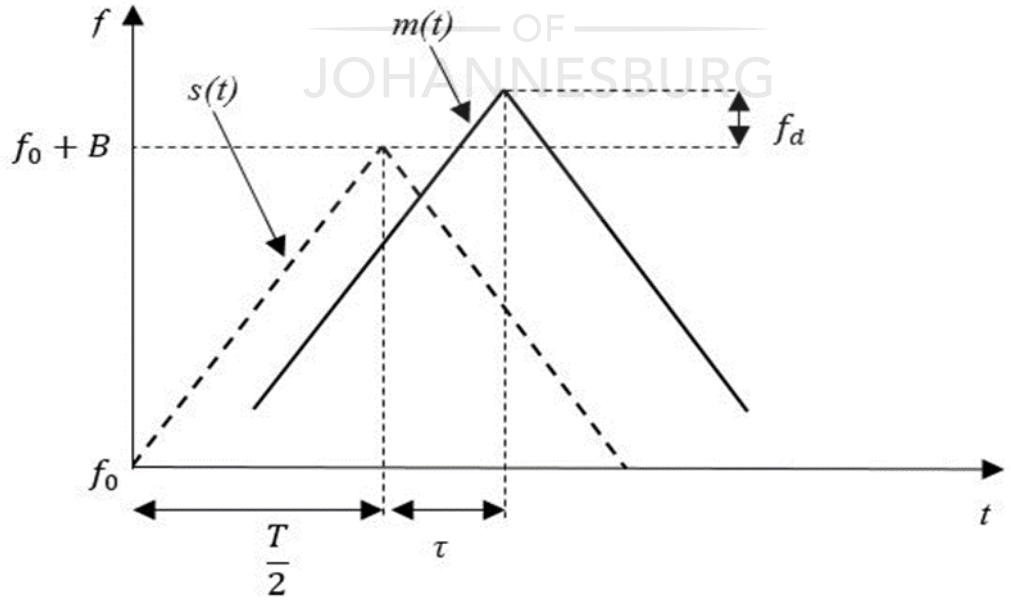

Figure 4.6: Signal transmitted and received.

In Figure 4.6, it can be observed that the received signal arrives at the radar after a certain delay, τ, and with a difference in frequency, f_d, which is a Doppler shift.

If one considers a human being walking with hands swinging along the body, the movements of the limbs and chest are seen as sources of EM wave modulation. If there is no obstruction between the target and the radar, the signal $s(t)$ sent by the transmitter is modulated by the movement of the limbs and the micro-movement of the chest. Consider the chest and limb movement as additive signal represented by

$$y(t) = y_c(t) + y_l(t), \tag{4.6}$$

where the

$$y_c(t) = A_c \cos(2\pi f_c t), \tag{4.7}$$

and

$$y_l(t) = A_l \cos(2\pi f_l t), \tag{4.8}$$

are signals due to the chest and limbs movement respectively. Thus, at the receiver side one can collect the signal:

$$m(t) = A_2 \cos[2\pi f(t_0 - t_1)]. \tag{4.9}$$

This signal has to be added to white Gaussian noise to yield:

$$m(t) = A_2 \cos[2\pi f(t_0 - t_1)] + n(t). \tag{4.10}$$

Taking into account that the target has micro-movement, one can intuitively assume the presence of the Doppler frequency f_d.

τ is the round trip time taken by the signal to bounce off the target and return to the radar. This can be determined as:

$$\tau(t) = |t_0 - t_1| = \frac{2r(t)}{c} \tag{4.11}$$

where $r(t)$ is the dynamic range between the target and the radar. $r(t)$ is determined as

$$r(t) = r + y(t)\ . \tag{4.12}$$

Incorporating (4.7) and (4.8) in (4.6) and then the resulting equation into (4.12) yields

$$r(t) = r + A_c \cos(2\pi f_c t) + A_l \cos(2\pi f_l t). \tag{4.13}$$

If (3.55) is then incorporated into (4.13), the result is:

$$\tau(t) = \frac{2[r + A_c \cos(2\pi f_c t) + A_l \cos(2\pi f_l t)]}{c}. \tag{4.14}$$

In order to deduce the target information from the received signal, a mixer multiplies $m(t)$ with the original signal transmitted $s(t)$ in the time domain. In practice this multiplication is known as the down-converting process. The result of the development is:

$$m(t) \cdot s(t) = \frac{A_2 A_1}{2}\{\cos\,[\,4(\pi f t_0)^2 - (2\pi f t_1) + n(t)] + \cos[\,n(t) - (2\pi f t_1)]\}. \quad (4.15)$$

A human being may be modelled as a metallic cylinder of the same height as the human being when the micro-Doppler is not of interest because the movement of the entire body is regarded as one unit. Representing a human by a metallic cylinder, a simulation was run in MATLAB to investigate the frequency impact on the RCS. To find the RCS behaviour of the target in the function of the frequency, the height and radius of the cylinder, a simulation was conducted.

Figure 4.7 represents the result of a simulation run at different frequencies while maintaining the same radius and same height of the cylinder. The X-axis represents the aspect angle at which the radar signal is impinging on the target. The Y-axis represents the normalised RCS of the target.

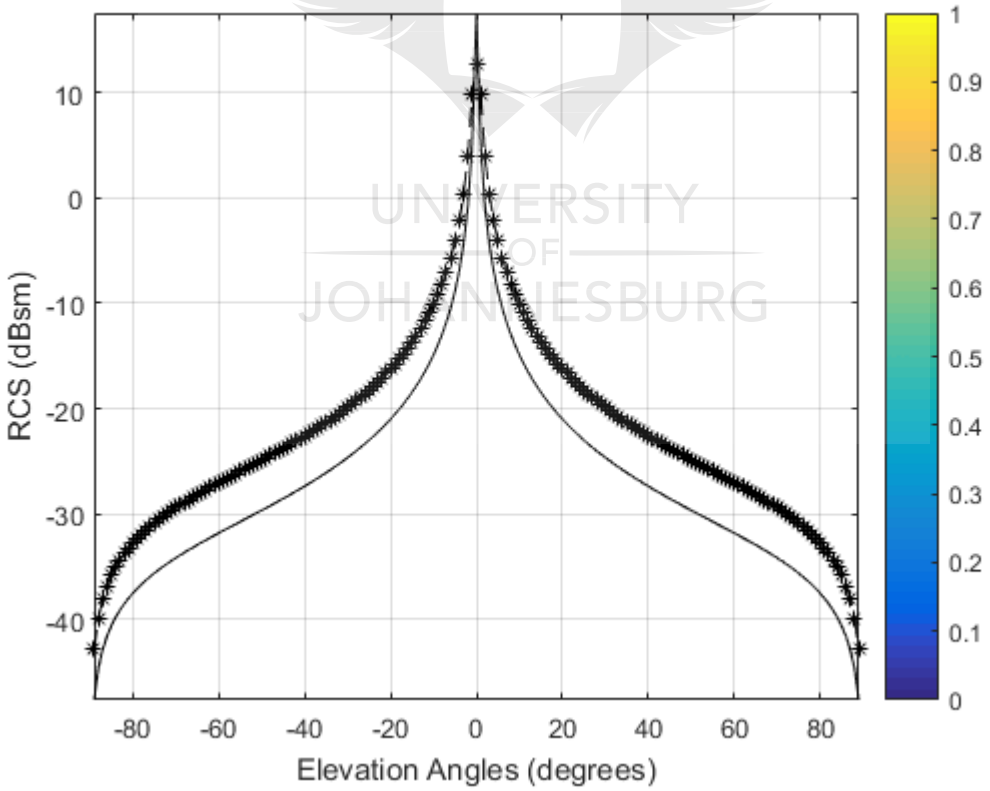

Figure 4.7: The same radius and same height at different frequencies (1 and 3 GHz).

In Figure 4.7, the frequencies used are 1 and 3 GHz because at 2 GHz the difference between the return signal at 1 and 3 GHz is not significant. In this simulation the body

width regarded as the radius was not varied. In Figure 4.7 the starred plot represents the curve of the RCS in the function of the elevation angle of a cylinder that is 1.9 m in height and 0.25 m in radius at a frequency of 1 GHz; on the other hand, the continuous curve represents the same target at 3 GHz. At a frequency of 1 GHz the target produces a higher RCS than at 3 GHz. The result shows that using a radar at a frequency of 1 GHz, the target is more likely to be detected than when using the same target at a frequency of 3 GHz. In addition, at zero-degree angle of elevation the target produced a higher RCS compared to the rest of the angles. The high specular or great RCS at zero-degree angle in the simulation is justified by the fact that the cylinder height is greater than its width at that position.

To extend the behavioural study of the cylinder size related to the RCS, another simulation was run. Figure 4.8 represents the simulation of the cylinder. This time the height and the radius have been modified. The X-axis represents the aspect angle at which the radar signal is impinging on the target. The Y-axis represents the normalised RCS of the target. In this condition, the influence of the height and the radius are studied.

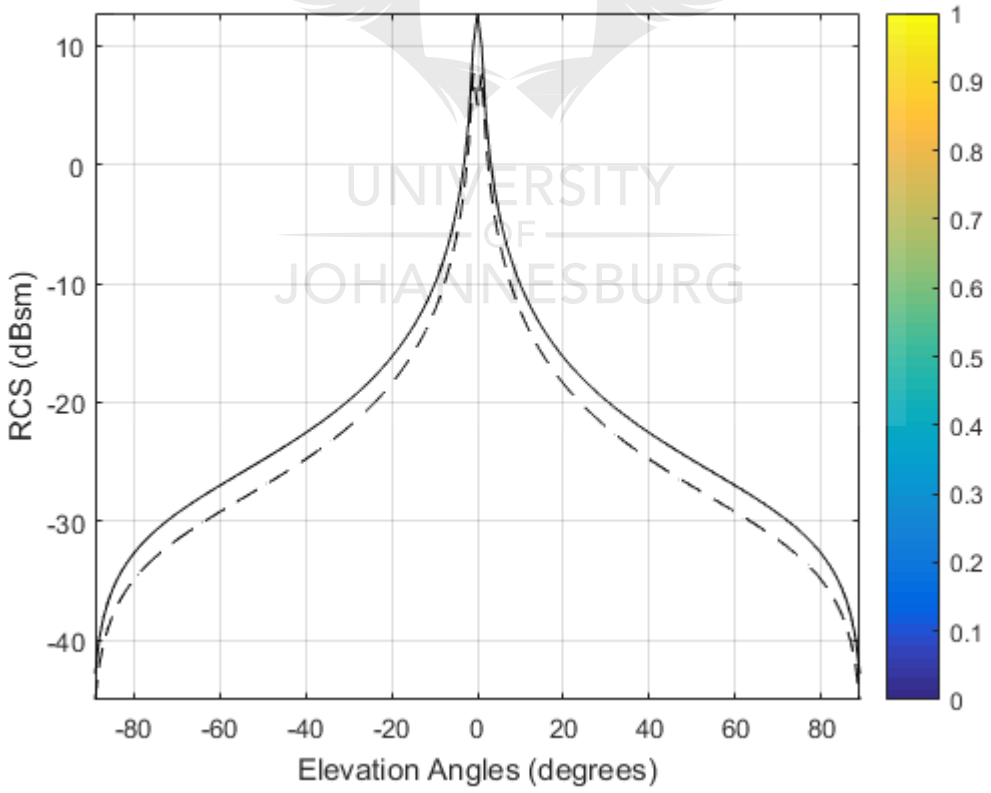

Figure 4.8: Frequency 1 GHz, radius of 0.25 and 0.15 m and height of 1.9 and 0.15 m.

Figure 4.8 reflects that, because the frequency of 1 GHz showed higher response compared to 3 GHz, in this simulation a frequency of 1 GHz was chosen. Using a frequency of 1

GHz, a height of 1.9 m and 1 m and a radius of 0.25 m and 0.15 m were used in the simulation. The dashed curve is the cylinder of 1 m in height and 0.15 m in radius, while the continuous curve is the cylinder of 1.9 m in height and 0.25 m in radius. A target with higher height and radius is more reflective than a shorter one. Care has to be taken when trying to detect both targets in the same scene.

As one can see, the cylinder with higher height and greater radius produced significant RCS compared to its counterpart of 1 m. Thus, the conclusion can be drawn that height cannot be neglected in the study of target behaviour.

4.2.2.2 Signal propagation in the presence of a wall

The backscatter model for walls is studied in this section. Backscattering of an EM wave impinging on a wall has been the object of many investigations for a long time [13, 71]. To model a wall, one has to consider the main elements in its makeup. The wall is built from different materials, with dielectric or electric properties as the reinforcement.

Figure 4.9 represents propagation of the signal passing through the wall before reaching the human behind the wall. The radar is placed at position *P*, then transmits the signal towards the wall.

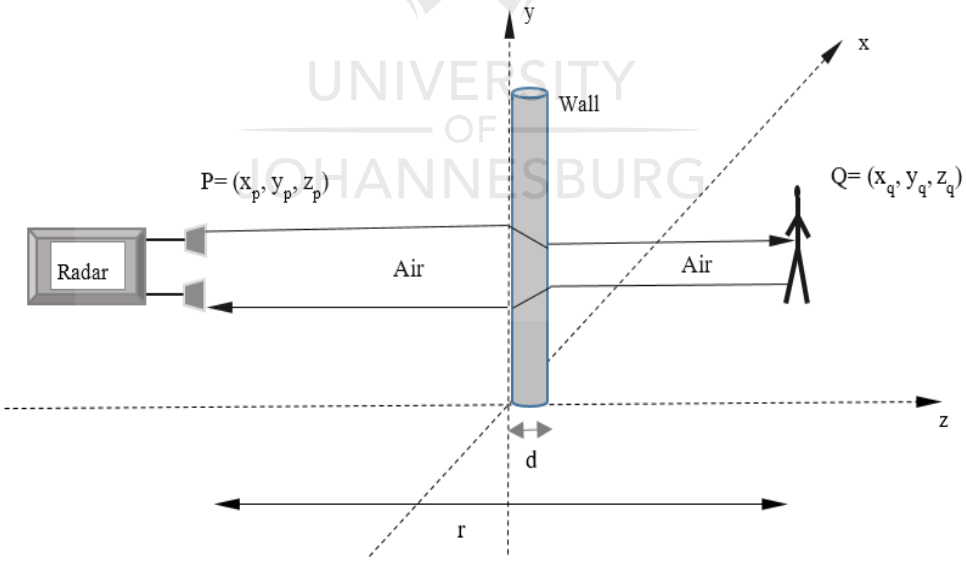

Figure 4.9: Signal propagating from the radar to the human through the wall.

In Figure 4.9, as the wave rays are passing through the wall, they bend before leaving the wall. From the wall the rays reach the human and are then reflected back to the wall. Again, the ray is bent before leaving the wall for the radar. The bending ray is the physical phenomenon that induces the ghost target if a strong algorithm is not used by the radar.

The width of the wall is an element that can influence detection. As shown in the figure, the bending can be significant if the wall is thick.

In this case it is assumed that a foundation is under the soil surface and consequently not visible. The wall is at an angle of 90 degrees to the soil surface. It is furthermore assumed that the ceiling and roof are above the level that will be illuminated by the EM wave. The wall is regarded as an inhomogeneous dielectric when hit by the EM wave.

The velocity of an EM wave inside a non-magnetic medium is given by:

$$v = \frac{1}{\sqrt{\varepsilon_0 \mu_0 \varepsilon_r}} = \frac{c}{\sqrt{\varepsilon_r}}\,. \tag{4.16}$$

The velocity of the EM wave will decrease while travelling from the air to the wall media; this can be observed in (3.58).

It is known that at the boundary point the incident angle θ_{air} and the refraction angle θ_{wall} are related by Snell's law, which is given by the following formula:

$$\sqrt{\varepsilon_{air}} sin\theta_{air} = \sqrt{\varepsilon_{wall}} sin\theta_{wall.} \tag{4.17}$$

The EM wave will experience multiple refraction as it travels twice through the air-wall-air. Thus, if the refraction angle is not taken into consideration while imaging the scene, incorrect imaging could result. The incorrect imaging can be seen as a non-focused image or ghost target.

In the interaction of an EM wave with a dielectric medium, it is known that the dielectric constant and the shape of a target are the main components that influence EM scattering.

The wall can be regarded as homogeneous material to simplify the numeric calculation. On the other hand, the wall can be seen as a stratified medium with different layers and it then becomes a heterogeneous medium. The scattering signal coming from a distant wall is represented as follows [101]:

$$\sigma = \lim_{r\to\infty} 4\pi r \frac{|E^s|}{|E^i|} \tag{4.18}$$

with r as the range between the radar and the target and E^s and E^i the scattering and the incident electric field. Because in this study the target is a wall with stratified layers, equation (3.60) is generalised as follows:

$$\sigma = \lim_{r\to\infty} 4\pi r(t) \frac{|\sum_{l=1}^{n} E^s|}{\left|\sum_{l=1}^{n} E^i\right|}\,. \tag{4.19}$$

When E^i impinges on the wall E^s and E^t, the forward electric field, result from the phenomenon. Thus, the relation of these three components is:

$$E^i = E^0 . e^{-jk_1 u_{ni} r} \tag{4.20}$$

$$E^s = \gamma E^0 . e^{-jk_1 u_{ns} r} \quad (4.21)$$

$$E^t = \rho E^0 . e^{-jk_2 u_{nt} r} \quad (4.22)$$

where E^0 is the electric field at the boundary position, σ and ρ are the reflection and the transmission coefficient, k is the wave number and u_{ni}, u_{ns} and u_{nt} are a unit vector of the incident, reflection and transmission wave.

4.3 CONCLUDING REMARKS

This chapter describes the radar built to collect the data. The choice of the FMCW has been justified by the fact that it sends different frequencies to the target at different time intervals. These different frequencies have the advantage of reflecting differently on different targets; as has been shown in this chapter, different frequencies impinging on the target vary the RCS of the same target. Thus, the choice of radar to be used is very important, according to the application. Combining Chapter 3 and Chapter 4 yielded a tool to run the experiment in order to justify the hypothesis formulated in Chapter 1.

The simulation covers the frequencies that the radar that was built did not cover. The simulation yielded a wider spectrum of viewing the problem in different angles. The software used for the theoretical simulation was MATLAB. The chapter presented the radar that was built and the experimental setup. A full description of each phase of the research and the radar used for data collection was given in Chapter 1 in the methodology section.

Finally, while the radar was built as a technology demonstrator, it was only a prototype. Medical or ethical clearance for using the radar on a human subject was outside the scope of this thesis. It has to be mentioned that all research involving human participants must be approved by human research ethics committees accredited by the National Health Research Ethics Council, a centralised body that is part of the Department of Health. For this reason, the thesis documents the prototype without the researcher having had the opportunity to test it. The simulation approach, with relevant emulation parameters, completely validates the hypothesis [82].

CHAPTER 5 MICRO-DOPPLER SIMULATION AND EXPERIMENT

5.1 INTRODUCTION

The radar discussed in this thesis has been presented in detail in previous chapters. In addition, the previous chapters served as introduction to this chapter by explaining the method adopted and the reason for choosing this method rather than others. Hence, this chapter presents experimental and simulation results to address the research questions. The results of the simulations and experiments are subsequently discussed.

To observe a human behind a wall or home appliance, echoes collected with radar are processed. These echoes are return signals from the target and any object the signal encounters on its way from the radar to the target and vice versa. The return signal is presented at the analogue-to-digital stage as an IF signal after the LNA, amplifier and filter. The IF signal is digitised, then processed to obtain the spectrogram of the sensed environment. Thus, the return signal is a function of time and frequency because at each instance of time the signal has a corresponding Doppler frequency.

To simulate a radar system and model the target, the signal has to be propagated to the target and the motion of the target has to be determined first. Therefore, the next section introduces the signal model. The model of the signal allows researchers to simulate the entire process of the radar sending a signal to the target, then getting the signal back to the radar and finally processing it.

5.2 SIGNAL MODEL

Consider a monostatic FMCW radar transmitting a time varying signal with a frequency $f(t)$ over the sensing period. The transmitted signal is expressed as:

$$S(t) = \exp[j2\pi f(t)t]. \tag{5.1}$$

Consider a point target located at a range of R_0 from the radar at a time $t_0 = 0$. If the target moves with a velocity $v(t)$ in the direction of the radar, forming an angle θ with the line of sight of the radar, the distance between the target and the radar at the time instant t_1 is:

$$R(t) = R_0 + \int_{t_0}^{t_1} v(t)dt. \tag{5.2}$$

Thus (5.2) can be expressed as follows if θ is taken into consideration:

$$R(t) = R_0 + \int_{t_0}^{t_1} v(u)\cos(\theta)du \tag{5.2}$$

where $v(t) = v(u)\cos(\theta)$.

Therefore, the radar returning signal from the target can be mathematically modelled as:

$$q(t) = \rho \exp\left\{j2\pi f(t)\left[t_0 - \frac{2R(t)}{c}\right]\right\} \tag{5.3}$$

where ρ is the reflectivity coefficient of the point target, the factor 2 in $2R(t)$ is the round trip of the signal from the radar to the target and c is the velocity of the EM wave propagation in the air. Thus, the Doppler frequency is represented mathematically as follows:

$$f_d(t) = \frac{2v(t)\,cos(\theta)}{\lambda_c(t)}. \tag{5.4}$$

The wavelength is determined as $\lambda_c(t) = c/f(t)$. This Doppler frequency is related to $q(t)$. For the current application the Doppler frequency return is of great importance, as it helps to detect the activities behind the wall. In addition, this helps to detect only animated objects and eliminate the presence of immobile objects behind the wall in the processing signal.

The target in this research being a human, the human is regarded as a special extended target because of its nature. To compute the return signal for this type of target, one has to consider the integration of the return signal for each point target over the region occupied by the target. Therefore, the integration is represented mathematically as follows:

$$Q(t) = \int_{\Omega} q(t)da. \tag{5.5.}$$

The total Doppler signature is the contribution of individual component Doppler frequencies for different parts of the body. Mathematically speaking, the contribution of the Doppler signature is known as the superposition of individual parts.

Thus, by observation, one can expect high Doppler frequency from limbs and torso motion because it can generate the time-varying Doppler frequency. In addition, these different parts of the body generate different Doppler frequency because of their geometric size. Therefore, these different signatures will drive the classification of distinct parts of the body. The next subsection focuses on wall attenuation. It will describe an experiment on signal propagation throughout the wall.

5.3 MATERIAL ATTENUATION AND SCATTERING

To be able to detect human activities behind the wall, the material that the signal is travelling through has to be taken into consideration. The wall and the appliances are the two materials through which the signal has to travel before reaching the human being.

Thus, responding to the first research question entails determining how the material through which the radar signal is travelling is affecting the signal. The following subsection is devoted to ascertaining the behaviour of the signal in the presence of a fan. It has to be mentioned that the fan can be a portable or a ceiling fan; both are found in many home environments. Fans are the means of cooling a room in the absence of an air conditioner, which may be too expensive for some areas. This research extends its application to regions where the temperature can easily reach 38 to 40 degrees Celsius. Therefore, people use fans as a means of cooling their rooms.

5.3.1 Wall attenuation and scattering

To test the hypothesis formulated to determine the effect of the wall on the signal propagating from the radar to the other side of the wall; the experiment described below has been introduced in this thesis. This experiment is intended to determine how the signal is affected by the medium. The first sub-section is devoted to the signal affected by the presence of the wall in the real environment, while the second sub-section is devoted to the simulation. Thus, knowing the signal on the other side of the wall, one can use this signal with its attenuation for simulation purposes.

5.3.1.1 Wall attenuation experiment

The signal travels through the wall before reaching the human behind the wall. Thus, studying human activities without taking the effect of the wall on the EM wave into account is an inaccurate approach. Therefore, the wall has to be taken into consideration because the signal has to travel through the wall twice before getting back to the radar receiver. The researcher ran experiments to evaluate the wall attenuation. Table 5-1 presents the measurement equipment used to run the experiment related to wall attenuation. The first column indicates the type of equipment used, the second the model of equipment used and the last the manufacturer of the equipment.

Table 5-1: Equipment used for wall attenuation experiment.

Equipment used for the experiment		
Type of equipment	**Model**	**Manufacturer**
Microwave generator	R&S SMB-B106 RF and Microwave Signal Generator	Rohde & Schwarz
Spectrum analyser	R&S ESR26	Rohde & Schwarz
Antenna	Appendix	UJ laboratory

To run this experiment, the researcher placed one antenna on each side of a wall, which was of brick. The first antenna was placed 1 m from the wall and connected to the wave generator. The antenna was placed 1 m above the floor and was used as a transmitter. The second antenna was placed on the other side of the room at a different distance of 50 cm from the wall as initial position. The antenna was at a height of 1 m as well. This antenna was moved from 50 cm to 3 m away from the wall, at intervals of 50 cm from the previous position. The interval between positions was chosen because the researcher did not expect any drastic change in signal below 50 cm.

It is crucial to know the way the signal is affected by the presence of the wall, because the signal has to travel through the wall. It is for this reason that the experiment described below was conducted.

Tables 5.2 to 5.6 present the results of the different experiments. The first column represents the frequency at which a signal was transmitted towards the wall. The second column represents the distance at which the receiver antenna was placed from the wall. The third column represents the strength of the signal received from the other side of the wall. The transmit power was 10 dBm for all the different frequencies and distances. It has to be mentioned that the position of the transmit antenna remained fixed while the receiver antenna was mobile.

Table 5-2: Through-the-wall signal at 1 GHz.

Received signal		
Frequency	**Distance**	**Power**
1 GHz	0.5 m	-49.28 dBm
1 GHz	1 m	-51.34 dBm
1 GHz	1.5 m	-53.45 dBm
1 GHz	2 m	-60.9 dBm
1 GHz	2.5 m	-63.7 dBm
1 GHz	3 m	-58.51 dBm

Table 5-3: Through-the-wall signal at 1.5 GHz.

Received signal		
Frequency	**Distance**	**Power**
1.5 GHz	0.5 m	-45.39 dBm
1.5 GHz	1 m	-58.48 dBm
1.5 GHz	1.5 m	-53.9 dBm
1.5 GHz	2 m	-49.6 dBm
1.5 GHz	2.5 m	-53.3 dBm
1.5 GHz	3 m	-63.2 dBm

Table 5-4: Through the wall signal at 2GHz.

Received signal		
Frequency	**Distance**	**Power**
2 GHz	0.5 m	-49.53 dBm
2 GHz	1 m	-54.01 dBm
2 GHz	1.5 m	-62.4 dBm
2 GHz	2 m	-64.6 dBm
2 GHz	2.5 m	-67.7 dBm
2 GHz	3 m	-74.2 dBm

Table 5-5: Through-the-wall signal at 2.5 GHz.

Received signal		
Frequency	**Distance**	**Power**
2.5 GHz	0.5 m	-40.43 dBm
2.5 GHz	1 m	-48.3 dBm
2.5 GHz	1.5 m	-54.3 dBm
2.5 GHz	2 m	-61.03 dBm
2.5 GHz	2.5 m	-68.47 dBm
2.5 GHz	3 m	-78.31 dBm

Table 5-6: Through-the-wall signal at 3 GHz

Received signal		
Frequency	**Distance**	**Power**
3 GHz	0.5 m	-47.1 dBm
3 GHz	1 m	-50.7 dBm
3 GHz	1.5 m	-53.11 dBm
3 GHz	2 m	-52.9 dBm
3 GHz	2.5 m	-61.2 dBm
3 GHz	3 m	-59.2 dBm

A signal generator was used to generate a signal at a power of 10 dBm; this was fed to the transmit antenna via a coaxial cable of 30 cm. In order to observe the signal properly in a different situation, the researcher plotted the results value in Figure 5.1. Figure 5.1 presents the received signal from the other side of the wall at different frequencies. The legend in the figure shows each frequency in a different colour. In the y-axis the received power is in dBm and the x-axis is the distance in metres.

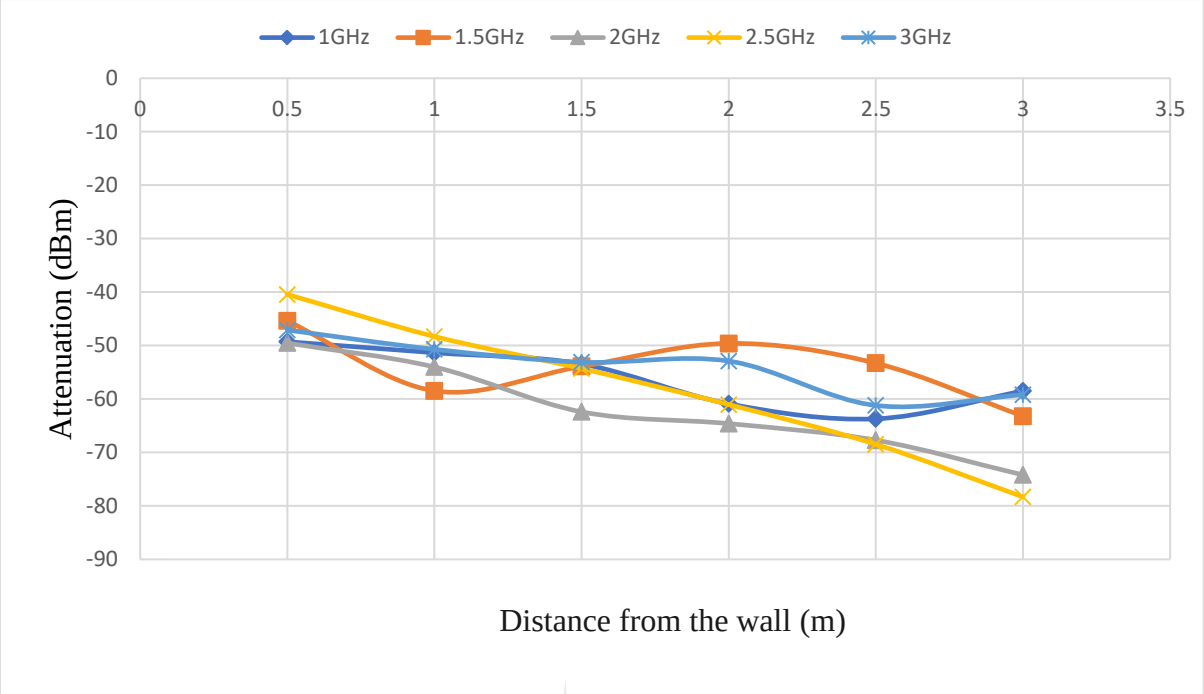

Figure 5.1: Received signal through the wall.

At 1 GHz and 3 GHz the signals passing through the wall are less affected compared to others in general up to a range of 1.5 m. While the signal is less affected at 1.5 GHz and 2.5 GHz at a range of 50 cm, the signal at 2 GHz is highly affected. At frequencies of 1.5 GHz and 2.5 GHz the signal fluctuated a lot more compared to the signal at 1 GHz and 3 GHz. At 2 GHz and at a distance of 50 cm the signal was even weaker than at the rest of the frequencies. Thus, up to 1.5 m the signals at 1 GHz and 3 GHz give better result than the rest of the rest of the signals in terms of fluctuation. On the other hand, at 2.5 GHz the signal has much higher power than at 1 GHz and 3 GHz, up to approximately 1.4 m. One can see that at 1.5 m the signal is weaker than the rest of the signals, even though it was initially stronger at a distance of 50 cm.

At half of the distance from the wall another behaviour was observed. The 1.5 GHz signal exhibited great fluctuation and much higher power. On the other hand, the 2 GHz and 2.5 GHz signals were subject to great attenuation in the second half of the range from 1.5 m to 3 m.

From an EM point of view, walls may be grouped into two major categories:

- Homogeneous walls, such as concrete or bricks walls, and
- Inhomogeneous walls, such as reinforced concrete, cinder block or dry wall.

In this study all the walls were regarded as homogeneous walls. Thus, with the results obtained in Tables 5.1 – 5.6, the researcher had adequate information on the way the signal is affected at different frequencies and ranges while passing through the wall.

5.3.1.2 Simulation of the wall slab

Viewing the result obtained in section 5.3.1.1, the conclusion can be reached that the wall consists of dispersive media. Thus, a wave propagating through the wall will be attenuated before reaching the target. This statement is confirmed in many research studies conducted previously [13, 47]

Consider a wave $E(z) = E(0)e^{-jkz}$ travelling in the direction of $+z$. $E(z)$ is space-dependent in the y and x directions, assuming that the wall is an isotopic and non-magnetic medium ($\mu = \mu_0$). In addition, the wall has an effective permittivity of $\epsilon(\omega)$, with k frequency-dependent as a complex-valued wavenumber defined as $k(\omega) = \omega\sqrt{\epsilon(\omega)\mu_0}$. Thus, the wave equation can be written in the frequency domain as follows:

$$\hat{E}(z,\omega) = e^{-jkz}\hat{E}(0,\omega). \tag{5.6}$$

A complete space time of this equation can be written as:

$$e^{j\omega t}\hat{E}(z,\omega) = e^{j(\omega t - kz)}\hat{E}(0,\omega). \tag{5.7}$$

Therefore, for a linear time-invariant system the input and the output will be represented in the function of the impulse response $h(t)$ and the corresponding frequency response $H(\omega)$. The two relations are multiplication in the frequency domain and convolution in the time domain.

Figure 5.2 presents the multiplication in the frequency domain and the convolution in the time domain. The top figure represents the frequency multiplication and the bottom figure the time convolution.

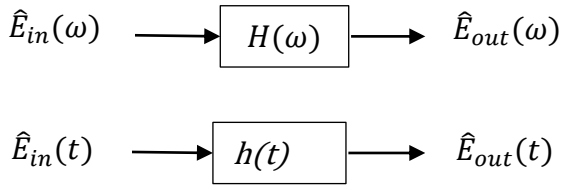

Figure 5.2: Multiplication in frequency domain and convolution in time domain.

Figure 5.2 can be written mathematically in the following way:

$$\hat{E}_{out}(\omega) = H(\omega)\hat{E}_{in}(\omega). \tag{5.8}$$

$$\hat{E}_{out}(t) = \int_{-\infty}^{\infty} h(t-t')\hat{E}_{in}(t')dt'. \tag{5.9}$$

Because micro-Doppler is used to detect the target, the reflection of the wall is ignored, as it has less influence on the micro-Doppler return. Figure 5.3 represents a rectangular wave passing through a dispersive medium. The signal in black is the original one sent and the signal in red is the signal after passing through the medium. The Y-axis represents the power in watts that is transmitted, and the X-axis represents the time that is taken by the signal to travel throughout the medium and when the signal has been transmitted.

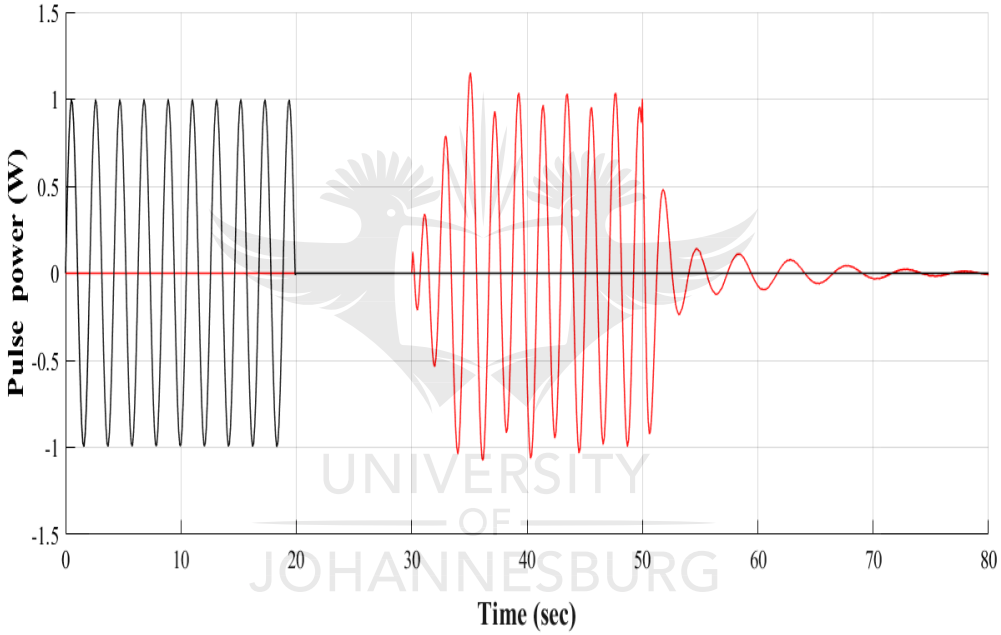

Figure 5.3: Transient propagation.

In Figure 5.3, one can observe that the signal does not change much in form, but instead a small change in amplitude is evident. In addition, the signal fades over a long distance.

5.3.1.3 Simulation of the wall slab with different permittivity and frequency

The simulations run in subsections a, b and c have been introduced in this study to determine how the signal is affected while passing through a wall composed of a single layer. The frequency, permittivity relative to the wall and the width of the wall were varied while observing the electric field before entering the wall and after emerging from the wall. In Figures 5.4 - 5.6, the blue line represents the permittivity, which started with a

value of 1; 1 is the relative permittivity of the air. Then at 2.5 m a wall is placed with different permittivity in a different simulation. The red solid line represents the electric field travelling in the direction of the X-axis positive. Two sizes of wall width have been retained for this simulation. The widths are 11 and 22 cm, which are common sizes found in house walls. The relative permittivities of the walls used in these simulations are 4 and 5.

a) Simulation of the wall slab at 1 GHz with different wall width and permittivity

Figures 5.4. a - 5.4.d represent the simulation run at a frequency of 1 GHz. Then in Figures 5.4.a and 5.4.b the simulations are run with a wall of 11 cm in width, while in Figures 5.4.c and 5.4.d the simulations are run with a wall having a width of 22 cm. In each case the relative permittivity has been modified.

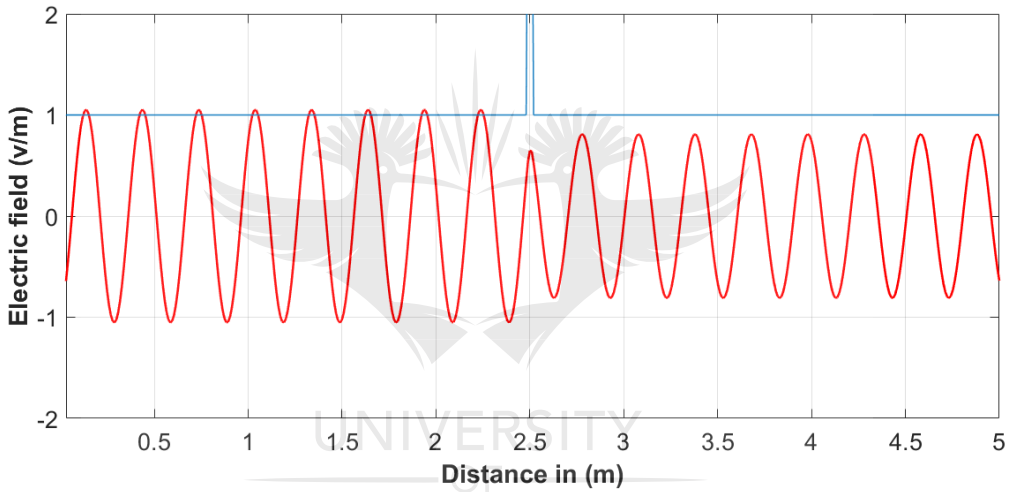

Figure 5.4.a: 1 GHz with a wall of 11 cm in width and permittivity of 4.

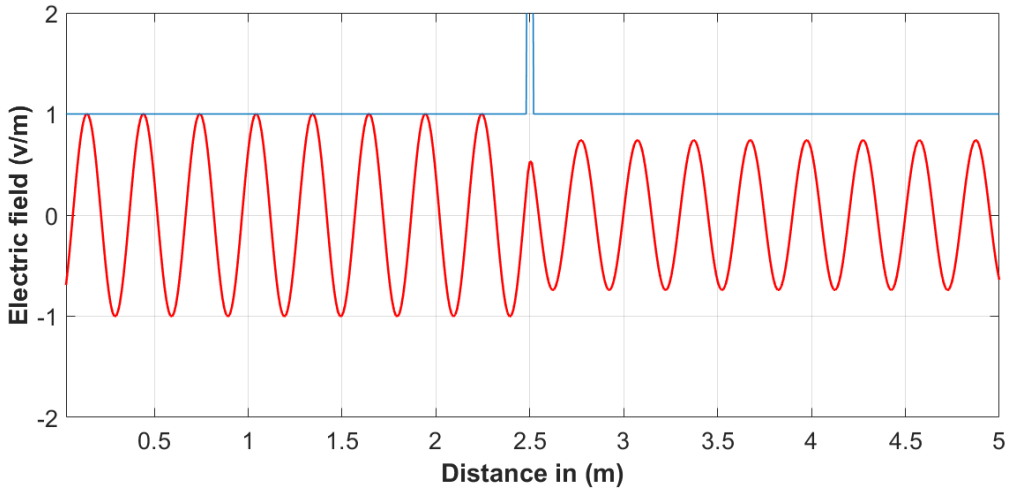

Figure 5.4.b: 1 GHz with a wall of 11 cm in width and permittivity of 5.

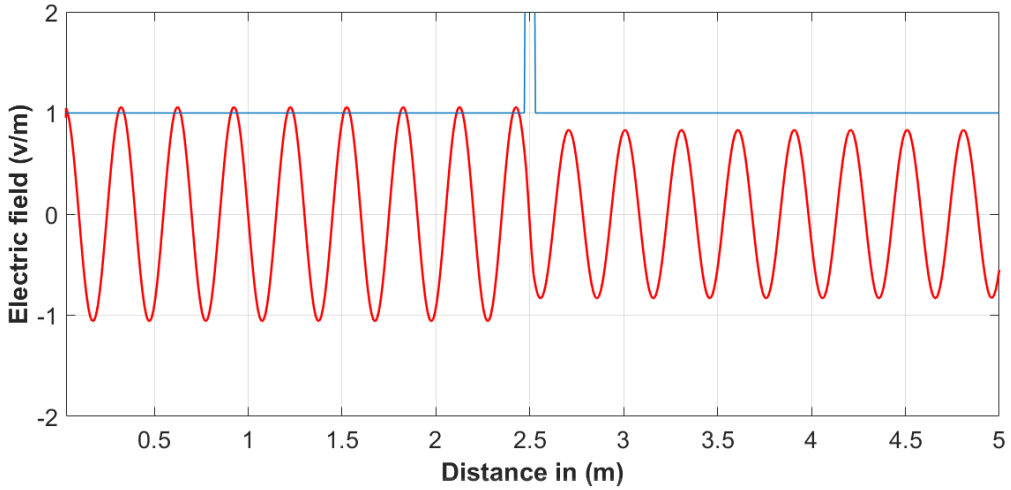

Figure 5.4.c: 1 GHz with a wall of 22 cm in width and permittivity of 4.

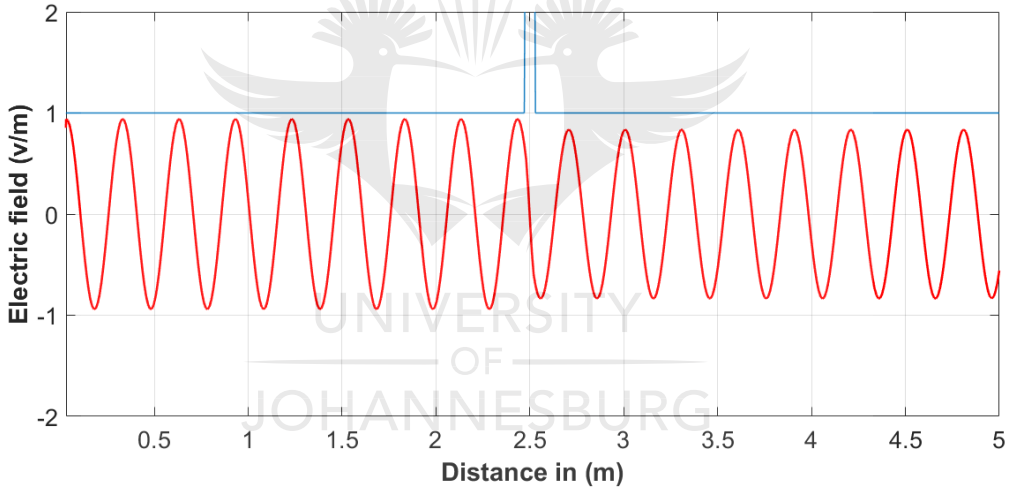

Figure 5.4.d: 1 GHz with a wall of 22 cm in width and permittivity of 5.

One can observe that at a frequency of 1 GHz there is attenuation of the signal, which is accounted as 20% of the signal injected on the other side of the wall. At this frequency the relative permittivity and the wall width do not have a great influence on the signal impinging on the wall. The forward signal is more or less 80% of the incident wave. Therefore, though there is attenuation, the forward signal is not affected sufficiently to make the target undetectable.

b) Simulation of the wall slab at 2 GHz with different wall width and permittivity

Figures 5.5. a - 5.5.d represent the simulation run at a frequency of 2 GHz. In Figures 5.5.a and 5.5.b the simulations are run with a wall of 11 cm in width, while in Figures 5.5.c and

5.5.d the simulations are run with a wall having a width of 22 cm. In each case the relative permittivity has been modified.

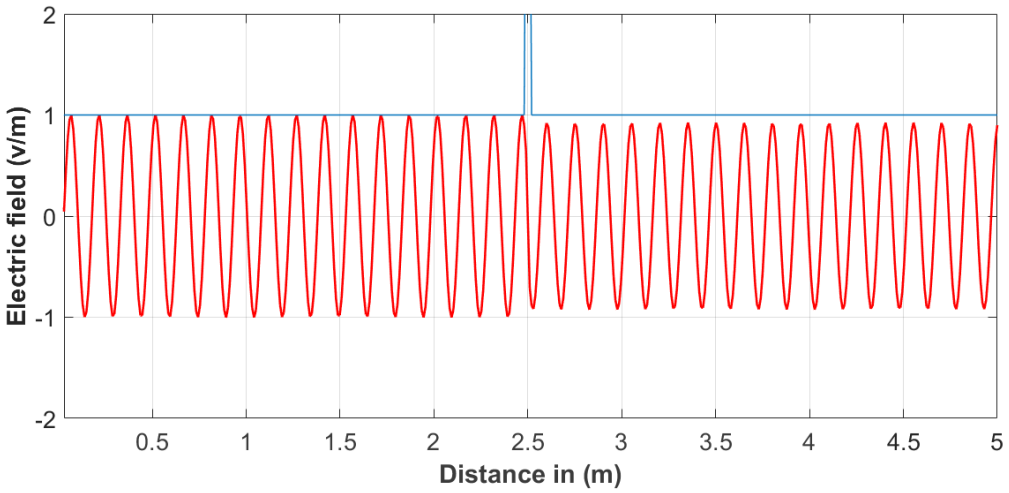

Figure 5.5.a: 2 GHz with a wall of 11 cm in width and permittivity of 4.

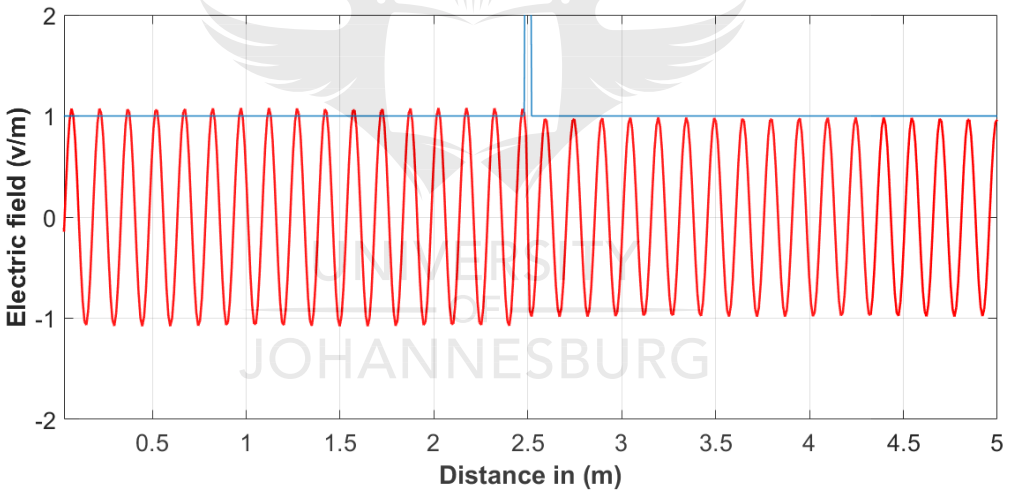

Figure 5.5.b: 2 GHz with a wall of 11 cm in width and permittivity of 4.

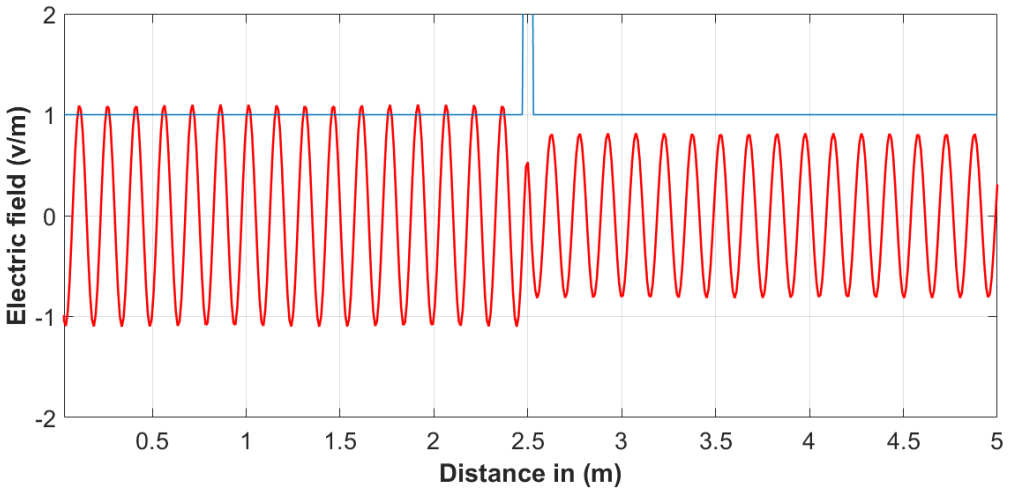

Figure 5.5: 2 GHz with a wall of 22 cm in width and permittivity of 4.

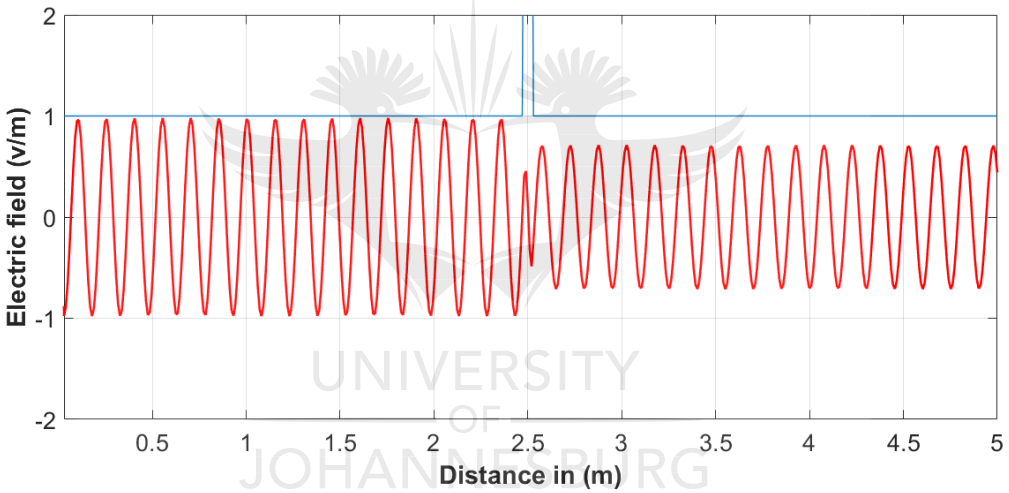

Figure 5.6: 2 GHz with a wall of 22 cm in width and permittivity of 5.

Observing Figures 5.5.a – 5.5.b, one can notice the difference in the signal attenuation compared to the previous simulation run in subsection a. At 2 GHz, with a wall width of 11 cm, the wall is almost transparent to the signal. The forwarding signal is around 95% compared to the incident signal. At this frequency the relative permittivity from 4 to 5 is not affecting the signal. On the other hand, in Figures 5.5.c and 5.5.d, at the same frequency, the forward signal is affected by the wall size and the permittivity. Though the forward signal is affected, the forward signal is 75% of the incident signal. This still makes the target detectable.

c) Simulation of the wall slab at 3 GHz with different wall width and permittivity

Figures 5.6. a - 5.6.d represent the simulation run at a frequency of 3 GHz. In Figures 5.6.a and 5.6.b the simulations are run with a wall of 11 cm in width, while in Figures 5.6.c and 5.6.d simulations are run with a wall with a width of 22 cm. In each case the relative permittivity has been modified.

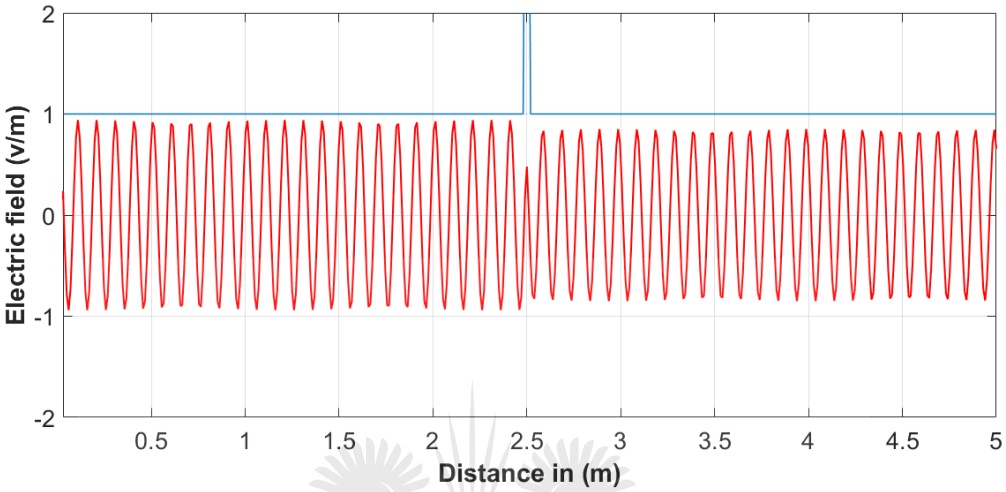

Figure 5.7: 3 GHz with a wall of 11 cm in width and permittivity of 4.

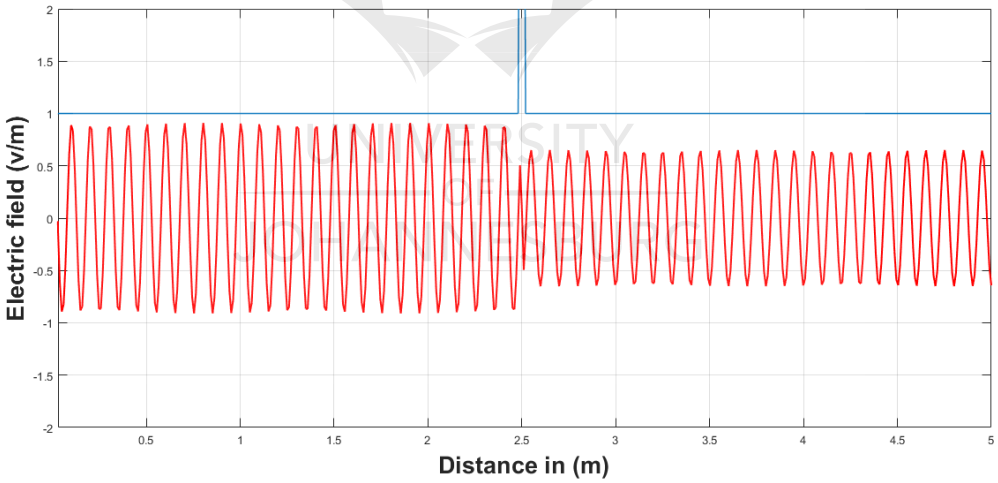

Figure 5.8: 3 GHz with a wall of 11 cm in width and permittivity of 5.

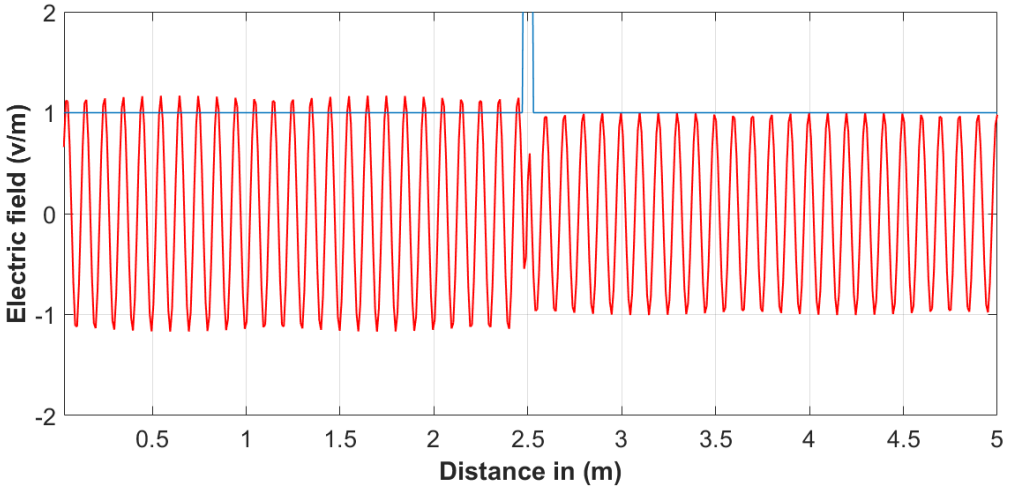

Figure 5.9: 3 GHz with a wall of 22 cm in width and permittivity of 4.

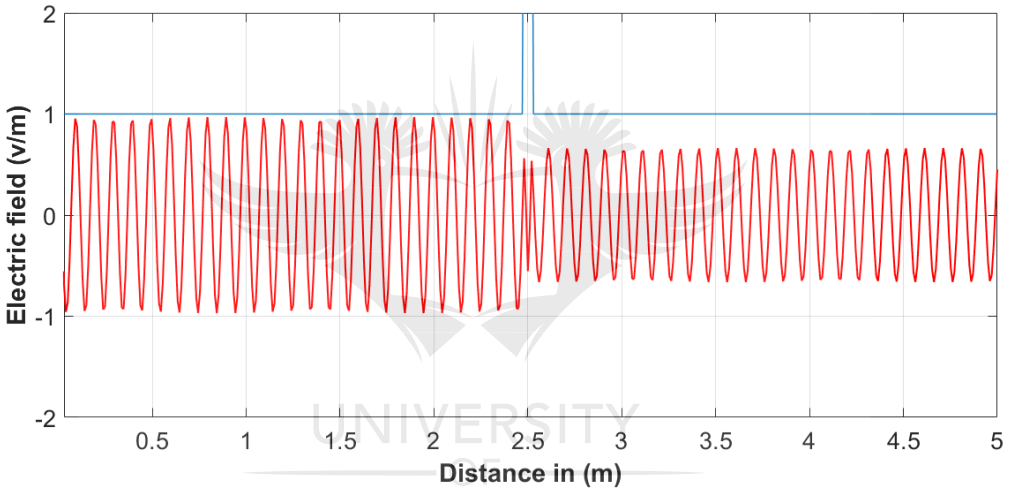

Figure 5.10: 3 GHz with a wall of 22 cm in width and permittivity of 5.

In Figure 5.6.a, one can observe that the forward signal is almost 95% of the incident signal. This means that the wall is transparent at this frequency and relative permittivity. In contrast, in Figure 5.6.b, at the same frequency and using a wall of the same width as in Figure 5.6.a, the signal is affected. This demonstrates that at certain frequencies the permittivity may influence the signal propagation. In Figure 5.6.c, the same phenomenon observed in Figure 5.6.a is observed, meaning that the width of the wall is not influencing the signal at this frequency. On the other hand, the forward signal in Figure 5.6.d is affected once the permittivity is changed. Therefore, the forward signal is strong enough to detect the target behind the wall.

5.3.2 Appliance attenuation and scattering experiment

Experimenting and simulating wall attenuation indicated that there are multiple materials the signal has to travel through before reaching the target. In households one frequently finds television sets (TV), refrigerators, fans, sofas, beds and other furniture and appliances. In the present case a TV, sofa or bed can easily be isolated because of their immobile nature. Since the researcher is using the micro-Doppler effect to detect human beings, immobile objects obstructing the target can be cancelled or regarded as clutter. On the other hand, an object such as a fan contains turning parts, which will produce a micro-Doppler effect. Thus, cancelling the fan's micro-Doppler effect is very important.

5.3.2.1 Scattering from moving object

In section 5.7 simulation of a human being is conducted. Different spectrograms of the human being return a signal while walking will be presented. Since the signal is expected to go through the wall, a home appliance, a fan, has been taken as one of the appliances that can produce significant disturbance to the signal. Thus, the following section investigates the signal return from a fan and rotating point target.

5.3.2.1.1 Three-point scattering

In this simulation, the researcher intends to determine the behaviour of a three-point scatterer when impinged on by an EM wave. Figure 5.7 represents three points scatterers presented in different colours. The first point in blue is placed in the centre of the line formed by the others. The second point is in green, rotating around the centre of the body, which is in the same position as the blue point. The last point is in red. The red point is rotating about the same point as the green one.

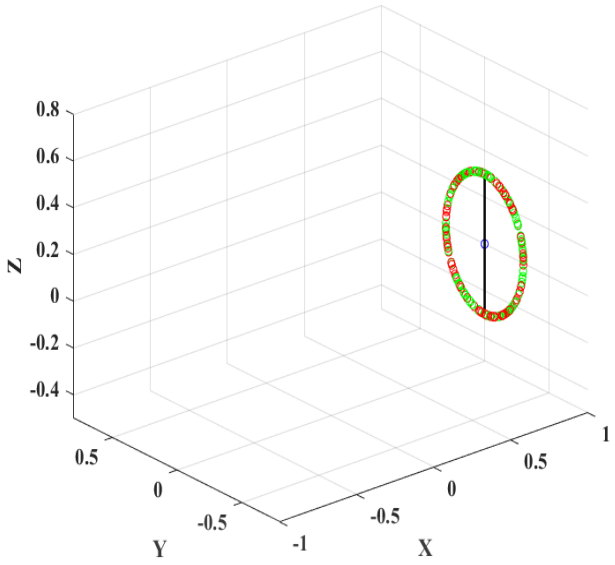

Figure 5.11: Representation of the three points in space.

In Figure 5.7, the radar is placed in front of the three points emitting the EM wave, while all the points are rotating about the centre. The radar is placed at 50 m from the centre of origin of the body-fixed system at a height of 2 m. The radar is transmitting a signal at a frequency of 2.4 GHz.

Figure 5.8 represents the micro-Doppler return of the three spinning point targets. The light solid line represents the first point, the dashed line the second point and the solid line the last target.

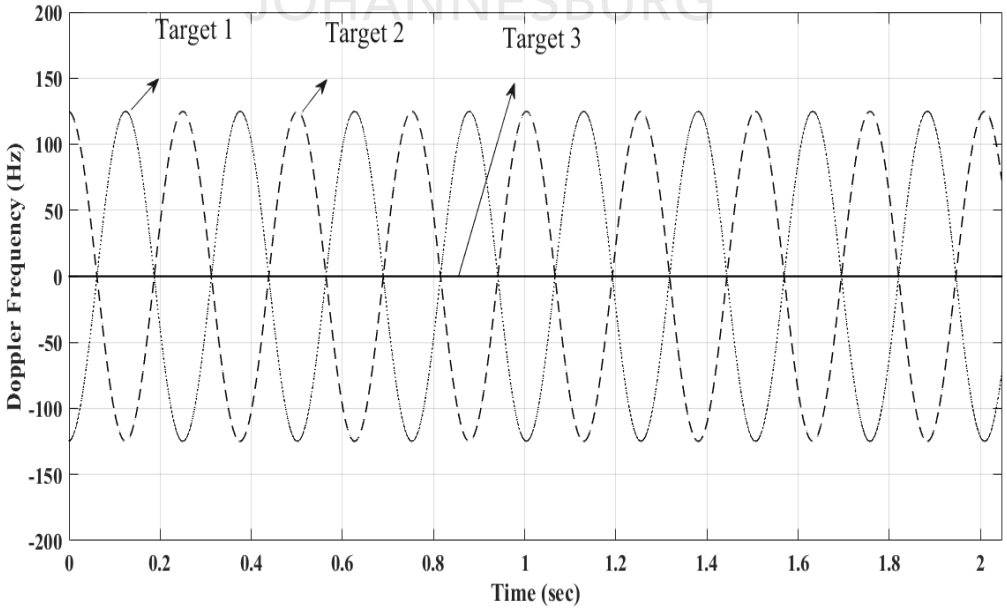

Figure 5.12: Micro-Doppler signature of three spinning point targets.

In Figure 5.8, it can be seen clearly that two points are exhibiting their micro-Doppler signature while the third one has a micro-Doppler effect of frequency 0 Hz. This is explained by the rotation about the centre of the body-fixed system. In addition, the centre of the body-fixed system is the position of the point. It means that its displacement is equal to zero, therefore the micro-Doppler frequency is zero.

5.3.2.2 Fan scattering

A simulation was run to detect the fan while rotating to find the return signal. A fan was chosen, as it is one of the appliances in the home environment and in this thesis micro-Doppler is used to detect activities inside a room. A fan can hide certain activities when a human is in front of this appliance.

Figure 5.8 represents the spectrogram of a fan with three blades. In this simulation, the researcher is transmitting a signal at a frequency of 2.4 GHz. The radar is placed 20 m from the fan and at a height of 2 m. The range resolution of the radar is 0.01 m. The fan is constructed with three rectangular metallic planes. For simplicity, to simulate the fan, the blades are considered to be flat and straight without any twist, as in the real world.

In Figure 5.9, one can observe the different blades of the fan. At this frequency the micro-Doppler radar frequency is in the frequency band of (400, -400 Hz). This frequency is justified by the fact that in equation (3.41) the Doppler frequency is related to the angular frequency. In short, (3.41) can be written as:

$$f_D = \frac{2 \cdot \Omega}{\lambda} = \frac{2 \cdot 25}{0.125} = 400Hz. \tag{5.10}$$

In the time axis the different blades can be seen. Therefore, if any human activities happen in the band of frequency at the same magnitude, some activities may be lost.

For this reason, the researcher ran another simulation, but this time with two blades to investigate how the signal could be affected with two blades of a rotating fan.

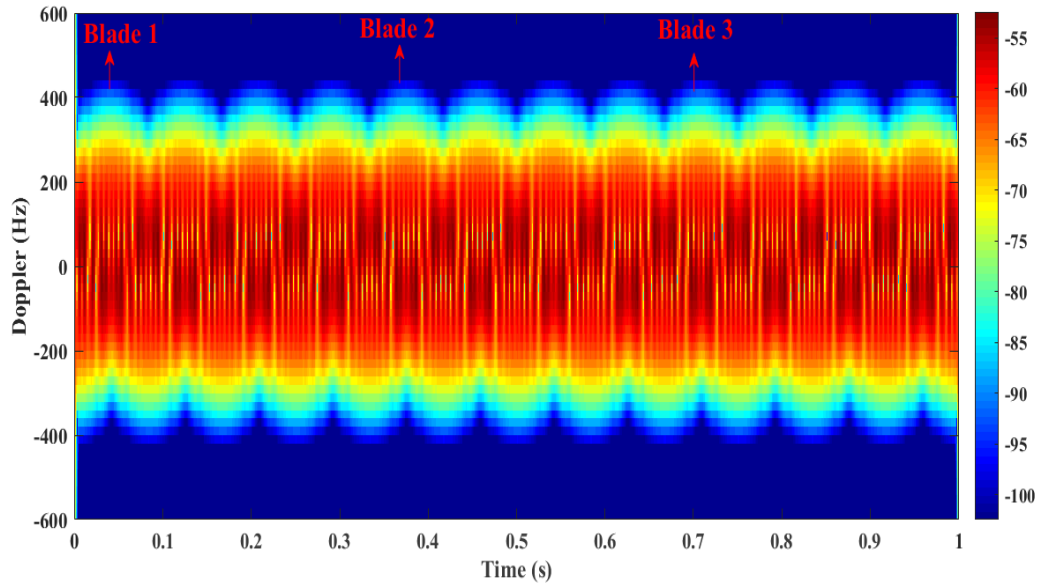

Figure 5.13: Fan with three blades spinning at 1500 rpm and radar working at 2.4 GHz.

Using the same setup of the simulation as in Figure 5.9, Figure 5.10 presents the spectrogram of the return signal of a fan with two rotating blades. One can see that the signal is in the same frequency band as the one in Figure 5.9. The main difference between Figures 5.9 and 5.10 is noticeable in the time domain. In the case of the three blades the spacing between the peaks is closer compared to the one with two blades.

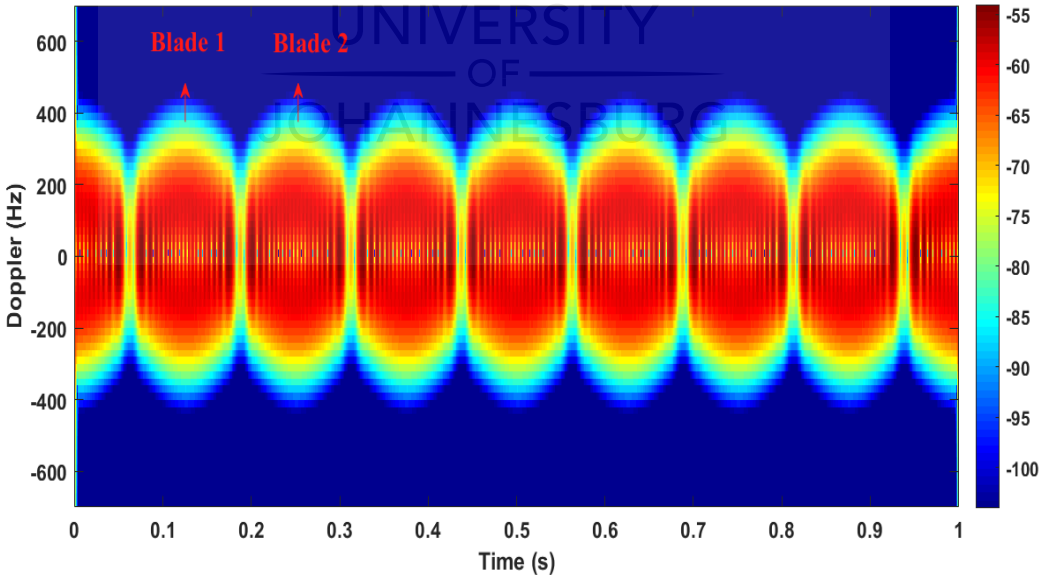

Figure 5.14: Fan with two blades spinning at 1500 rpm and radar working at 2.4 GHz.

Carrying out the simulation in the same conditions, but changing the frequency of the radar, influences the results. Figure 5.11 presents the spectrogram of a return signal for a three-blade rotating fan. The radar is transmitting its signal at a frequency of 20 GHz.

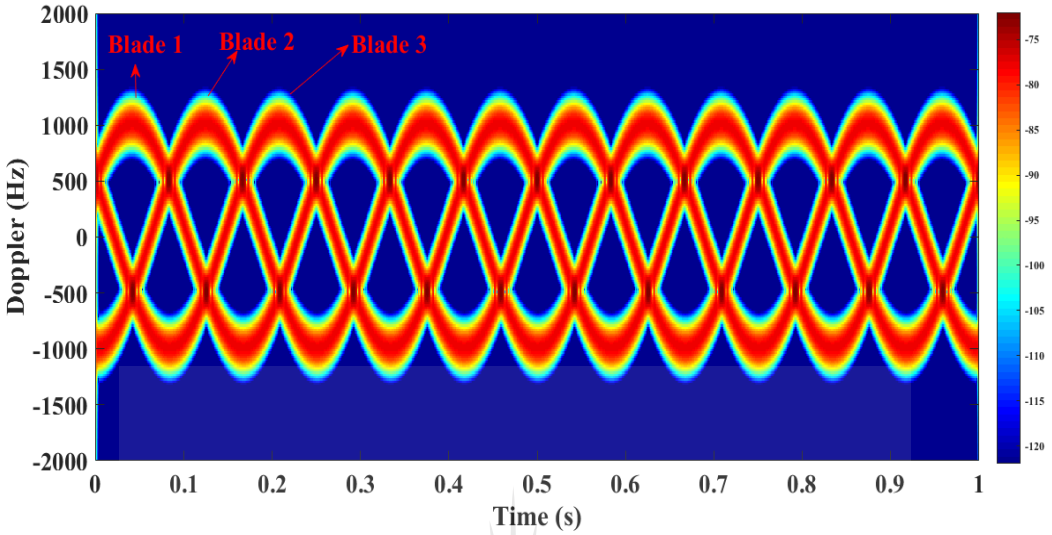

Figure 5.15: Fan with three blades spinning at 1500 rpm and radar working at 20 GHz.

By observing Figure 5.11, one can distinguish the three blades of the fan and even the corresponding blades better than while the radar is transmitting its signal at 2.4 GHz. Figure 5.11 also reveals the lapse of time between the different amplitude of frequencies of blades.

Figure 5.12 represents a two-blade simulation. This simulation is run in the same conditions as that illustrated in Figure 5.11, except that the number of blades is different. It has to be mentioned that all these simulations are run in a time of 1 second.

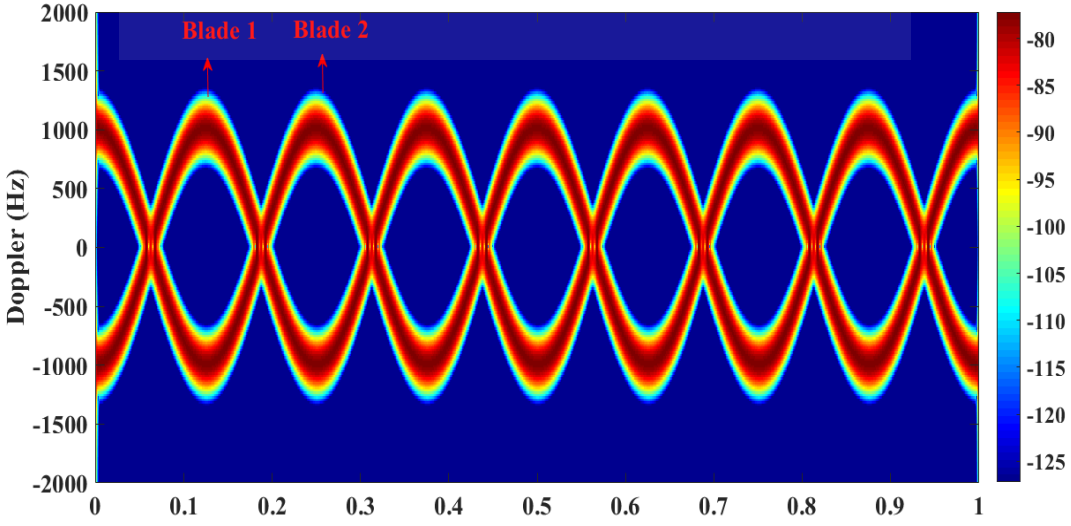

Figure 5.16: Fan with two blades spinning at 1500 rpm and radar working at 20 GHz.

By observing Figure 5.9 and Figure 5.11, one can detect the same number of ridges on both figures. Therefore, for the three-blade experiment, the entire simulation of 1 second comprises 12 ridges, while for the two blades nine ridges are observed for the same lapse of time. Thus, using a frequency of 2.4 GHz will enable one to detect the micro-Doppler of the fan, but not to classify the signal properly. In contrast, using a frequency of 20 GHz in the same conditions yields clear imaging of the three blades. While one can choose the frequency of 20 GHz for its capability to classify the target of interest, this might be affected when going through the wall.

Figure 5.10 and Figure 5.12 display the same similitude as Figure 5.9 and Figure 5.11. The entire simulation contains eight maximum amplitudes of all blades.

Hence, care is necessary when dealing with the radar return signal coming from a fan and human being overlapping in the time and frequency domain. The next section deals with radar return from a human being. As both human beings and fans may be found in space in different ranges, individual analyses of the fan and the human being are necessary. Therefore, the next section is devoted to radar return from the human being without the presence of the fan.

5.4 HUMAN SCATTERING

The target in this study is the human being. Simulations and experiments and the results of the examination of different materials through which the signal will pass before reaching the target are presented in Section 5.3. This section investigates the scattering of the EM wave on a human being. Because the target is human, the amount of EM wave energy to which the person is exposed has to be chosen carefully. In this area, the measurement of the amount of radio frequency (RF) energy absorbed by a body when using a wireless device is called the specific absorption rate. Thus, the values are:

- Whole body: 4 w/kg per minute exposure average,
- Head and torso: 3 w/kg per 5 minutes exposure per gram of tissue,
- Extremities: 12 w/kg per 5 minutes exposure per gram of tissue.

The following subsection is devoted to respond to the second and third research questions. The research questions are repeated here:

a) How can one detect a physically weak victim after an earthquake while the person's breathing and heartbeat signal strength is weak?

b) How can one detect a target with a lower chest RCS, such as a child?

After an earthquake the target is assumed to be breathing even though the breathing might be weak. The chest movement is a source of a micro-Doppler and will be simulated in the following section. On the other hand, to detect a low chest RCS, children are simulated in order to analyse the return signal.

5.4.1 Simulation of a walking human

In this section, multiple simulations were run to determine the effect of human height and radar responses. In addition to the height, simulation on two different frequencies was conducted to evaluate the human return signal in relation to the height and frequency. This section was divided into two subsections:

a) The simulation of a walking human being with a radar transmit frequency of 2.4 GHz with a resolution range of 0.5 m. This frequency was chosen as it is the frequency at which the built radar works.
b) The second section simulated a walking human being at a radar transmit frequency of 15 GHz with a resolution range of 0.01 m. This frequency was chosen in order to achieve a fine resolution range to be able to detect fine vibration.

5.4.1.1 Simulation of walking human with 2.4 GHz radar with 0.5 m resolution range

The following simulations were conducted with a radar frequency of transmission at 2.4 GHz. The transmit frequency was kept at 2.4 GHz while varying the height of the human and the velocity. Knowing that the fastest human in world can run at 10.43 m per second, the velocity used for this simulation was from 0.5 to 3 m/sec, as it was assumed that the possibility of finding a human running in the building was very low. The height varied because the researcher considered that people of different ages might be found inside the building. Considering that a human being with a height of 1 m can walk, 1 m was chosen as the starting height because below that height a human being may not be able to walk [102]. From an initial height of 1 m the researcher considered an additional 30 cm as reasonable to give the difference in the spectrum return signal. Therefore 1 m, 1.3 m, 1.6 m and 1.9 m were retained as simulation test height; 1.9 m was taken as the limit, because in only rare cases can one find people taller than 1.9 m. The following figures show the height mentioned with the model. For this simulation, the radar is located at position (X=10 m, Y=0 m, Z=2 m), while the human is located at the origin of the body fixed

system (X=0 m, Y=0 m, Z=0 m). In these simulations, the researcher is using the human model presented in [97].

Figure 5.17: 1 m walking human.

Figure 5.18: 1.3 m walking human.

Figure 5.19: 1.6 m walking human.

Figure 5.20: 1.9 m walking human.

5.4.1.1.1 Simulation of a walking human of 1 m at different velocities

In Figures 5.17 to 5.22, a 1 m human is simulated at different relative velocities. The velocities at which the human is walking are 0.5 to 3m/sec, increasing each time by 0.5 m/sec.

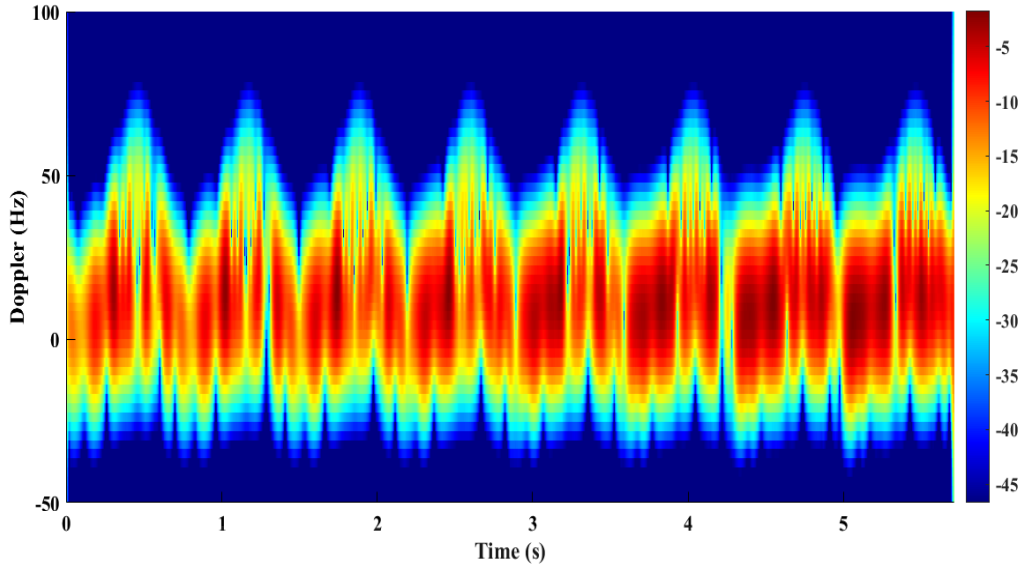

Figure 5.21: Micro-Doppler signature of 1 m human (child) at relative speed of 0.5 m/sec.

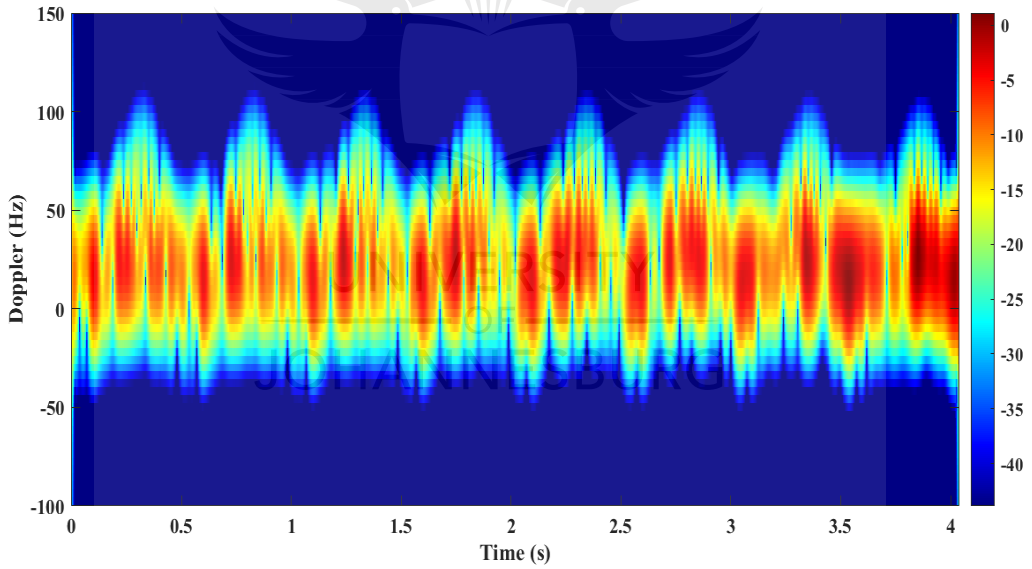

Figure 5.22: Micro-Doppler signature of 1 m human (child) at relative speed of 1 m/sec.

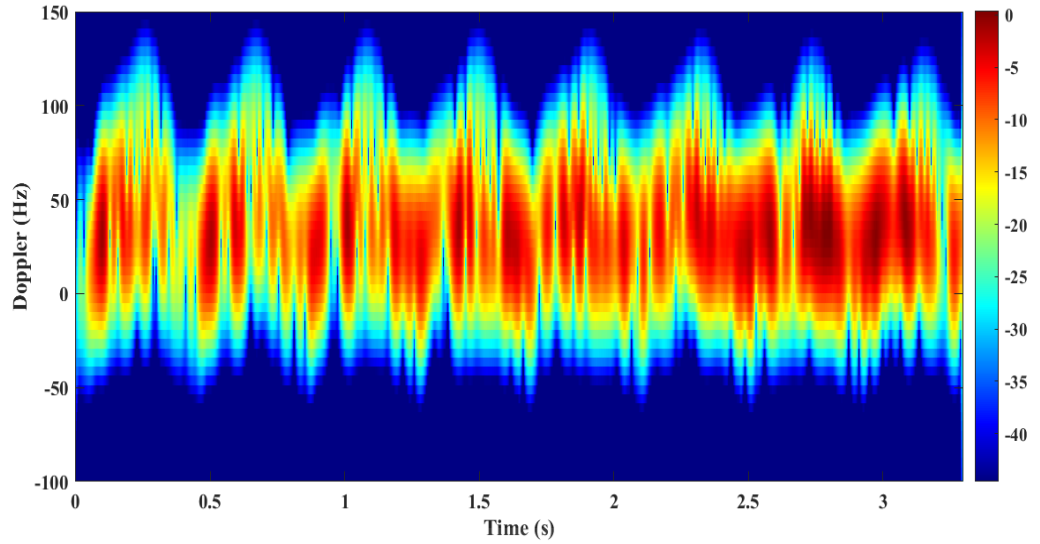

Figure 5.23: Micro-Doppler signature of 1 m human (child) at relative speed of 1.5 m/sec.

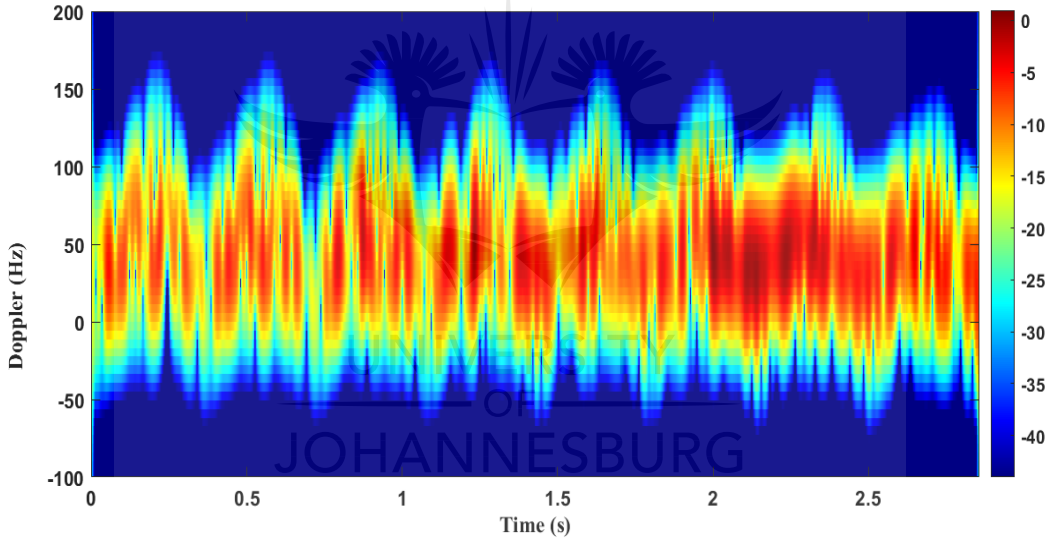

Figure 5.24: Micro-Doppler signature of 1m human (child) at relative speed of 2 m/sec.

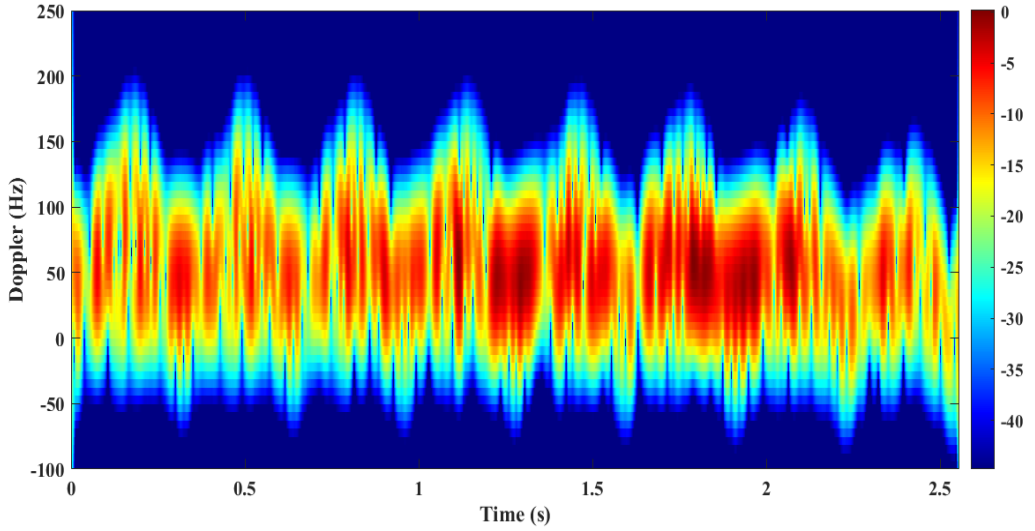

Figure 5.25: Micro-Doppler signature of 1 m human (child) at relative speed of 2.5 m/sec.

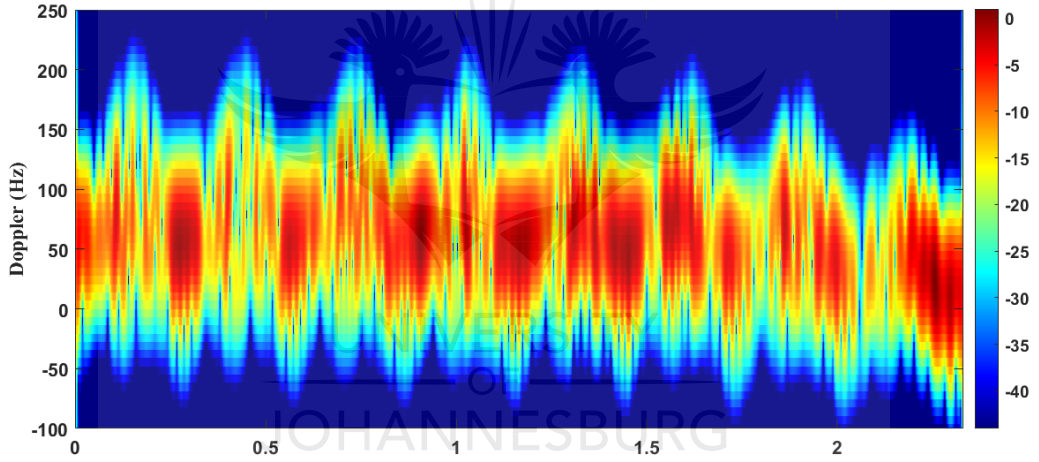

Figure 5.26: Micro-Doppler signature of 1 m human (child) at relative speed of 3 m/sec.

From Figures 5.17 to 5.22, one can see that in the frequency domain there are some small peaks of Doppler shift that are happening at a regular time interval. These peaks are the return signals from the legs, which are exhibiting high Doppler frequency return. At a lower speed the peaks' variation is found to be around 0 in the frequency domain. This can be observed in Figures 5.17 to 5.18. The return signal from the limbs is slightly clearer in Figures 5.19 to 5.22, but although some peaks are visible, there is no possibility of distinguishing the Doppler return from the different limbs. The results demonstrated that even though frequencies lower than 3 GHz are recommended for through-the-wall radar [4-13], extra care has to be taken because the height of the target could affect the results. Following these simulations, though the centre frequency of the radar has to be chosen

with care, the relative velocity of the target is another variable to take in consideration. While choosing the operating frequency of the radar, care has to be taken because the velocity of the target is proportional to the micro-Doppler return. The velocity may influence the detectability of the target unless the frequency has been well chosen.

5.4.1.1.2 Simulation of a walking human of 1.3 m at different velocities

In Figures 5.23 to 5.28, a 1.3 m human is simulated at different relative velocities. The velocities at which the human is walking are 0.5 to 3m/sec, increasing each time by 0.5 m/sec.

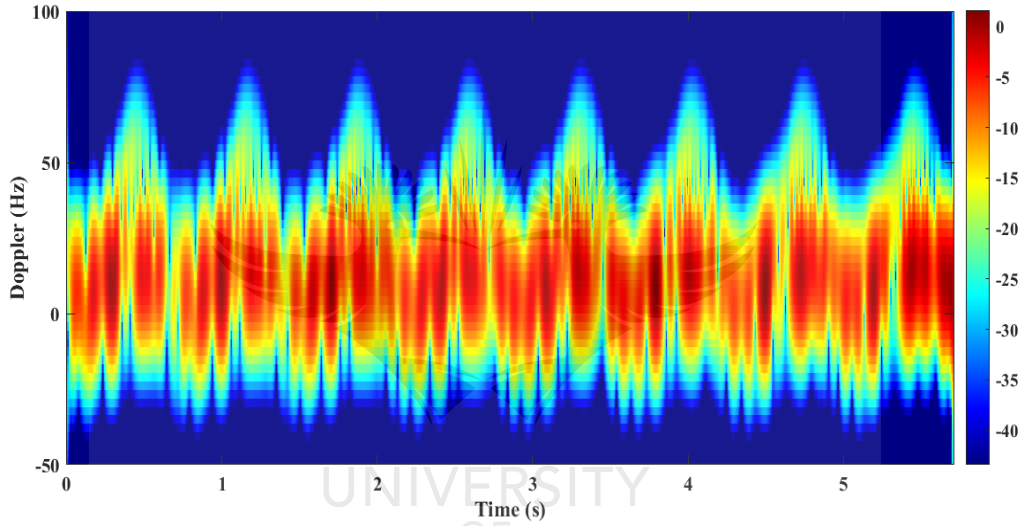

Figure 5.27: Micro-Doppler signature of 1.3 m human at relative speed of 0.5 m/sec.

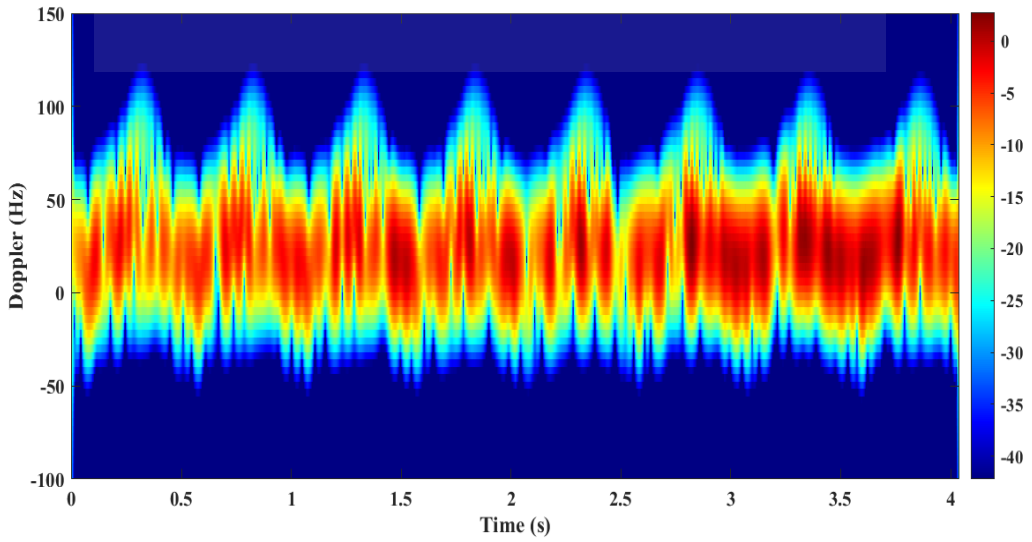

Figure 5.28: Micro-Doppler signature of 1.3 m human at relative speed of 1 m/sec.

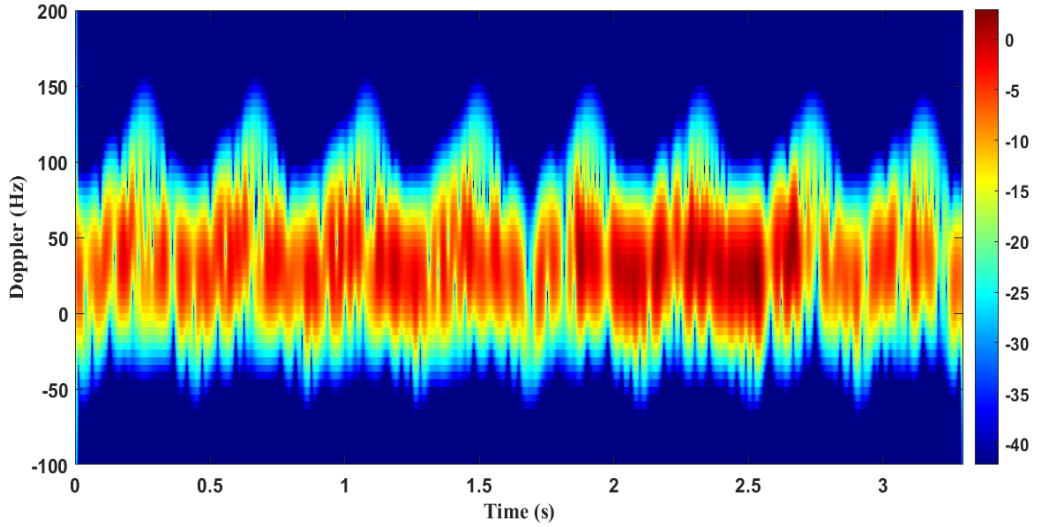

Figure 5.29: Micro-Doppler signature of 1.3 m human at relative speed of 1.5 m/sec.

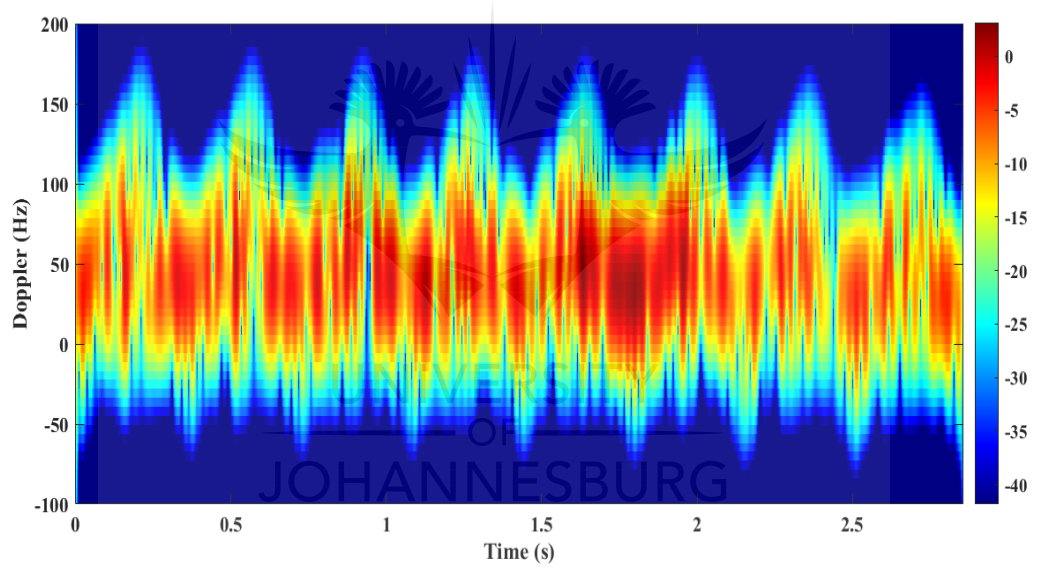

Figure 5.30: Micro-Doppler signature of 1.3 m human at relative speed of 2 m/sec.

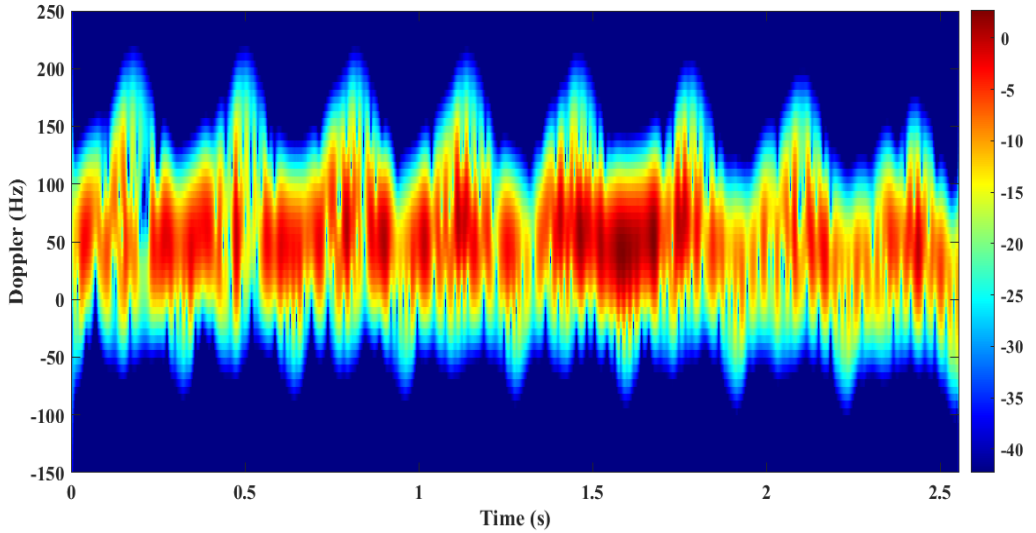

Figure 5.31: Micro-Doppler signature of 1.3 m human at relative speed of 2.5 m/sec.

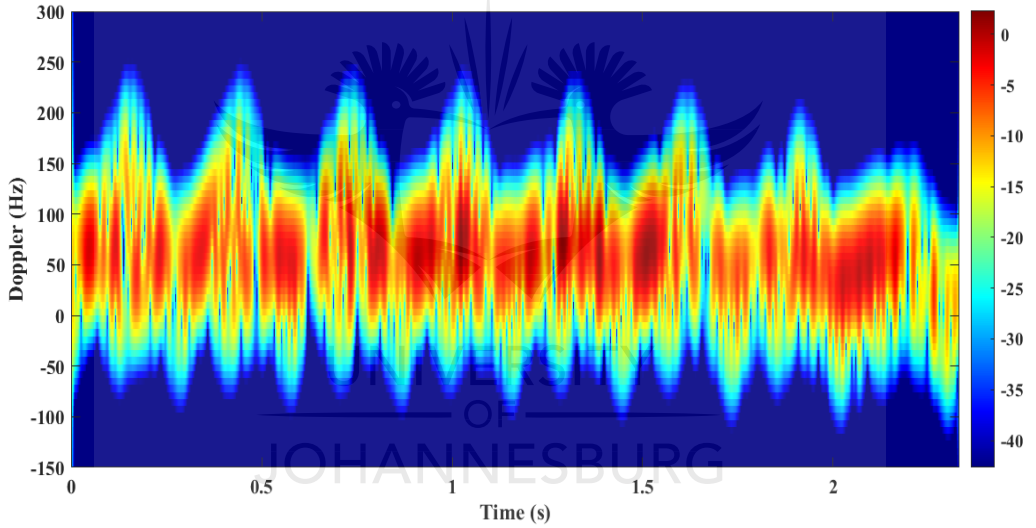

Figure 5.32: Micro-Doppler signature of 1.3 m human at relative speed of 3 m/sec.

In this simulation, compared to the simulation involving a 1 m tall human, one can observe that there are higher peaks coming from the legs and the hands. The red colour shows the torso and the rest of the body separately. Thus, different methods of analysing particular limb behaviour require different methods from the short-time Fourier transform to the Wigner distribution function. One can see that there is activity but there is no possibility to confirm whether it is a human being, even though the legs peaks are visible. In addition, this simulation sustains the researcher's statement on the consideration of the height in TWR. Research conducted in [4-13] did not take the height of the target into consideration. Thus, this work contributes to the body of knowledge by highlighting the height-frequency trade-off influencing the micro-Doppler returns.

5.4.1.1.3 Simulation of a walking human of 1.6 m tall at different velocities

In Figures 5.29 to 5.34, a 1.6 m tall human is simulated at different relative velocities. The velocities at which the human being is walking are 0.5 to 3m/sec, increasing each time by 0.5 m/sec.

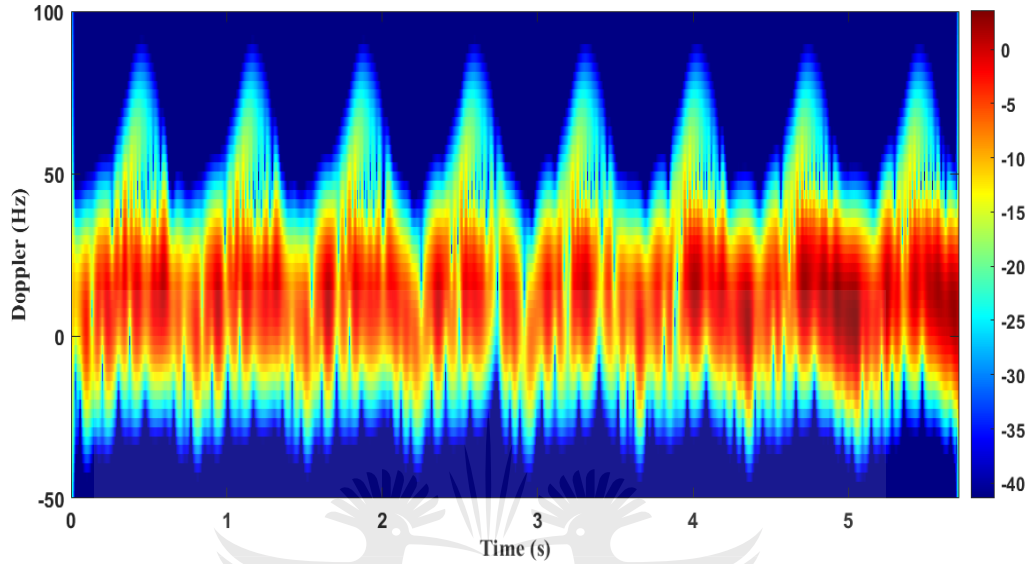

Figure 5.33: Micro-Doppler signature of 1.6 m human at relative speed of 0.5 m/sec.

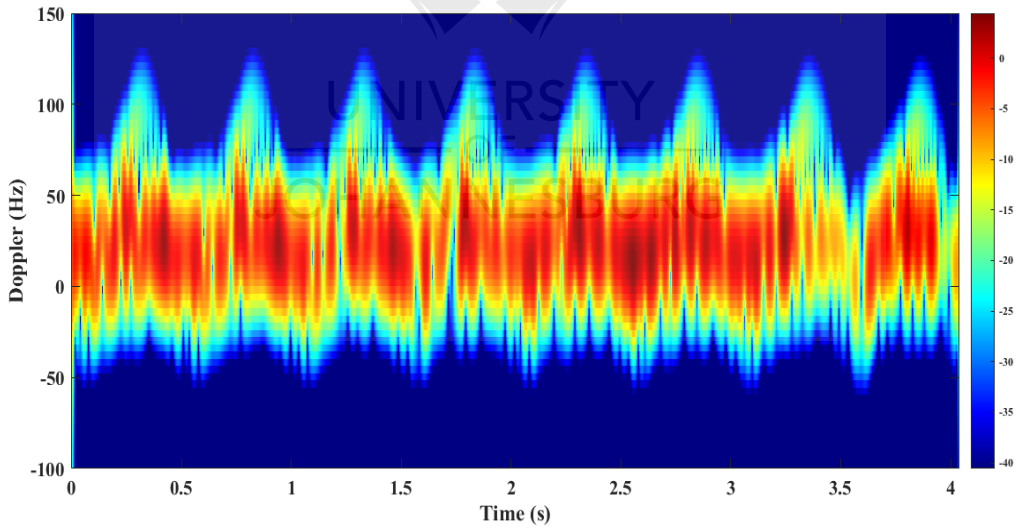

Figure 5.34: Micro-Doppler signature of 1.6 m human at relative speed of 1 m/sec.

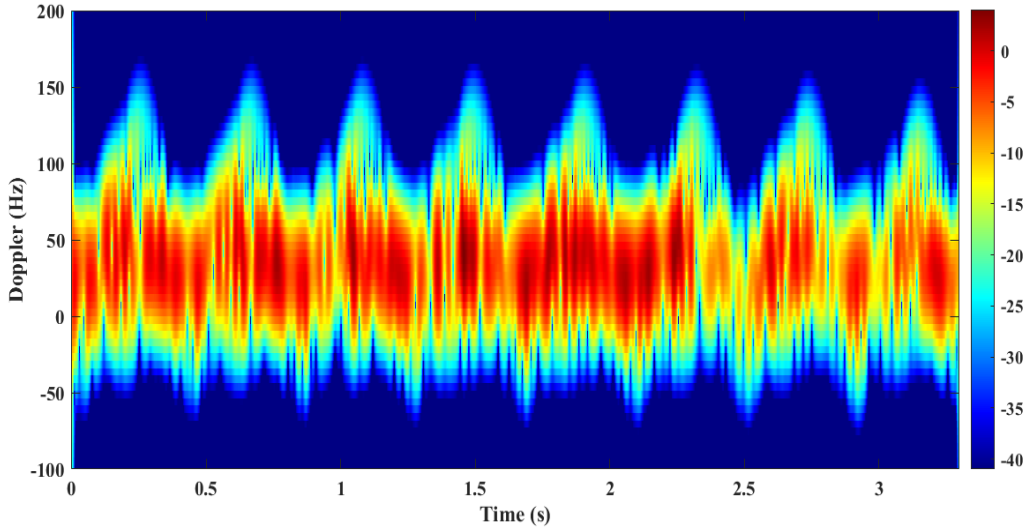

Figure 5.35: Micro-Doppler signature of 1.6 m human at relative speed of 1.5 m/sec.

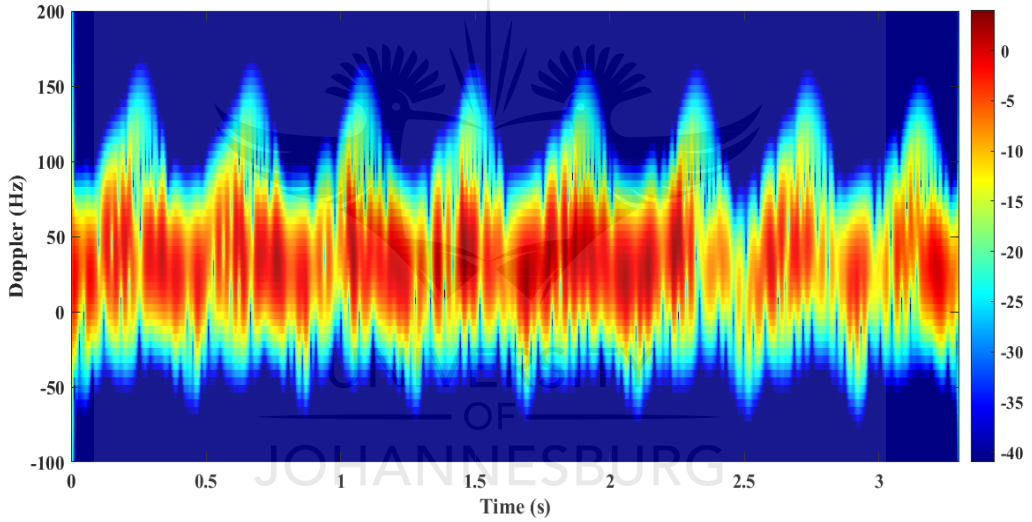

Figure 5.36: Micro-Doppler signature of 1.6 m human at relative speed of 2 m/sec.

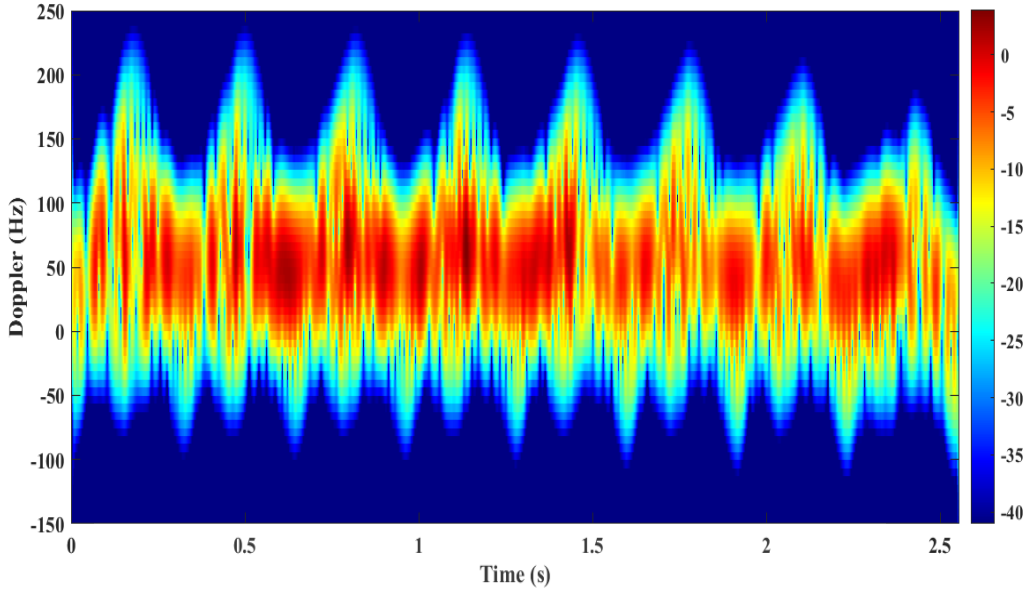

Figure 5.37: Micro-Doppler signature of 1.6 m human at relative speed of 2.5 m/sec.

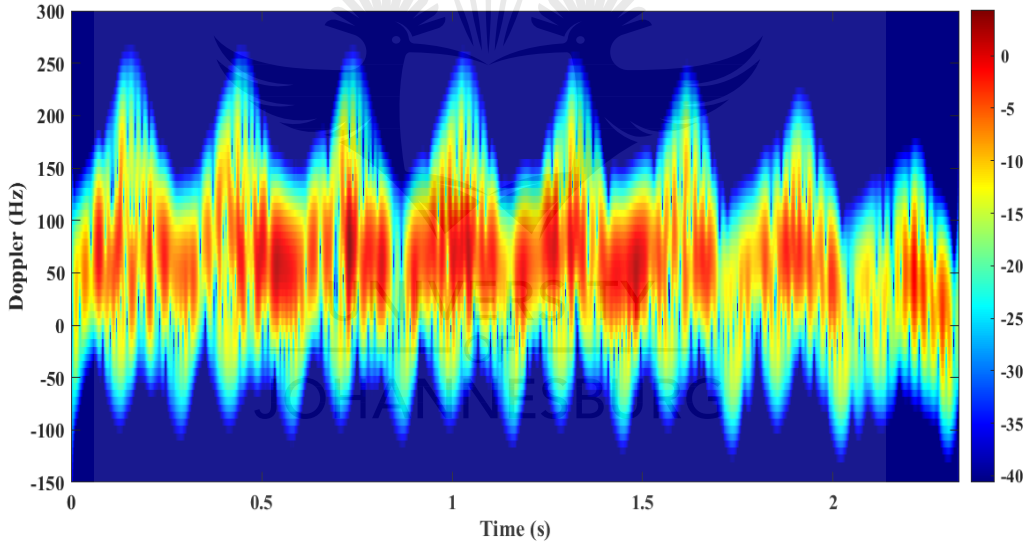

Figure 5.38: Micro-Doppler signature of 1.6 m human at relative speed of 3 m/sec.

The difference between the return signal from humans measuring 1.3 m and 1.6 m is not much. At a low speed of 0.5 m/sec the micro-Doppler shift is between 90 Hz and 100 Hz for both cases, which does not show much difference between the two spectrograms. Comparing the return signal at a velocity of 3 m/sec while at a height of 1.3 m, the micro-Doppler shift peaks are about 220 Hz, and at a height of 1.6 m the micro-Doppler shift peaks are about 250 Hz. Thus, one can say that from 1.3 m to 1.6 m the difference is not a great deviation from the lower height.

In contrast to the height of 1.3 m, the difference in the spectrograms from a human of 1 m to one of 1.6 m is prominent. Thus, one can observe a micro-Doppler shift with peaks about 70 Hz for a 1 m tall human walking at 0.5 m/sec, whereas a micro-Doppler shift at the same velocity but at a different height of 1.6 m resulted in 90 Hz micro-Doppler. With this result a 20 Hz difference can be observed, indicating a much higher probability of missing a target owing to its height.

5.4.1.1.4 Simulation of a walking human of 1.9 m with different velocities

In Figures 5.35 to 5.40, a 1.9 m tall human is simulated at different relative velocities. The velocities at which the human is walking are 0.5 to 3m/sec, increasing each time by 0.5 m/sec.

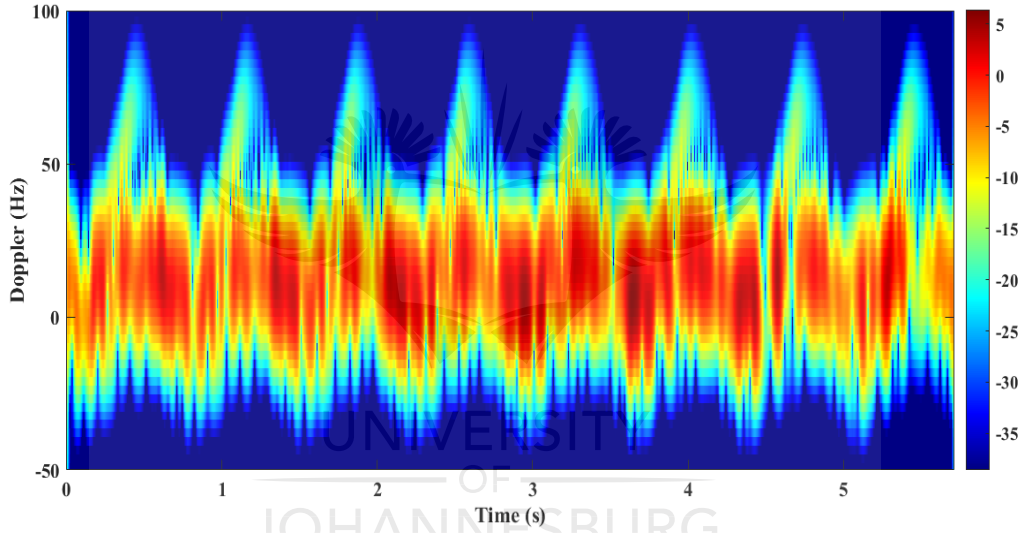

Figure 5.39: Micro-Doppler signature of 1.9 m human at relative speed of 0.5 m/sec.

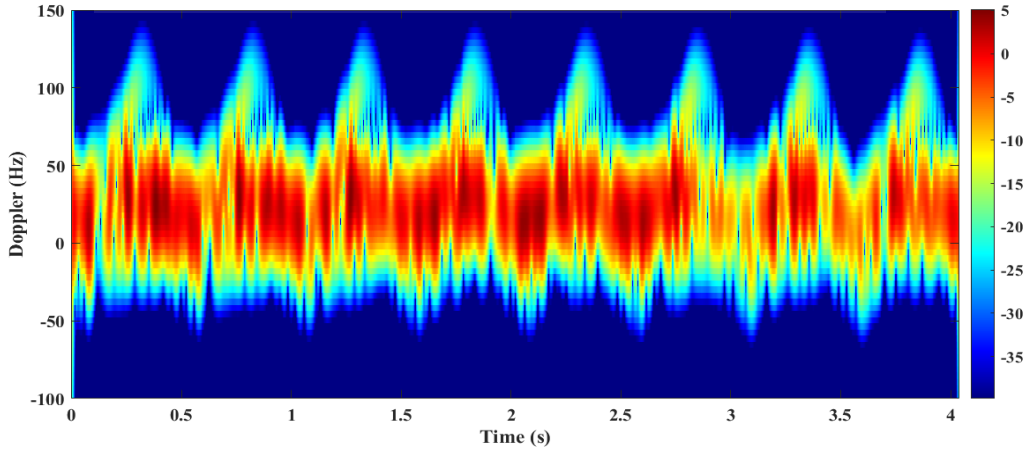

Figure 5.40: Micro-Doppler signature of 1.9 m human at relative speed of 1 m/sec.

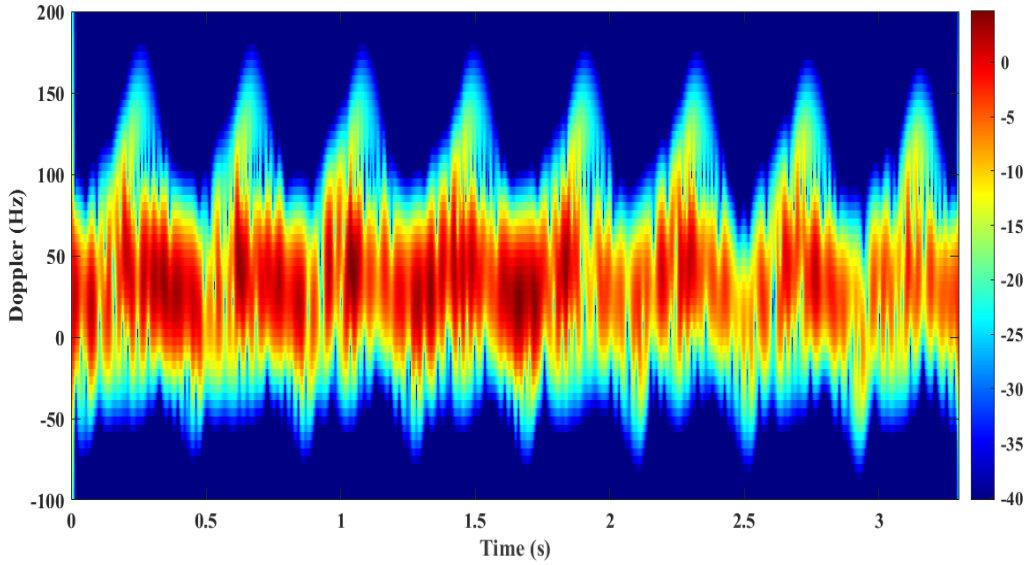

Figure 5.41: Micro-Doppler signature of 1.9 m human at relative speed of 1.5 m/sec.

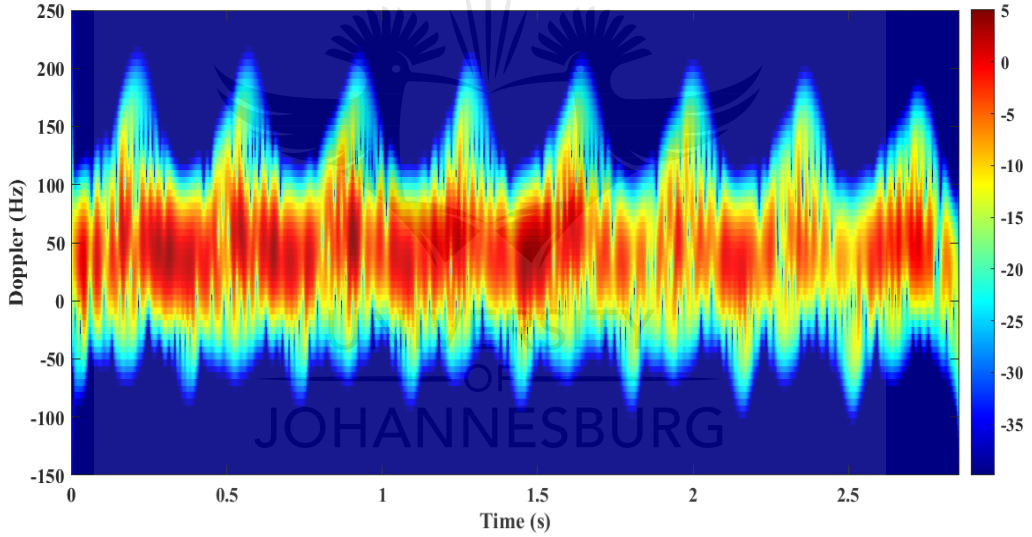

Figure 5.42: Micro-Doppler signature of 1.9 m human at relative speed of 2 m/sec.

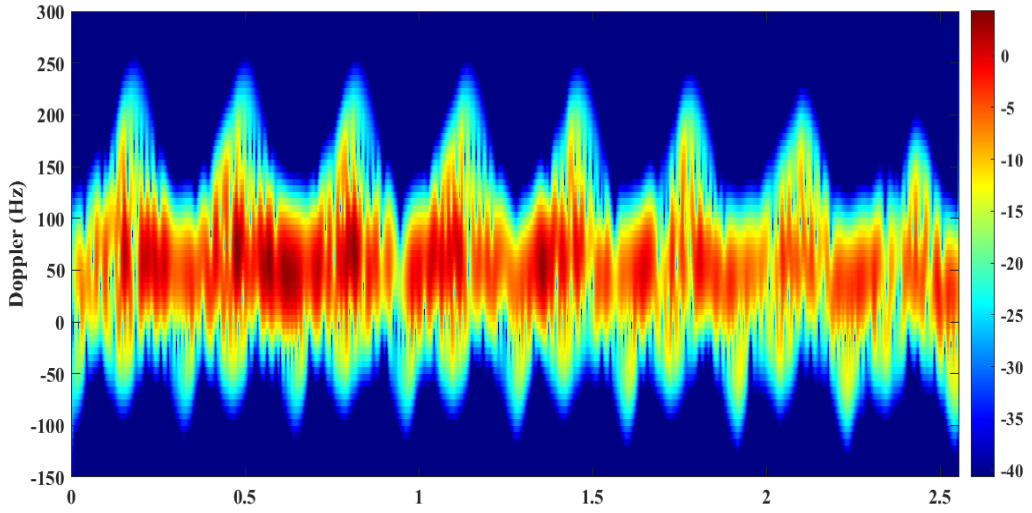

Figure 5.43: Micro-Doppler signature of 1.9 m human at relative speed of 2.5 m/sec.

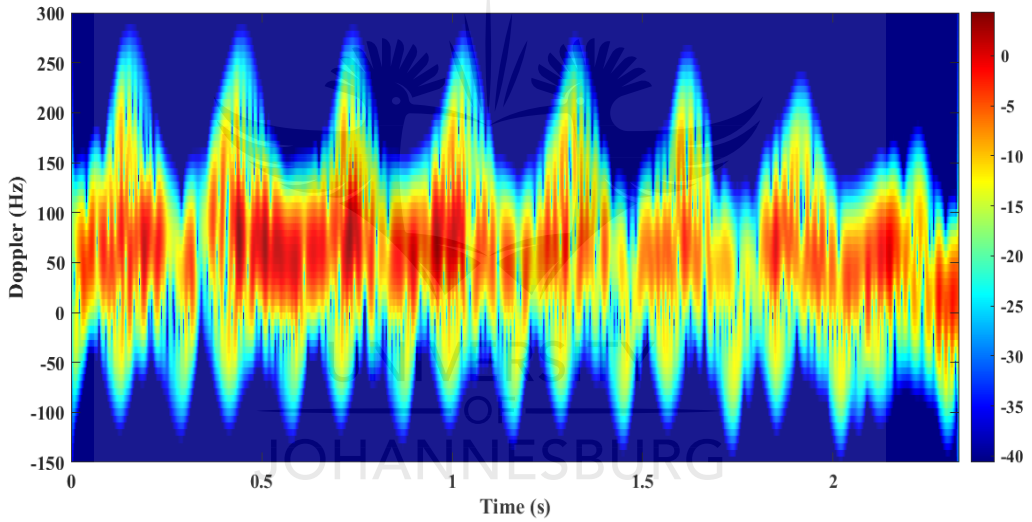

Figure 5.44: Micro-Doppler signature of 1.9 m human at relative speed of 3 m/sec.

Finally, at a frequency of 2.4 GHz, a simulation was run with a 1.9 m tall human being. This simulation revealed that height is a factor that cannot be neglected while investigating the human micro-Doppler.

At a lower speed of 0.5 m/sec, a human of 1 m tall recorded 70 Hz, one of 1.3 m recorded 80 Hz, one of 1.6 m recorded 90 Hz and eventually one of 1.9 m recorded 100 Hz. Thus, there is a significant difference from a human measuring 1 m to one of 1.9 m. This difference is justified by the length of the limbs. A 1 m tall human has short limbs, which produce lower micro-Doppler frequency shift. Contrary to one of 1 m, a person of 1.9 m exhibits higher micro-Doppler frequency shift due to the long limbs.

Another important observation that has to be mentioned is the chance of distinguishing the different limbs from the spectrogram observation. By observing all the spectrograms at 2.4 GHz, one cannot differentiate the limbs with accuracy. One can conclude that using a 2.4 GHz frequency as the centre frequency of the radar would allow one to detect a human but not to classify the return signal. At 2.4 GHz, the possibility of differentiating the micro-Doppler coming from the legs and hands is low while using the short-time Fourier transform (STFT). Therefore, the next section is devoted to another simulation at a higher frequency than 2.4 GHz. The simulation at a higher frequency than 2.4GHz enables one to analyse different spectrograms in respect of the frequency.

5.4.1.2 Simulation of a walking human at 15 GHz radar with 0.01 m resolution range

The following simulations are conducted with a radar centre frequency of transmission at 15 GHz. The transmit frequency has been kept at 15 GHz while varying the height of the human and the velocity. The velocity used for this simulation varies from 0.5 to 3 m/sec, as in the simulation at 2.4 GHz centre frequency. The height varies as well, as in the simulation at 2.4 GHz centre frequency from 1 m to 1.9 m. Therefore, 1 m, 1.3 m, 1.6 m and 1.9 m have been retained as simulation test height. Figures 5.13 to 5.16 showed the corresponding height with their model. For this simulation, the radar is located at position (X=10 m, Y=0 m, Z=2 m), while the human is located at the origin of the body fixed system (X=0 m, Y=0 m, Z=0 m). These simulations made use of the human model presented in [97].

5.4.1.2.1 Simulation of a walking human of 1 m tall at different velocities

From Figures 5.41 to 5.46, a 1 m tall human is simulated at different relative velocities. The velocities at which the human is walking are 0.5 to 3m/sec, increasing each time by 0.5 m/sec.

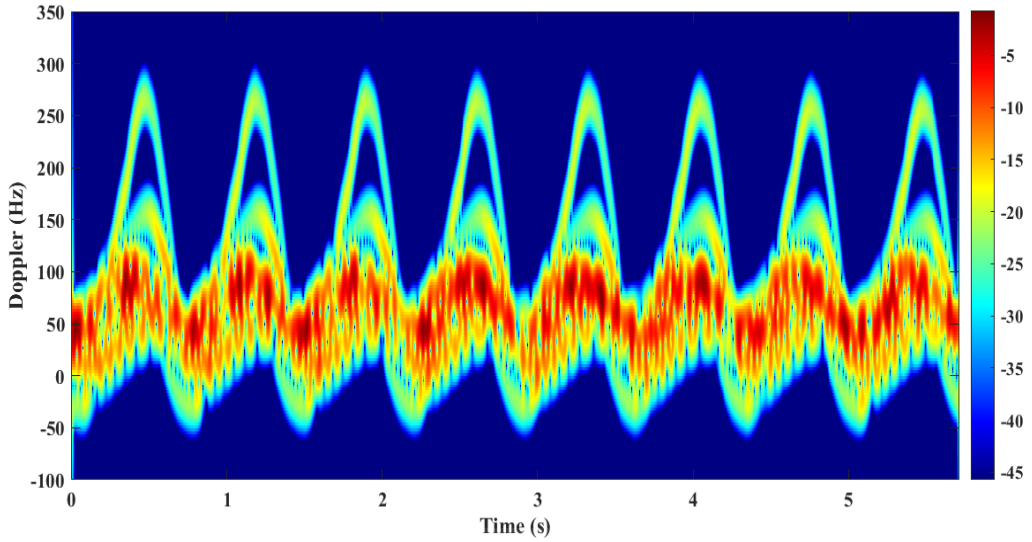

Figure 5.45: Micro-Doppler signature of 1 m human at relative speed of 0.5 m/sec.

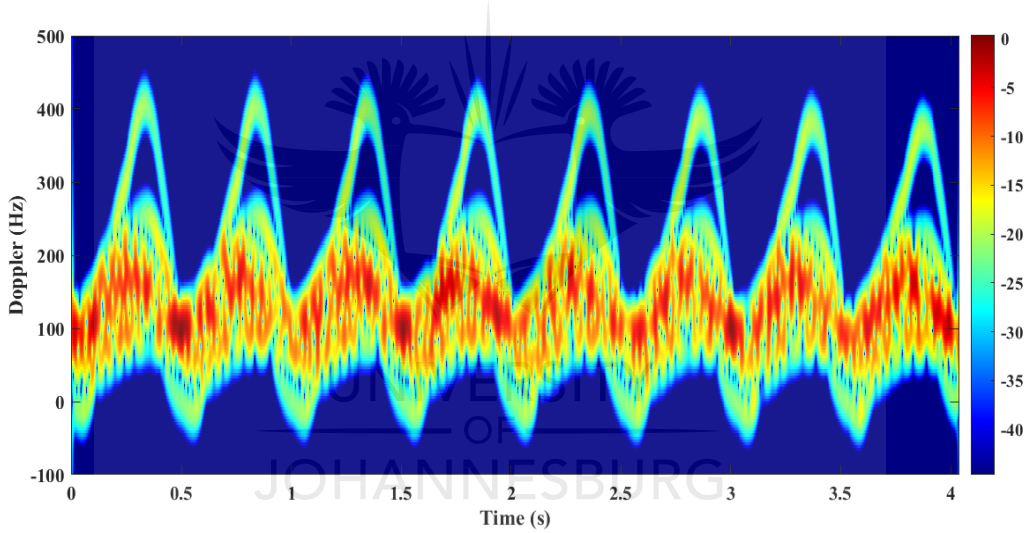

Figure 5.46: Micro-Doppler signature of 1 m human at relative speed of 1 m/sec.

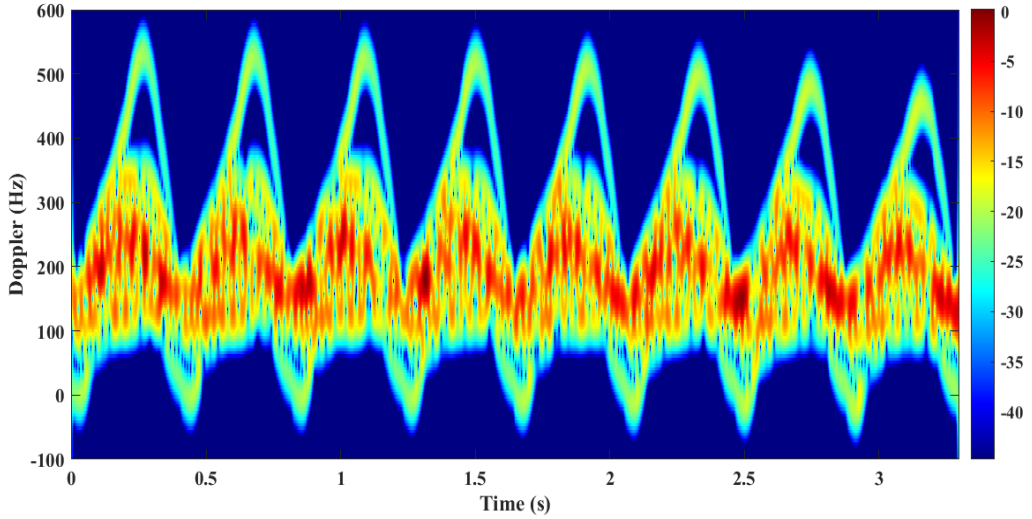

Figure 5.47: Micro-Doppler signature of 1 m human at relative speed of 1.5 m/sec.

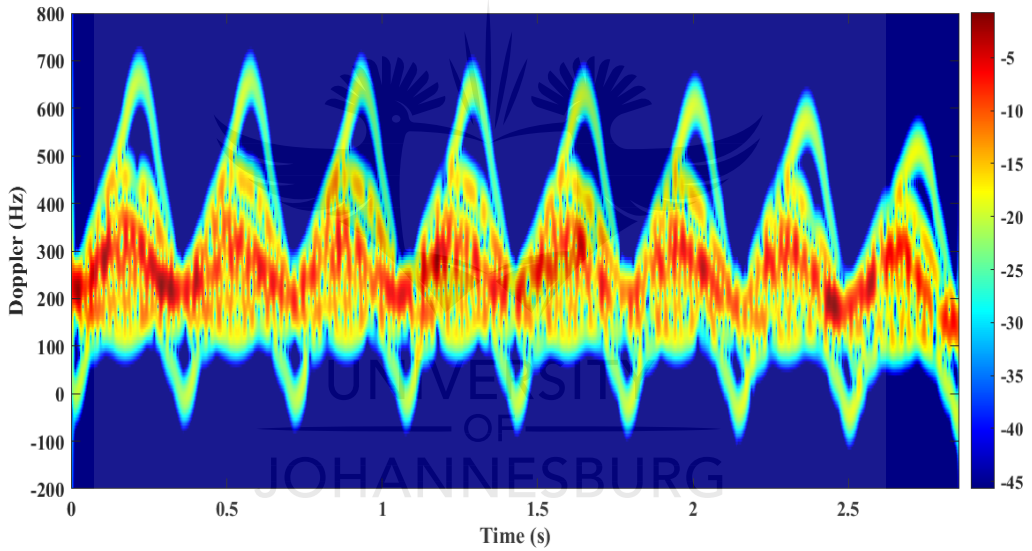

Figure 5.48: Micro-Doppler signature of 1 m human at relative speed of 2 m/sec.

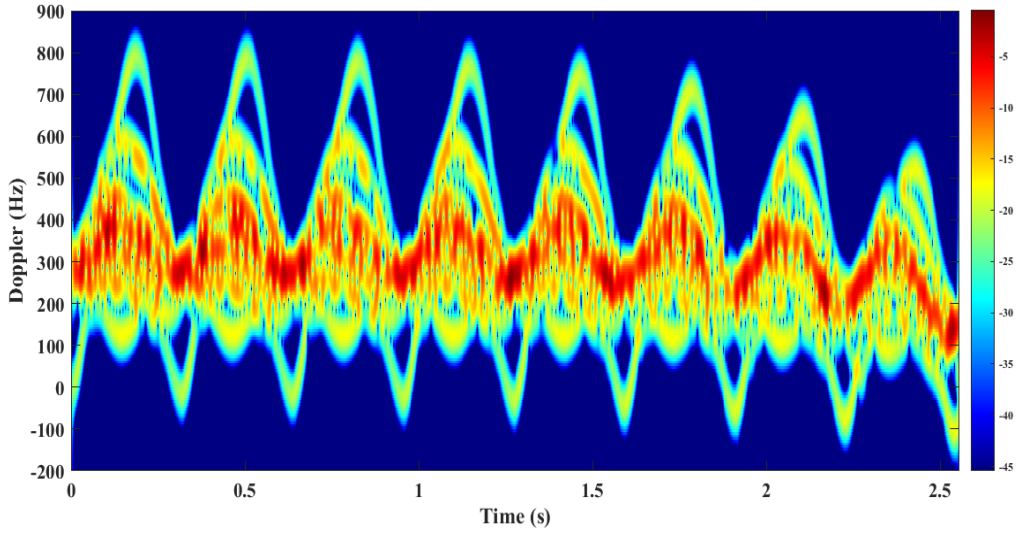

Figure 5.49: Micro-Doppler signature of 1 m human at relative speed of 2.5 m/sec.

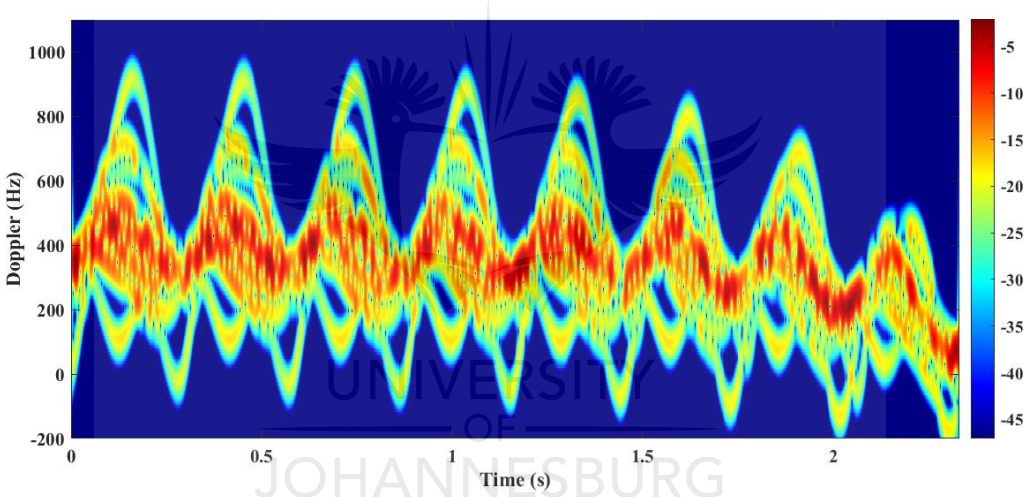

Figure 5.50: Micro-Doppler signature of 1 m human at relative speed of 3 m/sec.

By simply changing the operational frequency of the radar, one can observe how great the difference is when the radar is working at 2.4 GHz and when it is working at 15 GHz. Even at a velocity as low as 0.5 m/sec one is able to differentiate between the return signal coming from the legs and the one coming from the arms. In addition, using high frequency allows one to distinguish the different limbs from the torso. The torso spectrogram is seen clearly and is distinguishable from the legs and arms.

Furthermore, while at 2.4 GHz with a velocity of 0.5 m/sec the target modulated the signal to obtain the micro-Doppler frequency shift of 70 Hz, at 15 GHz the same velocity gave a micro-Doppler shift peak of 300 Hz. This micro-Doppler frequency is even higher than the

micro-Doppler generated by an adult human while radar is transmitting at 2.4 GHz frequency.

5.4.1.2.2 Simulation of a walking human of 1.3 m tall at different velocities

In Figures 5.47 to 5.52, a 1.3 m human is simulated at different relative velocities. The velocities at which the human is walking are 0.5 to 3m/sec, increasing each time by 0.5 m/sec.

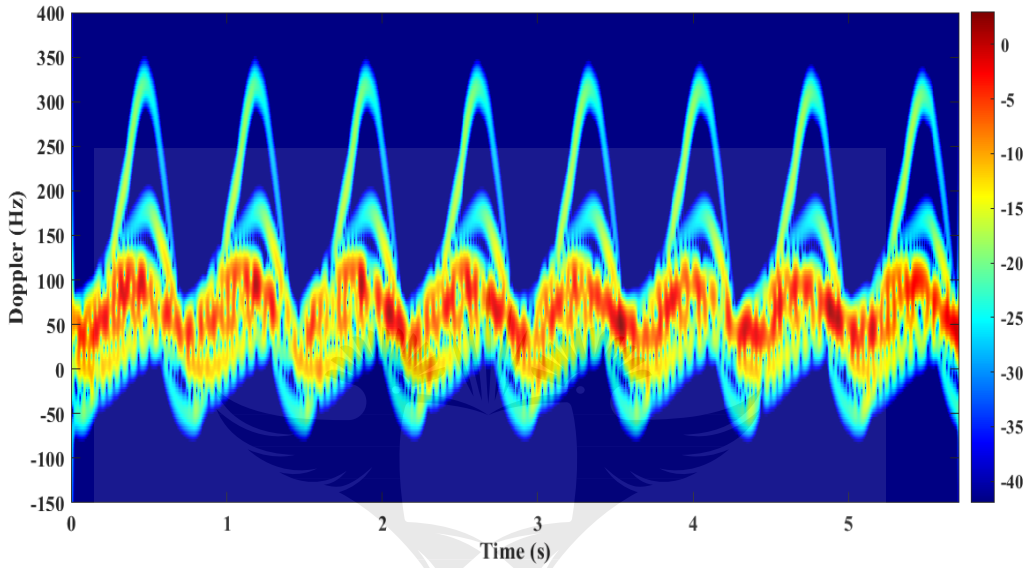

Figure 5.51: Micro-Doppler signature of 1.3 m human at relative speed of 0.5 m/sec.

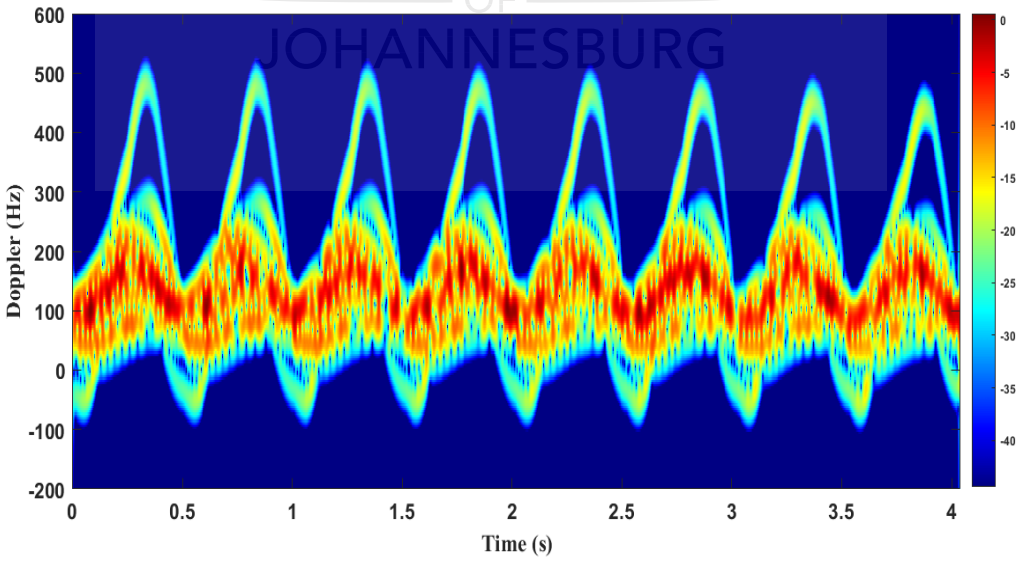

Figure 5.52: Micro-Doppler signature of 1.3 m human at relative speed of 1 m/sec.

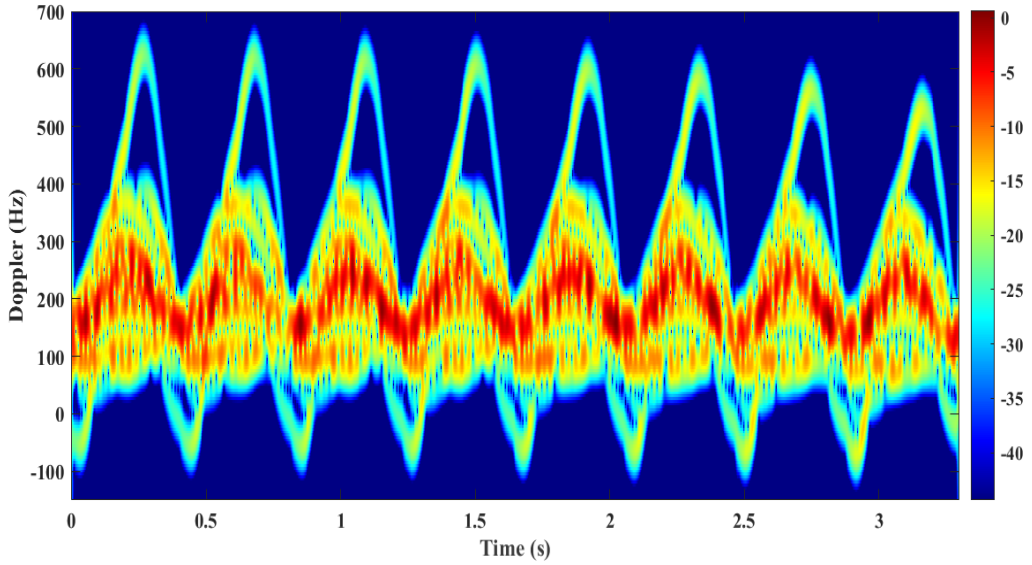

Figure 5.53: Micro-Doppler signature of 1.3 m human at relative speed of 1.5 m/sec.

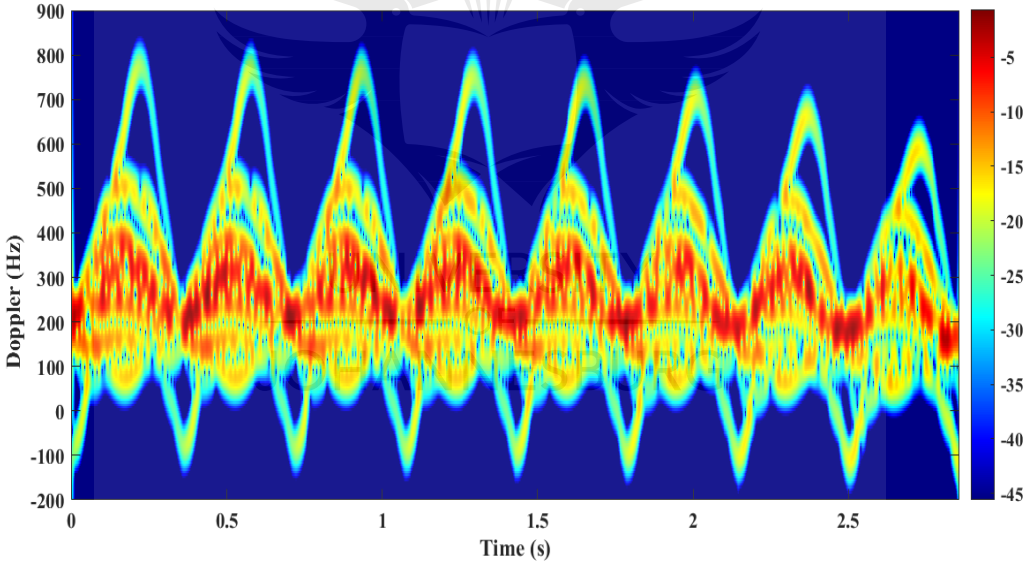

Figure 5.54: Micro-Doppler signature of 1.3 m human at relative speed of 2 m/sec.

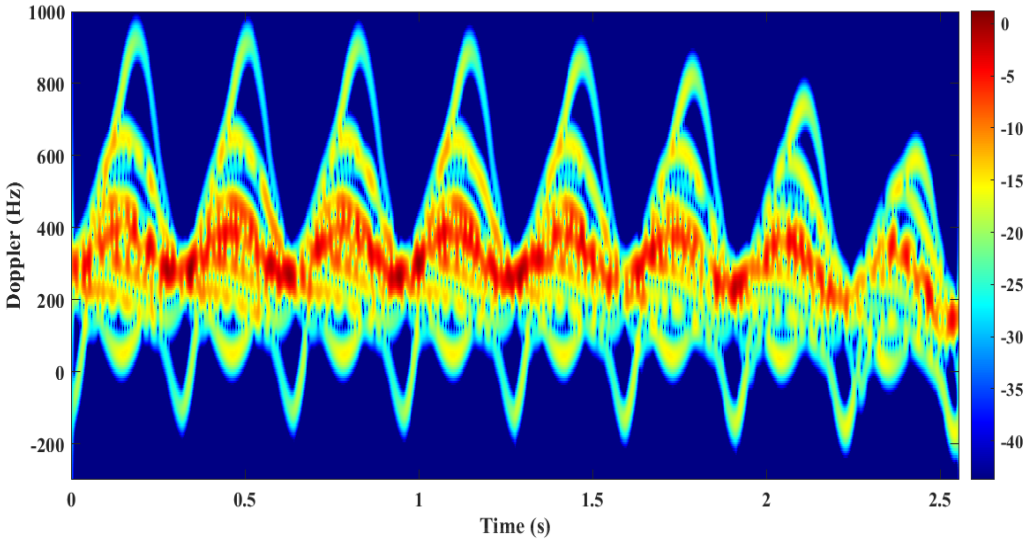

Figure 5.55: Micro-Doppler signature of 1.3 m human at relative speed of 2.5 m/sec.

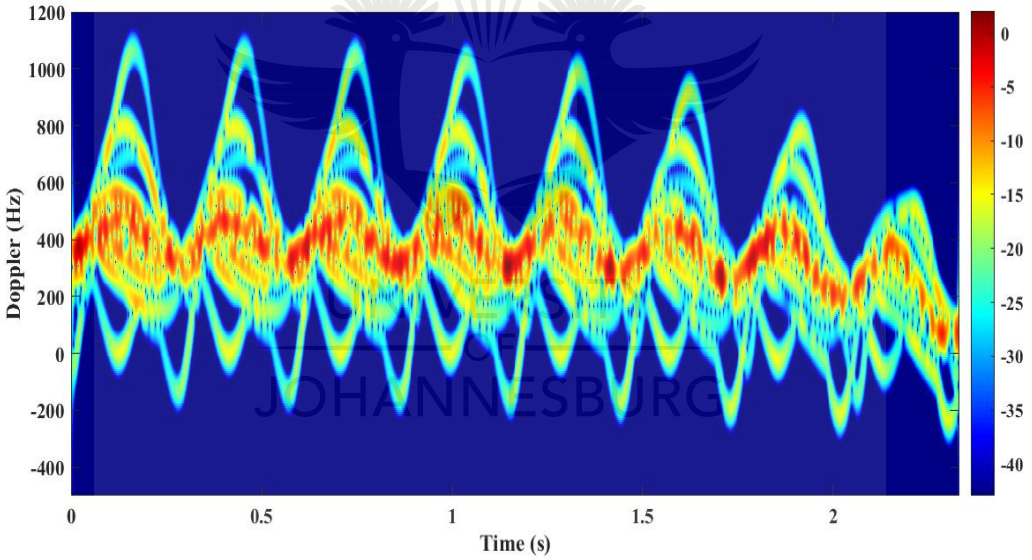

Figure 5.56: Micro-Doppler signature of 1.3 m human at relative speed of 3 m/sec.

Comparing a human being of 1 m tall with one of 1.3 m, a difference in micro-Doppler peak can be observed. Taking the case when the person is walking at 0.5 m, a peak of 300 Hz is observed when the human is 1 m tall, while 380 Hz is observed when the human is 1.3 m tall, thus a 80 Hz difference in micro-Doppler is reported for a 30 cm increase in height.

The main differences are observed in the frequency and time domain. When the velocity of the human increases, this decreases the time taken by the human to complete one complete cycle. This is the case when observing the human at a velocity 0.5 m/sec rather than 3

m/sec. In the first case the period of one cycle is 0.8 s, while in the second case the period is 0.3 s. This factor is necessary to reveal the human velocity.

5.4.1.2.3 Simulation of a walking human of 1.6 m tall at different velocities

In Figures 5.53 to 5.58, a 1.6 m human is simulated at different relative velocities. The velocities at which the human is walking are 0.5 to 3m/sec, increasing each time by 0.5 m/sec.

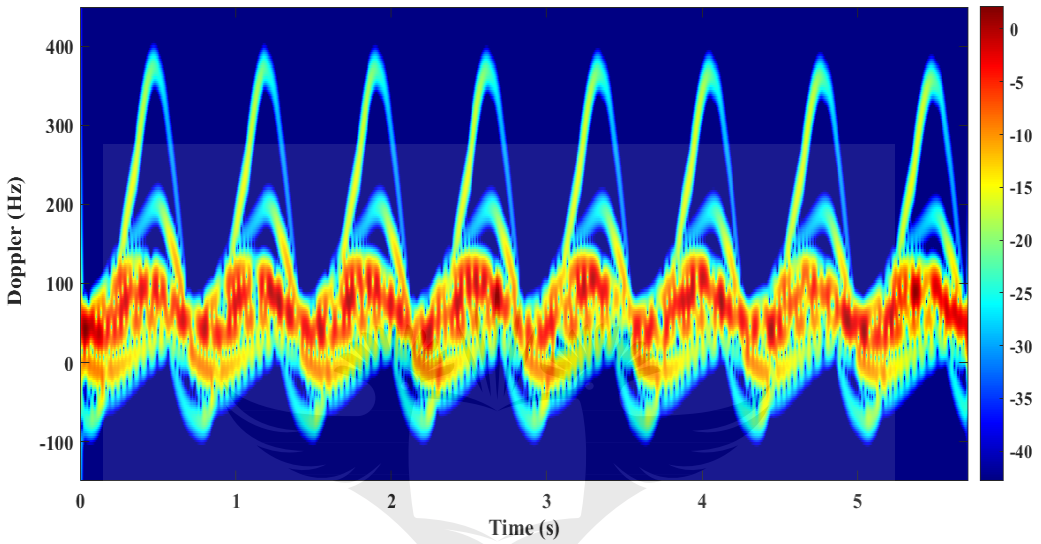

Figure 5.57: Micro-Doppler signature of 1.6 m human at relative speed of 0.5 m/sec.

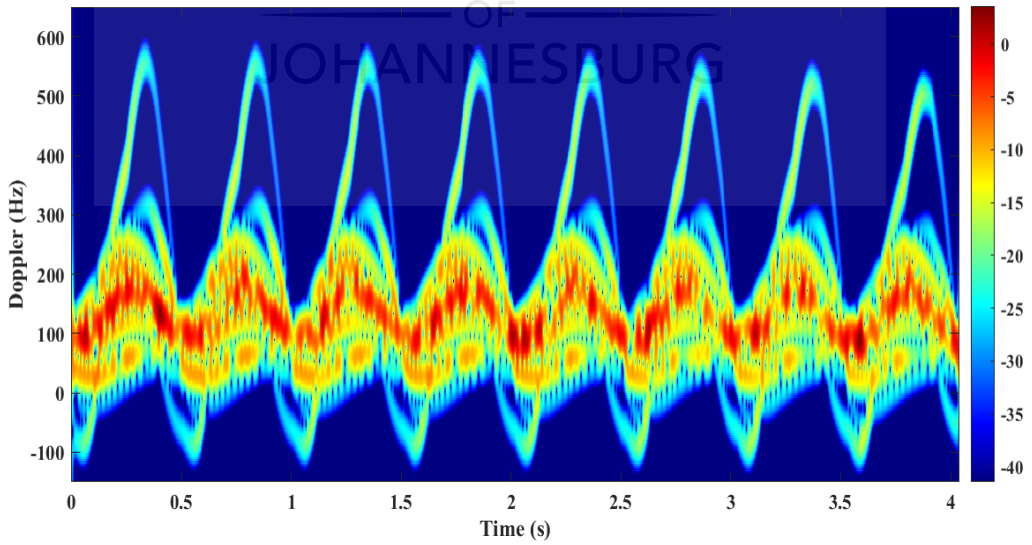

Figure 5.58: Micro-Doppler signature of 1.6 m human at relative speed of 1 m/sec.

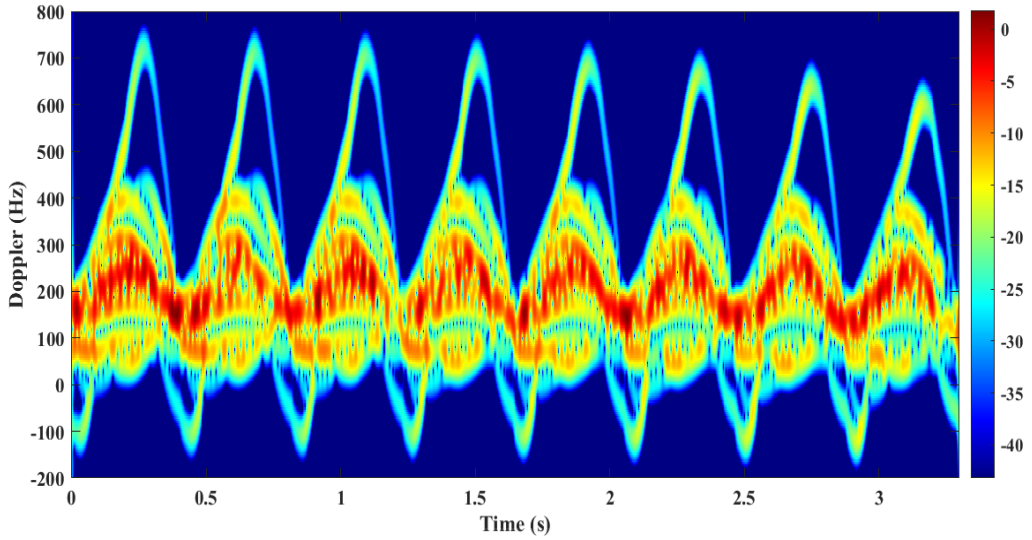

Figure 5.59: Micro-Doppler signature of 1.6 m human at relative speed of 1.5 m/sec.

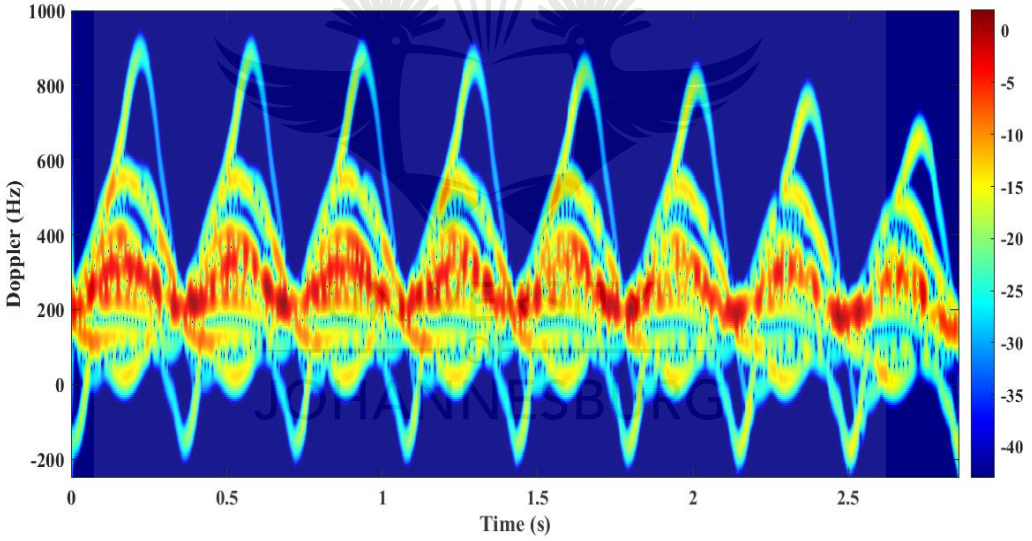

Figure 5.60: Micro-Doppler signature of 1.6 m human at relative speed of 2 m/sec.

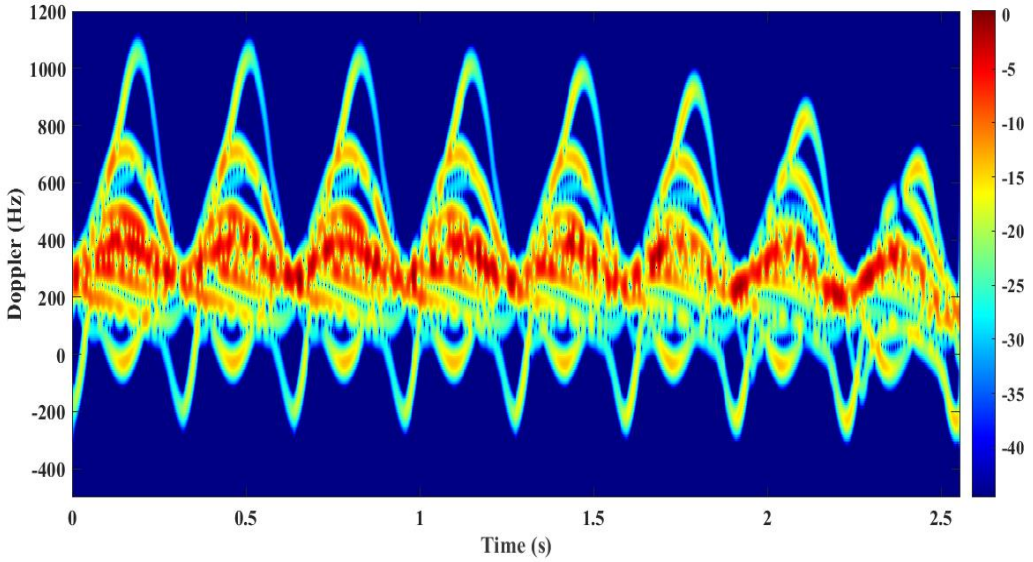

Figure 5.61: Micro-Doppler signature of 1.6 m human at relative speed of 2.5 m/sec.

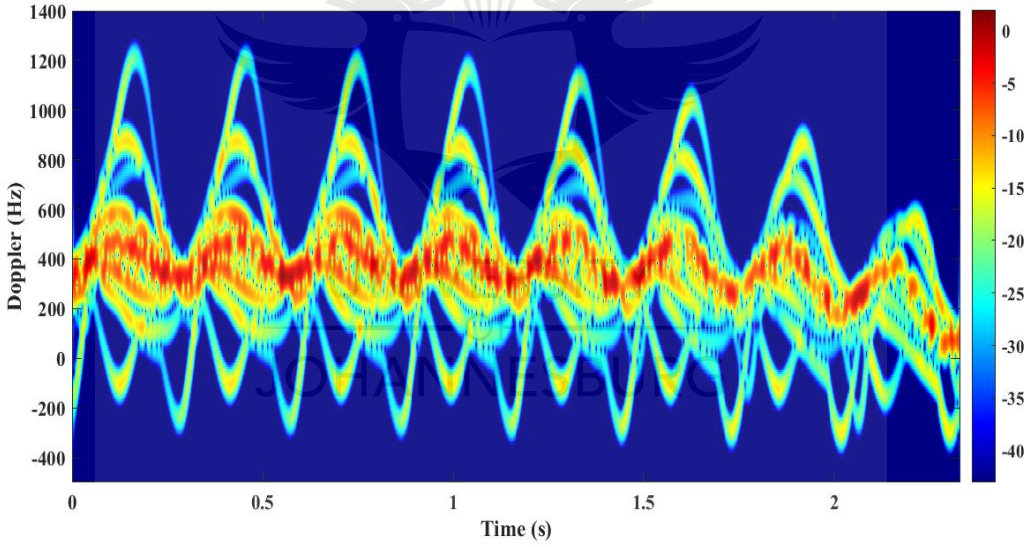

Figure 5.62: Micro-Doppler signature of 1.6 m human at relative speed of 3 m/sec.

The same behaviour observed from 1 m to 1.3 m is observed again here. Though the micro-Doppler increases, it does not increase in the same proportion as the proportion from 1 m to 1.3 m. This reveals that the height of a human is not proportional to the micro-Doppler that the human produces when impinged on by a radar signal. This simulation confirmed the result of the cylinder. When the height is increased, greater reflection is expected. The non-proportionality of the height and the return signal, in this case micro-Doppler frequency, deserves attention. The height related to the micro-Doppler frequency is non-linear.

5.4.1.2.4 Simulation of a walking human of 1.9 m tall at different velocities

In Figures 5.59 to 5.64, a 1.9 m tall human is simulated at different relative velocities. The velocities at which the human is walking are 0.5 to 3m/sec, increasing each time by 0.5 m/sec.

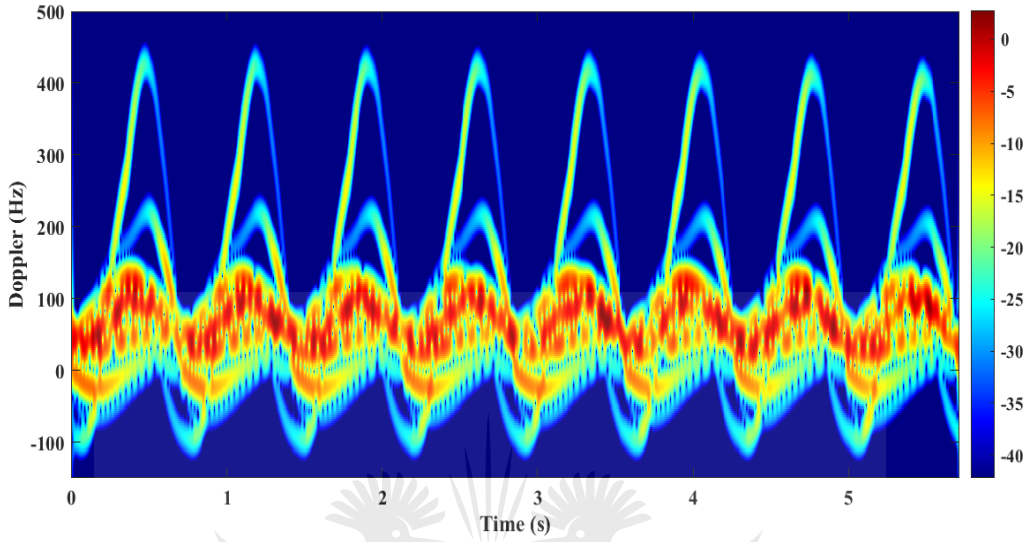

Figure 5.63: Micro-Doppler signature of 1.9 m human at relative speed of 0.5 m/sec.

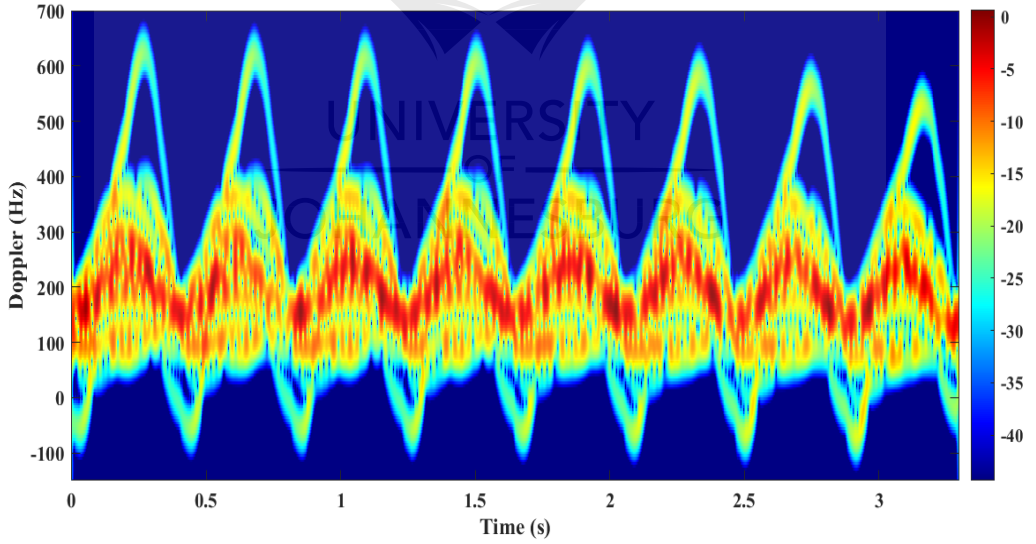

Figure 5.64: Micro-Doppler signature of 1.9 m human at relative speed of 1 m/sec.

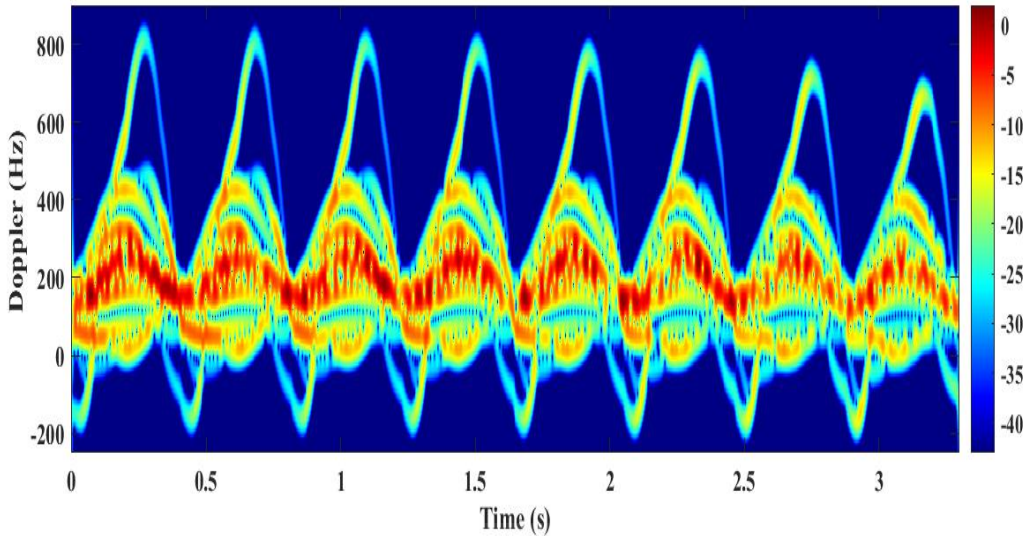

Figure 5.65: Micro-Doppler signature of 1.9 m human at relative speed of 1.5 m/sec.

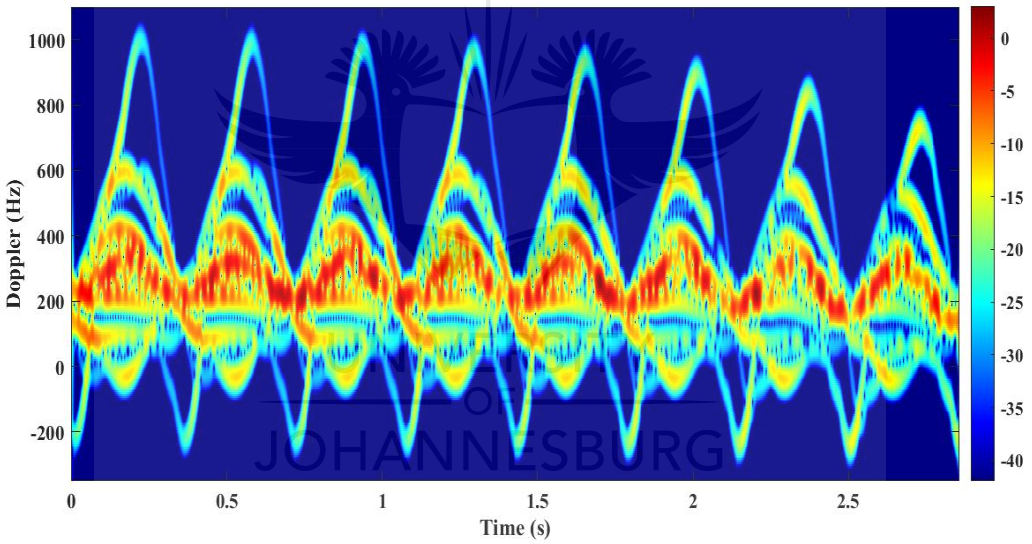

Figure 5.66: Micro-Doppler signature of 1.9 m human at relative speed of 2 m/sec.

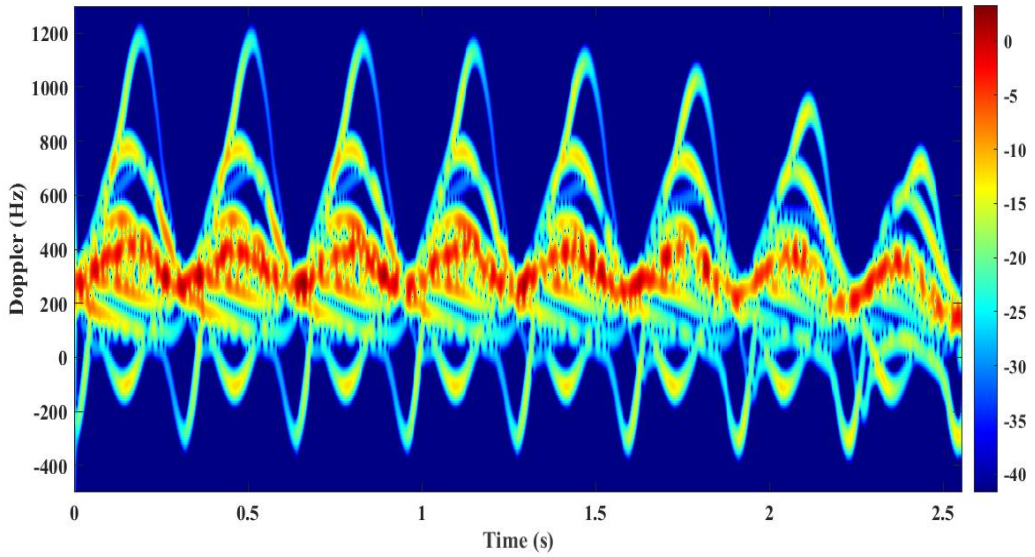

Figure 5.67: Micro-Doppler signature of 1.9 m human at relative speed of 2.5 m/sec.

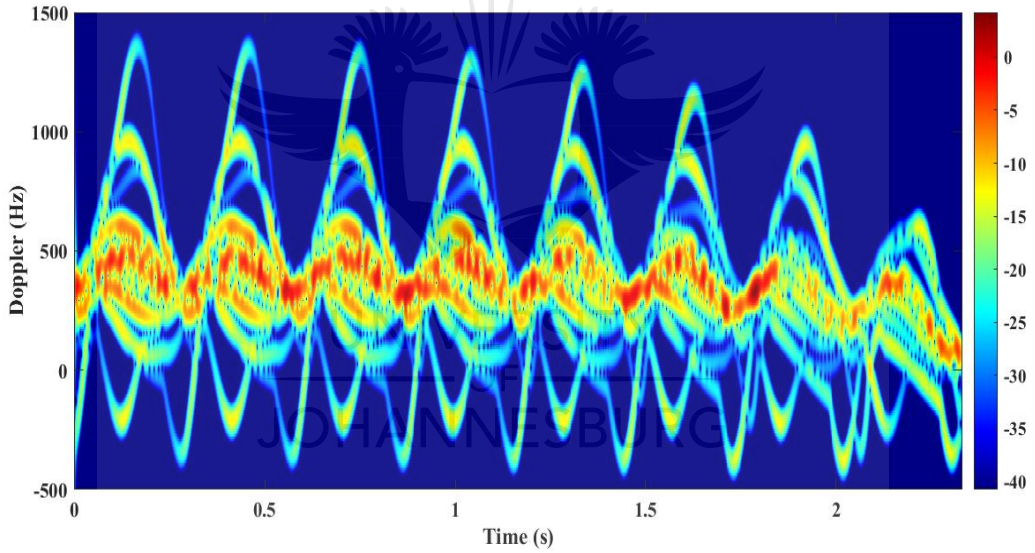

Figure 5.68: Micro-Doppler signature of 1.9 m human at relative speed of 3 m/sec.

In conclusion to this section, one can see that the micro-Doppler frequency return is related to the operational frequency of the radar, the height of the human being and finally the velocity of this human being. Therefore, it is imperative to analyse the human return spectrogram by considering the operational frequency of the radar, the height of the human being and the velocity of the human being. To illustrate the relationship between the operational frequency of the radar, the height of the human being and finally the velocity of the human being, Tables 5.7 and 5.8 present the peak micro-Doppler frequency of each simulation at different velocities, heights and frequencies.

Table 5-7: Peak return at 2.4 GHz frequency.

		Frequency of 2.4 GHz					
	Velocity	**0.5 m/sec**	**1 m/sec**	**1.5 m/sec**	**2 m/sec**	**2.5 m/sec**	**3 m/sec**
Height	1 m	70	100	120	150	190	210
	1.3 m	80	110	150	180	210	240
	1.6 m	90	120	170	200	220	280
	1.9 m	100	140	180	210	260	290

Table 5-8: Peak return at 15 GHz frequency.

		Frequency of 15 GHz					
	Velocity	**0.5 m/sec**	**1 m/sec**	**1.5 m/sec**	**2 m/sec**	**2.5 m/sec**	**3 m/sec**
Height	1 m	300	450	590	720	880	1000
	1.3 m	340	520	680	820	990	1150
	1.6 m	400	590	750	940	1100	1280
	1.9 m	450	680	800	1080	1200	1400

Figure 5.62 gives a graphical representation of the two tables above. The Y-axis represents the micro-Doppler frequency peaks of each simulation at a specific velocity. On the other hand, the X-axis represents the velocity at which the human was walking in the simulation while the micro-Doppler frequency was sampled. The dashed line represents the simulation done at 2.4 GHz while the solid line represents the simulation done at a frequency of 15 GHz. Series 1 and 5 curves represent the micro-Doppler frequency of a 1 m human being. Series 2 and 6 represent the micro-Doppler frequency of a 1.3 m human being. Series 3 and 7 represent the micro-Doppler frequency of a 1.6 m human being. Series 4 and 8 represent the micro-Doppler frequency of a 1.9 m human being. One can observe the difference in micro-Doppler return in the same condition but at a different frequency.

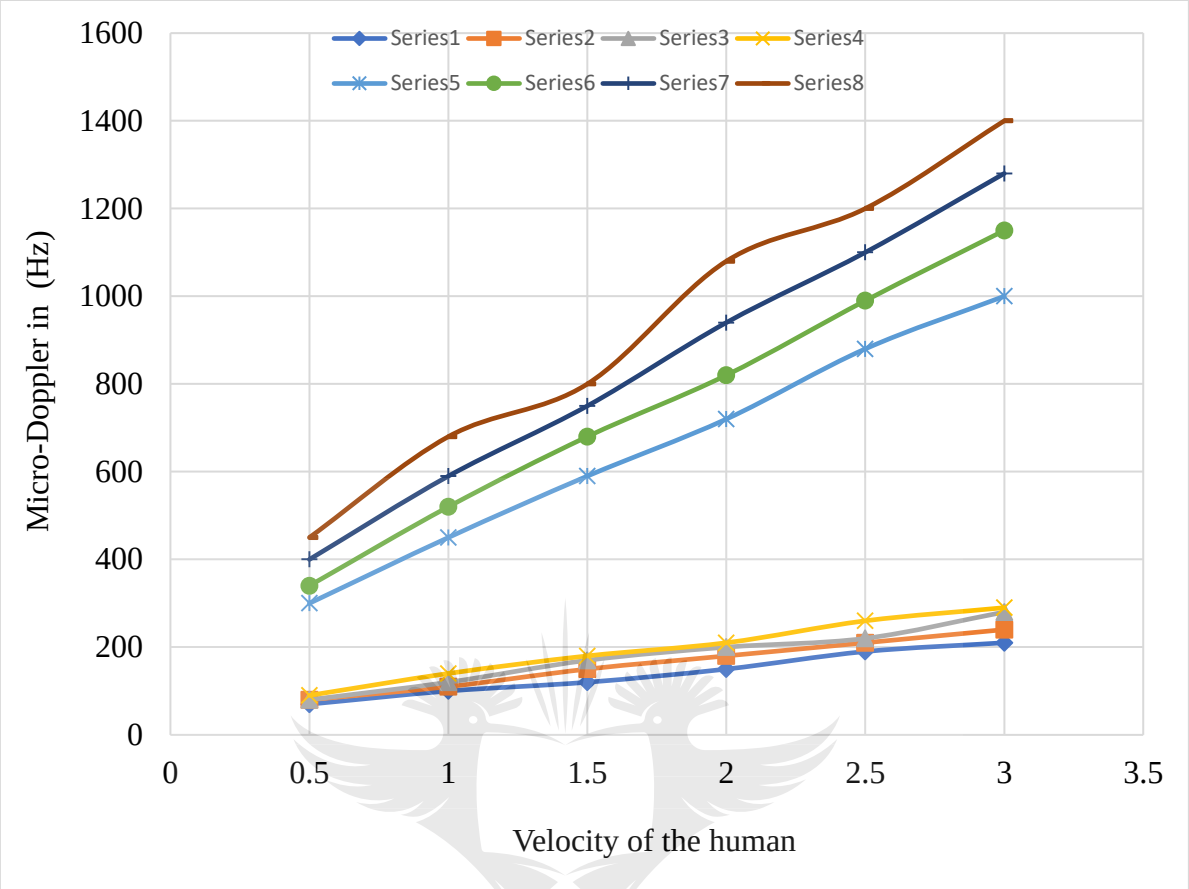

Figure 5.69: Peak micro-Doppler at different heights and frequency.

All the micro-Doppler frequencies are below 290 Hz when the radar is working at 2.4 GHz, while at 15 GHz the lower frequency is at 300 Hz. Thus, using a radar working at 2.4 GHz and trying to classify the micro-Doppler may be almost impracticable when using STFT. If one would like to classify a target at this frequency, investigation of different processing algorithms will be important.

5.5 CONCLUDING REMARKS

The results obtained after simulation and experiments prove that one can detect the presence of a human being despite the presence of an appliance. Thus, while using a micro-Doppler as human signature, care must be taken when selecting the radar frequency. Starting with the three-blade fan, one can see that at 2.4 GHz the number of ridges is the same as for the two ridges at a frequency of 20 GHz. The same behaviour has been observed with a two-blade fan at 2.4 GHz and 20 GHz, demonstrating that using a higher frequency produced a high micro-Doppler frequency.

On the other hand, the simulation involving a human revealed that at 2.4 GHz one is able to detect the human being even though there is no possibility of detecting different limbs of the body. However, at 24 GHz the different limbs can be detected at a height lower than 1 m. In addition, the spectrogram revealed a different pace at different heights. This characteristic allows one to distinguish between tall and short humans. For example, when comparing Figure 5.41 and Figure 5.59, both simulations are conducted at the same speed but at different heights of 1 m and 1.9 m, respectively. At 1 m height the time taken for one pace is 0.4 second, while at 1.9 m height the time is 0.8 second. Thus, at a height of 1 m a human covers a shorter distance than at 1.9 m. From that one can establish the height of the person.

CHAPTER 6 CONCLUSION AND FUTURE WORK

6.1 THESIS CONTRIBUTION

In Chapters 1 and 2 of this thesis, a considerable number of TWRI techniques have been enumerated, among them the medium through which the signal travels from the radar to the target, the possibility of detecting a weak target behind the wall, the possibility of detecting a human being lying against the wall and the possibility of detecting a target with a lower RCS.

In this thesis, the use of the micro-Doppler frequency of the return signal to differentiate the target from clutter was presented. Micro-Doppler frequency is an efficient way of extracting and classifying micro-movement from different objects exhibiting different movements as a whole. It was demonstrated in Chapter 3 how a human and a moving object are subject to micro-movement related to micro-Doppler frequency, though the entire object is subject to Doppler frequency. It was demonstrated after simulation that the influence of the wall while using the Doppler effect is minimised. These results correlated with previous findings in the literature [76]. In the same perspective, using an FMICW removes the strong return of a transmitted signal from the wall [69, 70]. Thus, using the micro-Doppler effect to differentiate the different parts of the body and the FMCW radar minimised the effect of the wall on the signal significantly. This research considered activities happening in residential accommodation.

The research for this thesis achieved the primary scientific objective of detecting human activities behind a wall in the presence of appliances. The target was mobile and non-cooperative and micro-Doppler return was sensed with an FMCW radar. In addition, this research achieved more scientific objectives by designing a low-cost FMCW radar to collect and analyse radar signatures. The choice of the FMCW radar has been justified by the fact that the wall effect had to be minimised.

Research reported in the literature did not consider a small chest area when detecting human beings. The additional contribution of this thesis is to consider that in the home environment people of different height may live together. Therefore, assuming that the subject behind the wall will always be adult might disregard some parameters necessary for the evaluation of the radar. Simulation considering human beings of different height

has thus been presented. The simulation revealed that a spectrogram produced by an adult is significantly different from one produced by a child. A highly sensitive radar is recommended to be used to be able to detect children as targets. The experiment with children responded to the research question considering humans with lower chest RCS.

A significant contribution of this thesis was the simulation, experimentation, processing, and analysis of diverse micro-Doppler signatures coming from the vicinity under investigation. The micro-Doppler signature of what was suspected of being the most mobile object in a home environment was simulated and discussed. The object that was assumed to be inducing the Doppler effect was a fan.

To answer the research question on weak victims after an earthquake, velocity discrimination had to be used. Therefore, the radar had to be set up to detect any micro-Doppler frequency near to the zero value.

It was concluded that using a radar working at a frequency of 2.4 GHz while a fan and a human are positioned behind each other will make the target undetectable, even if it is exhibiting motion. For this reason, the radar frequency has to be chosen with particular care to satisfy two conditions. The first is to choose a radar signal that can penetrate building material with less disintegration. The second is that the higher the radar frequency is, the higher the probability that the return signal will be capable of being classified with a high degree of certainty. It has been simulated and demonstrated that at 2.4 GHz frequency, the radar can detect the presence of activities without distinguishing the provenance of the micro-Doppler. This is the case in Figure 5.22, while in the same conditions but different frequency as shown in Figure 5.41 the micro-Doppler coming from the legs, arms and torso can be seen clearly.

On the other hand, using a frequency as high as 15 GHz demonstrated that one can detect the presence of a human being regardless of the person's age. Thus, to be able to detect children with a high probability of distinguishing different parts of the body, a high frequency is recommended.

In this research, computer simulation analysis played a crucial role in theoretical development. In addition, because of the limitation in terms of the frequency of the radar the researcher built, the simulation provided more flexibility. This was seen when the simulation could run at different frequencies without requiring hardware design.

The design and evaluation of the cost-effective FMCW radar emanated from this thesis. Because of its modularity, the FMCW that was built yielded high performance and was

less sensible to noise. In addition, the modularity aspect of the FMCW radar reduced the complexity and made it a practical sensor for industrial and research applications.

This dissertation contributed to the design and detailed analysis of the classification of a target behind a wall based on micro-Doppler features. In addition, the researcher demonstrated the way to extract human micro-Doppler in the presence of a fan. This is the case when two micro-Doppler signals are overlapping. Besides that, the antenna used in the experiment was made in the laboratory. Furthermore, a printed circuit board was designed and tested for radar signal generation.

6.2 FUTURE WORK

Micro-Doppler signals coming from a human being need more investigation and further improvement. In this thesis, the researcher considered a moving object as an element that can obstruct a target behind a wall. This thesis can be continued by investigating the propagation of the signal through other appliances before it reaches the human being. Taking the case where the signal has to travel through the wall, then through a fridge and thereafter to the target may reveal the incapacity of the radar to detect a target in these conditions.

A frequency of 2.4 GHz can penetrate building material with less deterioration of the signal, but another method that will extract overlapping signals is required.

BIBLIOGRAPHY

[1] K. Sarabandi, Electromagnetic Scattering from Vegetation Canopies, Ph.D. Dissertation: The University of Michigan, 1989.

[2] Y. Yang and A. E. Fathy, "See-through-wall imaging using ultra wideband short-pulse radar system," in *IEEE Antennas and Propagation Society International Symposium*, 2005, pp. 334-337.

[3] M. Farwell, J. Ross, R. Luttrell, D. Cohen, W. Chin and T. Dogaru, "Sense through the wall system development and design considerations," *Elsevier Journal of the Franklin Institute*, vol. 345, no. 6, pp. 570-591, September 2008.

[4] T. Jin, B. Chen and Z. Zhou, "Image-domain estimation of wall parameters for autofocusing of through-the-wall SAR imagery," *IEEE Transactions on Geoscience and Remote Sensing*, vol. 51, no. 3, pp. 1836-1843, August 2012.

[5] F. H. C. Tivive, A. Bouzerdoum and M. G. Amin, "A subspace projection approach for wall clutter mitigation in through-the-wall radar imaging," *IEEE Transactions on Geoscience and Remote Sensing*, vol. 53, no. 4, pp. 2108-2122, September 2015.

[6] V. John, B. Joshua and L. Elizabeth, "DHS and NASA technology helps save four in Nepal earthquake disaster," U.S. Department of Homeland Security Science and Technology Directorate, 5 May 2015. [Online]. Available: http://www.jpl.nasa.gov/news/news.php?feature=4574. [Accessed 28 May 2015].

[7] ENCA, "Hope fades as Lily mine rescue efforts halted for weeks," ENCA, 18 February 2016. [Online]. Available: https://www.enca.com/south-africa/hope-fades-lily-mine-rescue-efforts-halted-weeks. [Accessed 6 April 2016].

[8] M. Dehmollaian and K. Sarabandi, "Refocusing through building walls using synthetic aperture radar," *IEEE Transactions on Geoscience and Remote Sensing*, vol. 46, no. 6, pp. 1589-1599, June 2008.

[9] G. Wang and M. G. Amin, "Imaging through unknown walls using different standoff distances," *IEEE Transactions on Signal Processing*, vol. 54, no. 10, pp. 4015-4025, October 2006.

[10] L.-P. Song, C. Yu and Q. H. Liu, "Through-wall imaging (TWI) by radar: 2-D tomographic results and analyses," *IEEE Transactions on Geoscience and Remote Sensing*, vol. 43, no. 12, pp. 2793-2798, December 2005.

[11] J. J M de Wit and W. L van Rossum, "Extraction of building features from stand-off measured through-wall radar data," *IEEE journal of Selected Topics in Applied Earth Observations and Remote Sensing*, vol. 9, no. 1, pp. 149-158, January 2016.

[12] J. Moulton, A. S. Kassam, F. Ahmad, G. M. Amin and K. Yemelyanov, "Target and change detection in synthetic aperture radar sensing of urban structures," in *IEEE Radar Conference*, Rome, 2008, pp. 1-6.

[13] F. Ahmad, Y. Zhang and G. M. Amin, "Three-dimensional wideband beamforming for imaging through a single wall," *IEEE Geoscience and Remote Sensing Letters*, vol. 5, no. 2, pp. 176-179, April 2008.

[14] Y.-S. Yoon and G. M. Amin, "Spatial filtering for wall-clutter mitigation in through-the-wall radar imaging," *IEEE Transactions on Geoscience and Remote Sensing,* vol. 47, no. 9, pp. 3192-3208, June 2009.

[15] Y. Wang and A. E. Fathy, "Advanced system level simulation platform for three-dimensional UWB through-wall imaging SAR using time-domain approach," *IEEE Transactions on Geoscience and Remote Sensing,* vol. 50, no. 5, pp. 1986-2000, November 2012.

[16] M. Dehmollaian and K. Sarabandi, "Analytical, numerical, and experimental methods for through-the-wall radar imaging," in *IEEE International Conference on Acoustics, Speech and Signal Processing,* Las Vegas, 2008, pp. 5181-5184.

[17] Y. -J. Ren, C. -P. Lai, P.-H. Chen and R. M. Narayanan, "Compact ultrawideband UHF array antenna for through-wall radar applications," *IEEE Antennas and Wireless Propagation Letters,* vol. 8, pp. 1302-1305, December 2009.

[18] Y. Kim and H. Ling, "Human activity classification based on micro-Doppler signatures using a support vector machine," *IEEE Transactions on Geoscience and Remote Sensing* , vol. 47, no. 5, pp. 1328-1337, 2009.

[19] B. Lyonnet, C. Ioana and M. G Amin, "Human gait classification using microDoppler time-frequency signal representations," in *Radar Conference,* Washington DC, 10-14 May 2010.

[20] Y. Seo Koo, L. Ren, Y. Wang and A. E. Fathy, "UWB microDoppler radar for human gait analysis, tracking more than one person, and vital sign detection of moving persons," in *International Microwave Symposium Digest (IMS) IEEE MTT-S,* Seattle, WA, USA, June 2013, pp. 1-4.

[21] L. Chioukh, H. Boutayeb and D. Deslandes, "Noise and sensitivity of harmonic radar architecture for remote sensing and detection of vital signs," *IEEE Transactions on Microwave Theory and Techniques,* vol. 62, no. 9, pp. 1847-1855, September 2014.

[22] O. Yechiam, K. S. Porter, J. Hughes, C. F Dillon and T. Nwankwo, "Resting pulse rate reference data for children, adolescents, and adults: United States, 1999-2008," National Center for Biotechnology Information, Hyattsville, August, 2011.

[23] P. K. M. Nkwari, S. Sinha and H. C. Ferreira, "Through-the-wall radar imaging: A review," *IETE Technical Review,* vol. 34, no. 5, pp. 461-462, September 2017.

[24] R. Solimene, F. Soldovieri, G. Prisco and R. Pierri, "Three-dimensional through-wall imaging under ambiguous wall parameters," *IEEE Transactions on Geoscience an Remote Sensing,* vol. 47, no. 5, pp. 1310-317, May 2009.

[25] B. R Mahafza, "Radar fundamentals," in *Introduction to Radar Analysis,* Huntsville, CRC Press LLC, March 1998, p. 33.

[26] B. B Mahafza, "Radar fundamentals," in *Introdution to Radar Analysis,* Washington D C, CRC Press, 1998, p. 38.

[27] V. C Chen, "Introduction," in *Micro-Doppler Effect in Radar,* Boston, London, Artech House, 2011, p. 1.

[28] B. Dilpreet, R. Jean-Michel and R. Y. Mehmet, "Blood pressure estimation using pulse transit time from bioimpedance and continuous wave radar," *IEEE Transactions on Biomedical Engineering,* vol. 64, no. 4, pp. 917-927, April 2017.

[29] F. Mohamad, M. Mohamed, R. Sreeraman, B. Miodrag, R. D. Hilmi and Z. G. Voicu, "Event recognition for contactless activity monitoring using phase-modulated continuous wave radar," *IEEE Transactions on Biomedical Engineering,* vol. 64, no. 2, pp. 479-491, February 2017.

[30] R. Solimene, R. Di Napoli, F. Soldovieri and R. Pierri, "TWI for an unknown symmetric lossless wall," *IEEE Tranactions on Geoscience Remote Sensing,* vol. 49, no. 8, p. 2876–2886, August 2011.

[31] L. Ja-Chen, "Noninvasive microwave measurement of respiration," *Proceedings of the IEEE,* vol. 63, no. 10, p. 1530, October 1975.

[32] D. D. Amy, B.-L. Olga, M. L. Victor, L. Jenshan and T. A. K. Gregory, "Range correlation an I/Q performance benefits in single-chip silicon Doppler radars for noncontact cardiopulmonary monitoring," *IEEE Transactions on Microwave Theory and Techniques,* vol. 52, no. 3, pp. 839 - 848, March 2004.

[33] X. Yanming, L. Jenshan, B.-L. Olga and M. L. Victor, "Frequency-tuning technique for remote detection of heartbeat and respiration using low-power double-sideband transmission in Ka_band," *IEEE Transactions on Microwave Theory and Techniques,* vol. 54, no. 5, pp. 2023 - 2032, May 2006.

[34] V. Mehrnoosh and S. Kamal, "Millimeter-wave Doppler spectrum and polarimetric response of walking bodies," *IEEE Transactions on Geoscience and Remote Sensing,* vol. 50, no. 7, pp. 2866-2879, January 2012.

[35] F. Soldovieri and R. Solimene, "Through-wall imaging via a linear inverse scattering algorithm," *IEEE Geoscience and Remote Sensing Letters,* vol. 4, no. 4, pp. 513-517, October 2007.

[36] G. Gennarelli and F. Soldovieri, "A linear inverse scattering algorithm for radar imaging in multipath environments," *IEEE Geoscience and Remote Sensing Letters,* vol. 10, no. 5, pp. 1085-1089, September 2013.

[37] F. H. Chi Tivive, A. Bouzerdoum and M. G Amin, "A subspace projection approach for wall clutter mitigation in through-the-wall radar imaging," *IEEE Transactions on Geoscience and Remote Sensing,* vol. 53, no. 4, pp. 2108-2122, April 2015.

[38] V. Ha Tang, A. Bouzerdoum and S. Lam Phung, "Multipolarization through-wall radar imaging using low-rank and jointly-sparse representations," *IEEE Transactions on Image Processing,* vol. 27, no. 4, pp. 1763-1776, April 2018.

[39] R. Solimene, F. Soldovieri, G. Prisco and R. Pierri, "Three-dimensional through-wall imaging under ambiguous wall parameters," *IEEE Transaction on Geoscience Remote Sensing,* vol. 47, no. 5, pp. 310-1317, May 2009.

[40] F. Soldovieri, R. Solimene and F. Ahmad, "Sparse tomographic inverse scattering approach for through-the-wall radar imaging," *IEEE Transactions on Instrumentation and Measurment,* vol. 61, no. 12, pp. 3340-3350, December 2012.

[41] . W. Zhang and A. Hoorfar, "Three-dimensional real-time through-the-wall radar imaging with diffraction tomographic algorithm," *IEEE Transactions on Geoscience and Remote Sensing,* vol. 51, no. 7, pp. 4155-4163, December 2012.

[42] W. Zhang, "Two-dimensional microwave tomographic algorithm for radar imaging through multilayered media," *Progress in Electromagnetics Research,* vol. 144, pp. 261-270, January 2014.

[43] W. Zhang and A. Hoorfar, "Three-dimensional synthetic aperture radar imaging through multilayered walls," *IEEE Transactions on Antennas and Propagation,* vol. 62, no. 1, pp. 459-462, January 2014.

[44] W. Zhang, "Three-dimensional through-the-wall imaging with multiple-input multiple-output MIMO radar," *Journal of Electromagnetic Waves and Applications,* vol. 28, no. 15, pp. 1935-1943, September 2014.

[45] C. Zhang, Y. Kuga and A. Ishimaru, "Hard-wall radar imaging: localization of objects shadowed by metallic walls with MIMO radar," *IEEE transactions on antennas and propagation,* vol. 66, no. 8, pp. 4240-4251, August.

[46] M. Dehmollaian and K. Sarabandi, "Analytical, numerical, and experimental methods for through-the-wall radar imaging," in *Proceedings of 2008 IEEE Acoustics, Speech and Signal Processing*, Las Vegas, NV, USA, 4 April 2008, pp. 5181-5184.

[47] F. Ahmad, M. Amin and S. A Kassam, "Synthetic aperture beamformer for imaging through a dielectric wall," *IEEE Transactions on Aerospace and Electronic Systems,* vol. 41, no. 1, p. 271–283, January 2005.

[48] G. Wang, M. Amin and Y. Zhang, "New approach for target locations in the presence of wall ambiguities," *IEEE Transactions on Aerospace and Electronic Systems,* vol. 42, no. 1, pp. 301-315, January 2006.

[49] L. Li, W. Zhang and F. Li, "A novel autofocusing approach for real time through-wall imaging (TWI) under unknown wall characteristics," *IEEE Transaction on Geoscience and Remote Sensing,* vol. 48, no. 1, pp. 423-431, September 2009.

[50] K. F. Anny and J. E. Hyo, "A theory of wave scattering from an inhomogeneous layer with an irregular interface," *IEEE Transactions on Antennas and Propagation,* vol. 29, no. 6, pp. 899-910, November 1981.

[51] M. G Amin, Compressive Sensing for Urban Radar, Pennsylvania: CRC Press , 2014.

[52] W. Zhang and A. Hoorfar, "A generalized approach for SAR and MIMO radar imaging of building interior targets with compressive sensing," *IEEE Antennas and Wireless Propagation Letter*, vol. 14, pp. 1052-1055, January 2015.

[53] W. Zhang, M. G Amin, F. Ahmad, A. Hoorfar and G. E Smith, "Ultra-wideband impulse radar through- the-wall imaging with compressive sensing," *International journal of Antennas and Propagation,* vol. 2012, pp. 1-11, 2012.

[54] D. Bi, Y. Xie, L. Ma, X. Li, X. Yang and Y. Rosa Zheng, "Multifrequency compressed sensing for 2-D near-field synthetic aperture radar image reconstruction," *IEEE Transactions on Instrumentation and Measurement,* vol. 4, no. 67, pp. 777-791, April 2017.

[55] S. Caorsi and M. Stasolla, "A layer stripping approach for EM reconstruction of stratified media," *IEEE Transactions on Geoscience and Remote Sensing,* vol. 52, no. 9, pp. 5855-5869, September 2014.

[56] A. E Yagle, "A layer stripping fast algorithm for the two-dimensional direct current inverse resistivity roblem," *IEEE Transactions on Geoscience and Remote Sensing,* Vols. GE-25, no. 5, pp. 558-563, September 1987.

[57] A. E Yagle, "A layer-stripping fast algorithm for reconstructing an elastic medium from its commessional wave reflectign response," *IEEE Journal of Oceanic Engineering,* Vols. OE-1, no. 2, pp. 423-432, April 1987.

[58] S. Rao, Time Domain Electromagnetics, Amsterdam: Elsevier, 1999.

[59] A. Maunder, O. Taheri and M. Reza Ghafouri Fard, “Calibrated layer-stripping technique for level and permittivity measurement with UWB radar in metallic tanks,” *IEEE Transactions on Microwave Theory and Techniques,* vol. 63, no. 7, pp. 2322-2334, July 2015.

[60] A. Martone, C. Le and K. Ranney, “Coherent and non-coherent change detection for through the wall sensing of moving targets,” in *in Proceeding Radar Conference,* Kansas City, 2011, 256-261.

[61] J. Hu, Y. Song, T. Jin, B. Lu, G. Zhu and Z. Zhou, “Shadow effect mitigation in indication of moving human behind wall via MIMO TWIR,” *IEEE Geoscience and Remote Sensing Letters,* vol. 12, no. 3, pp. 453-457, March, 2015.

[62] J. Liu, L. Kong, X. Yang and Q. Huo Liu, “First-order multipath ghosts' characteristics and suppression in MIMO through-wall imaging,” *IEEE Geoscience and Remote Sensing Letters,* vol. 13, no. 9, pp. 1315-1319, September 2016.

[63] W. Zhang and A. Hoorfar, “Fast data acquisition and real-time processing techniques for through-the wall radar imaging,” *Forum for Electromagnetic Research Methods and Application Technologies,* vol. 3, pp. 1-9, 2014.

[64] E. Emre and M. Randolph L, “Through-the-wall SAR attributed scattering center feature estimation,” *IEEE Transactions on Geoscience and Remote Sensing,* vol. 47, no. 5, pp. 1338-1348, May 2009.

[65] N. Subotic, E. Keydel, J. Burns, A. Morgan, K. Cooper, B. Thelen, B. Wilson, W. Williams, S. McCarty, B. Lampe, B. Mosher and D. Setterdahl, “Parametric reconstruction of internal building structures via canonical scattering mechanisms,” in *IEEE International Conference on Acoustics, Speech and Signal Processing, 2008. ICASSP 2008.*, Las Vegas, 31 March-4 April 2008.

[66] O. Yechiam, P. Kathryn S, H. Jeffery, D. Charles F and N. Tatiana, “Resting pulse rate reference data for children, adolescents, and adults: United States, 1999-2008,” in *National Health Statistics Reports*, Hyattsville, August 2011.

[67] E. Alec, The search for Christian Doppler, New York: Springer-Verlag Wein GmbH, 1992, pp. 46-48.

[68] T. Dogaru, C. Le and G. Kirose, “Analysis of the radar Doppler signature of a moving human,” U.S. Army research laboratory technical report, Maryland, 2004.

[69] V. C Chen, “Basics of the micro-Doppler effect in radar,” in *Micro-Doppler effect in radar*, Boston, London, Artech House, 2011, p. 35.

[70] T. Gowers, J. Barrow-Green and I. Leader, “William Rowan Hamilton,” in *The princeton companion to mathematics*, Princeton and Oxford, Princeton University press, January 2008, p. 765.

[71] F. Harfoush, A. Taflove and G. A. Kriegsmann, “A numerical technique for analyzing electromagnetic wave scattering from moving surfaces in one and two dimensions,” *IEEE Transactions on Antennas and Propagation,* vol. 37, no. 1, pp. 55 - 63, January 1989.

[72] M. Abdelazeez, L. Peach and S. Borkar, “Scattering of electromagnetic waves from moving surfaces,” *IEEE Transactions on Antennas and Propagation,* vol. 27, no. 5, pp. 679 - 684, September 1979.

[73] M. Pastorino and M. Raffetto, "Scattering of electromagnetic waves from a multilayer elliptic cylinder moving in the axial direction," *IEEE Transactions on Antennas and Propagation,* vol. 61, no. 9, pp. 4741 - 4753, September 2013.

[74] V. Dang and O. Kilic, "Simulation framework for compressive sensing-based through-wall detection of moving targets," *IET Radar, Sonar & Navigation* , vol. 11, no. 9, pp. 1349 - 1358, September 2017.

[75] "Doppler spectrum from moving scatterers in a random environment," *IEEE Transactions on Wireless Communications,* vol. 8, no. 6, pp. 1536-1276, June 2009.

[76] V. C Chen, Micro-Doppler effect in radar, Boston, London: Artech House, 2011.

[77] V. C Chen, "Analysis of radar micro-Doppler signature with time-frequency transform," in *Proceedings of the tenth IEEE workshop on statistical signal and array processing*, Pocono Manor, August 2000.

[78] B. R Mahafza, "Radar cross section," in *Radar systems analysis and design using MATLAB*, Huntsville, Alabama, Chapman & Hall/CRC, 2000, p. 100.

[79] G. Charvat, J. Williams, A. Fenn, S. Kogon and J. Herd, "RES.LL-003 Build a Small Radar System Capable of Sensing Range, Doppler, and Synthetic Aperture Radar Imaging," Massachusetts Institute of Technology: MIT OpenCourseWare, IAP January 2011. [Online]. Available: https://ocw.mit.edu. [Accessed 27 January 2016].

[80] F. Ahmad, M. G Amin and G. Mandapati, "Autofocusing of through-the-wall radar imagery under unknown wall characteristics," *IEEE Transactions on Image Processing*, vol. 16, no. 7, pp. 1785-1795, July 2007.

[81] M. I. Skolnik, Radar Handbook Second edition, New York: McGraw-Hill, 1990.

[82] D. Koepsell, . W.-P. Brinkman and S. Pon, "Human participants in engineering research: notes from a fledgling ethics committee," *Science and Engineering Ethics,* vol. 21, no. 4, pp. 1033-1048, August 2015.

[83] A. David, Biomechanics and motorcontrol of human movement, John Wiley & Sons.

[84] X. Liu, H. Leung and G. A Lampropoulos, "Effects of non-uniform motion in through-the-wall SAR imaging," *IEEE Transactions on Antennas and Propagation,* vol. 57, no. 11, pp. 3539-3548, November 2009.

[85] F. Fioranelli, S. Salous and X. Raimundo, "Frequency-modulated interrupted continuous wave as wall removal technique in through-the-wall imaging," *IEEE Transactions on Teoscience and Remote Sensing,* vol. 52, no. 10, pp. 6272-6283, October 2014.

[86] F. Fioranelli, S. Salous, I. Ndip and X. Raimundo, "Through-the-wall detection with gated FMCW signals using optimized patch-like and vivaldi antennas," *IEEE Transactions on Antennas and Propagation,* vol. 63, no. 3, pp. 1106-1117, March 2015.

[87] C. Li, Z. Peng, T. -Y. Huang, T. Fan, F. -K. Wang, T. -S. Horng, J. -M. Muñoz -Ferreras, R. Gómez-García, L. Ran, J. Lin and J. -M. Muñoz -Ferreras, "A review on recent progress of portable short-range noncontact microwave radar systems," *IEEE Transactions on Microwave Theory and Techniques,* vol. 65, no. 5, pp. 1692-1706, May 2017.

[88] F.-K. Wang, T.-S. Horng, K.-C. Peng, J.-K. Jau, J.-Y. Li and C.-C. Chen, "Detection of concealed individuals based on their vital signs by using a see-through-wall imaging system with a self-injection-locked radar," *IEEE Transactions on Microwave Theory and Techniques,* vol. 61, no. 1, pp. 696-704, January 2013.

[89] S. Sundar Ram, C. Christianson, Y. Kim and H. Ling, "Simulation and analysis of human micro-Dopplers in through-wall environments," *IEEE Transactions on Geoscience and Remote Sensing,* vol. 48, no. 4, pp. 2015-2023, April 2010.

[90] Y. Kim and H. Ling, "Human activity classification based on micro-Doppler signatures using a support vector machine," *IEEE transactions on geoscience and remote sensing,* vol. 47, no. 5, pp. 1328-1337, May 2009.

[91] P.-H. Chen, M. C. Shastry, C.-P. Lai and R. M. Narayanan, "A portable real-time digital noise radar system for through-the-wall imaging," *IEEE Transactions on Geoscience and Remote Sensing,* vol. 50, no. 10, pp. 4123-4134, October 2012.

[92] Y. Wang, Q. Liu and A. E Fathy, "CW and pulse–Doppler radar processing based on FPGA for human sensing applications," *IEEE Transactions on Geoscience and Remote Sensing,* vol. 51, no. 5, pp. 3097-3107, May 2013.

[93] Y. Kim and B. Toomajian, "Hand gesture recognition using micro-Doppler signatures with convolutional neural network," *IEEE Access,* vol. 4, pp. 7125-7130, October 2016.

[94] L. Xu, D. Feng and X. Wang, "Improved synthetic aperture radar micro-Doppler jamming method based on phase-switched screen," *IET Radar, Sonar & Navigation,* vol. 10, no. 3, pp. 525-534, March 2016.

[95] B. Tekeli, S. Zubeyde Gurbuz and M. Yuksel, "Information-theoretic feature selection for human micro-Doppler signature classification," *IEEE Transactions on Geoscience and Remote Sensing,* vol. 54, no. 5, pp. 2749-2762, May 2016.

[96] P. Setlur, F. Ahmad and M. Amin, "Maximum likelihood and suboptimal schemes for micro-Doppler estimation using carrier diverse Doppler radars," *IET Signal Processing,* vol. 5, no. 2, pp. 194-208, April 2011.

[97] L. Hong, F. Dai and X. Wang, "Micro-Doppler analysis of rigid-body targets via block-sparse forward–backward time-varying autoregressive model," *IEEE Geoscience and Remote Sensing Letters,* vol. 13, no. 9, pp. 1349-1353, September 2016.

[98] L. Du, L. Li, B. Wang and J. Xiao, "Micro-Doppler feature extraction based on time-frequency spectrogram for ground moving targets classification with low-resolution radar," *IEEE Sensors Journal,* vol. 16, no. 10, pp. 3756-3763, May 2016.

[99] P. Xia, X. R Wan, J. X Yi and H. Tang, "Micro-Doppler imaging for fast rotating targets using illuminators of opportunity," *IET Radar, Sonar and Navigation,* vol. 10, no. 6, pp. 1024-1029, July 2016.

[100] D. P Fairchild and R. M Narayanan, "Multistatic micro-doppler radar for determining target orientation and activity classification," *IEEE Transactions on Aerospace and Electronic Systems,* vol. 52, no. 1, pp. 512-521, February 2016.

[101] F. Fioranelli, M. Ritchie and H. Griffiths, "Performance analysis of centroid and SVD features for personnel recognition using multistatic micro-Doppler," *IEEE Geoscience and Remote Sensing Letters,* vol. 13, no. 5, pp. 725-729, May 2016.

[102] A. Sume, M. Gustafsson, M. Herberthson, A. Janis, S. Nilsson, J. Rahm and A. Orbom, "Radar detection of moving targets behind corners," *IEEE Transactions on Geoscience and Remote Sensing,* vol. 49, no. 6, pp. 2259-2267, June 2011.

[103] R. M Narayanan and M. Zenaldin, “Radar micro-Doppler signatures of various human activities,” *IET Radar, Sonar and Navigation,* vol. 9, no. 9, pp. 1205-1215, December 2015.

APPENDIX A: SUMMARY OF LITERATURE RELATED TO THIS RESEARCH

Table A-1: Summary of literature related to this research.

Reference	Journal	Journal Impact Factor (IF)[1]	Frequency band of interest	Contribution to body of scholarly knowledge
[67]	*IEEE Transactions on Microwave Theory and Techniques*	2.897	–	This paper reviewed different techniques used in radar communication for motion detection, displacement and localisation. In this publication, the radar is assisted by using on-board signal-processing algorithms; these are capable of playing crucial roles in various areas, such as health care and care of the elderly, veterinary monitoring, human–computer interaction, structural monitoring and wind engineering. Thus, one can see that portable short-range non-contact microwave radar systems could be applied in many areas.
[68]	*IEEE Transactions on Microwave Theory and Techniques*	2.897	2.3 to 2.8 GHz	Merging the FMCW and sum-difference pattern detection approaches, the authors could determine the distance and azimuth from the radar to the target (human) hidden by a wooden partition wall. To distinguish a human being from a stationary object, the authors used dynamic spectral subtraction, which allowed the extraction of human motion or vital signs. The authors were able to distinguish between two different humans when using the decomposition of the Doppler signal.

[1]WoS journal IF as listed on the IEEE Xplore website (www.ieeexplore.org) [May 2018]

Table A-1: Summary of literature related to this research.

Reference	Journal	Journal IF	Frequency band of interest	Contribution to body of scholarly knowledge
[69]	*IEEE Transactions on Geoscience and Remote Sensing*	4.942	0.7-2.2 GHz	The authors used frequency-modulated interrupted continuous wave (FMICW) signals to remove the strong return of the transmitted signal from the wall. The effectiveness of the technique has been validated through numerical simulations and experiments. FMICW is typically an FMCW that is switched on and off with a complementary sequence of the transmitter and the receiver. The technique is effective in detecting stationary and mobile targets and breathing owing to the removal of the wall returns. Combining FMICW with other wall removal techniques could be of great interest to mitigate the influence of the wall on the desired target under investigation.
[70]	*IEEE Transactions on Antennas and Propagation*	2.957	0.5-2 GHz	In TWRI systems, antennas are fundamental to the system to radiate power towards the area of interest. As the radar is transmitting in a wide range, the antenna should have well-matched impedance across the bandwidth. In addition, the radiation has to be focused towards the target under investigation. The publication presents an FMCW while using a patch-like antenna. After simulation and design of the antenna, the paper finds agreement between the simulated result and the antenna that was designed. After design, the antenna was fine-tuned using simulation results and subsequently showed strong wall-removal for through-wall detection of stationary targets and moving people. Furthermore, the antenna had a smaller factor and was made of a less expensive substrate compared to its counterpart.

[1] WOS journal IF as listed on the IEEE Xplore website (www.ieeexplore.org) [May 2018]

Table A-1: Summary of literature related to this research.

Reference	Journal	Journal IF	Frequency band of interest	Contribution to body of scholarly knowledge
[71]	*IEEE Transactions on Image Processing*	4.828	-------	While comparing conventional contrast measures such as the sum of squared intensity to the higher order statistics, the publication finds that higher order statistics are more sensitive to errors in wall parameters. Thus, the publication presents an autofocusing technique based on high-order statistics to mitigate error implied by an unknown wall. By running many simulations to compare their proposed technique to others, the publication claims greater effectiveness from their approach.

[1] WoS journal IF as listed on the IEEE Xplore website (www.ieeexplore.org) [May 2018]

Table A-2: Summary of previous works related to through-the-wall imaging using micro-Doppler effect.

Reference	Journal	Journal IF[2]	Type of radar used	Frequency band of interest	Algorithm used	Summary
[18]	*IEEE Transactions on Geoscience and Remote Sensing*	4.942	Doppler radar	2.4 GHz	Support vector machine	The researchers investigated a method to classify different human activities from their returned micro-Doppler activities. Thereafter, collecting the Doppler spectrogram, a support vector machine (SVM) was trained for different activities. Using the SVM, the authors found the optimal parameters through fourfold cross-validation. Their classification was more than 90% accurate. In addition, different possibilities of classification of human activities were investigated, such as classification over an extended time, at oblique angles with respect to the radar, and through a wall. The classification was challenging when the experiment was done through a wall. At an oblique approach angle above 30° with respect to the radar the degradation of the signal was significant. It was recommended that distributed sensors be investigated to classify the activities of humans moving in any direction.

[2] WoS Journal IF as listed on the IEEE Xplore website (www.ieeexplore.org) [May 2018]

[72]	*IEEE Transactions on Geoscience and Remote Sensing*	4.942	Doppler radar	2.4 GHz	Finite-difference time domain (FDTD)	A simulation of a TWR is run to detect micro-Doppler movement behind the wall. The wall is modelled using the FDTD and the human motion is modelled from a primitive based prediction applied to model the scattered returns. The core of the authors' investigation was to determine the effect of a homogenous and inhomogeneous wall on human-generated micro-Doppler. Contrary to [73], the paper found that TWR exposed only very minor distortions on the actual Doppler frequencies. Experimental and theoretical analysis supported the findings. The paper compared the two and three dimensions and found that even though the 3-D one offered improved performance, the 2-D one did not deviate significantly from the 3-D one. In terms of range, the method used in the paper could be used for high-range resolution even though the preliminary results showed significant degradation of the signal.
[74]	*IEEE Transactions on Geoscience and Remote Sensing*	4.942	Noise radar	400–720 MHz	Empirical mode decomposition and Hilbert transform	The paper presents a noise radar that combines real-time ranging, an imaging and Doppler capability as a single portable package. The paper uses different stand-off up to 9 metres and could detect the micro-Doppler. To remove the effect of the wall, the paper presents a time-gating method. In addition, the back and side walls effect

						could be removed using time gating if the layout of the building was known or if background radar data were available to use a background subtraction method.
[75]	*IEEE Transactions on Geoscience and Remote Sensing*	4.942	Continuous wave Doppler radar (CWDR) and ultra-wideband pulse–Doppler (UWBPD)	3 GHZ	Short-time Fourier transform (STFT)	The authors built two prototype radars based on field programmable gate arrays. The CWDR was cost-effective; on the other hand, it was only capable of detecting a single human at a time. This method was used in applications where range detection was not required. On the other hand, the UWBPD was capable of multiple-object detection and real-time target tracking. In addition, UWBPD demonstrated both a high-resolution range profile and micro-Doppler signature simultaneous acquisition. After comparison the conclusion was that the UWBPD offers more advantage than the CWDR if used in TWRI or where there is debris.
[76]	*IEEE Transactions on Antennas and Propagation*	1.873	SAR	24 GHz	Generalised likelihood ratio test technique	When SAR is used in a through-the-wall system, it provides high resolution and recognition of the target, using the SAR to collect the Doppler spectrum and analyse the non-uniform motion induced by the Doppler effect and target focusing. After analysis, the authors found that the wall parameters could have a strong impact on target focusing while using an SAR image. This influence on the target motion complicated the

						range estimation. In addition, the authors affirm that the presence of the wall has less impact on the micro-Doppler while using the SAR. In contrast, the presence of the wall is responsible for target smearing, defocusing and target displacement in the azimuth. While using the time-frequency analysis, a target with micro-Doppler demonstrated a high detection performance gain over that of the stationary one.
[77]	*IEEE Access*	3.244	Doppler radar	5.8 GHz	Deep convolutional neural network (DCNN)	Recognising human gesture is research of great interest in micro-Doppler radar. Human gesture aids recognition of the target. The authors investigated the use of micro-Doppler to recognise human hand gestures. They used 10 gestures to validate their concept. The gesture spectrum was collected in the absence of any obstruction between the radar and the target. The Doppler spectrogram was analysed with a DCNN. The DCNN showed an improvement up to 93.1% of recognition accuracy while using seven gestures. Lower performance was observed when using 10 gestures. With 10 gestures the paper reports an accuracy of 85.6%. The paper finds that depending on the distance to the radar and the aspect angle, the micro-Doppler signatures could vary. Multiple human gesture recognition has been identified as a

						research gap that has not been bridged.
[78]	*IET Radar, Sonar and Navigation*	1.509	SAR	9.375 GHz	Phase-switched screen	Knowing that micro-Doppler induces defocusing on the target, the authors used the micro-Doppler effect to introduce jamming in SAR imaging. This method is used to protect an aerial object, which is a micro-Doppler generator.
[79]	*IEEE Transactions on Geoscience and Remote Sensing*	4.942	Pulse Doppler radar transmitting a linear-frequency-modulated	15 GHz	Information-theoretic (IT)	Using IT feature selection techniques, the authors could classify different activities performed by a human subject. The IT technique was used because it did not require many features to classify the different activities. At a signal-to-noise ratio over 10 dB and with a minimum of 1 s of data, the results showed that their approach yielded 96% correct classification for the target moving along the radar line of sight. On the other hand, correctness of over 65% has been observed for tangential motion. A meticulous choice of features is necessary, as all the features do not contain a high level of information. Thus, by reducing the number of features to be analysed, the computational requirement is decreased as well.
[80]	*IET Signal Processing*	1.298	Dual-frequency radars	903 MHz and 921 MHz	Maximum likelihood (ML)	Using dual-frequency radars, the authors derived the ML as an estimator of the micro-Doppler motion parameters. By applying the iteratively reweighted non-linear least

						squares algorithm to solve the ML estimator for the micro-Doppler returns, their method has shown improvement while being applied to simulated data.
[81]	*IEEE Geoscience and Remote Sensing Letters*	2.761	Pulse radar	8 GHz	Block-sparse forward-backward time-varying autoregressive (BS-FBTVAR).	To analyse the micro-Doppler signatures produced by rigid-body targets, a parametric time-frequency method was used. By using the basis expansion method, the authors presented the conventional FBTVAR model in linear form. Subsequently, the BS-FBTVAR model was developed by applying the block sparsity lying in the time-invariant parameters' vectors owing to the rigidity of the targets. The complex value block sparse Bayesian learning algorithm was used to solve the BS-FBTVAR model. While comparing the conventional joint time–frequency (TF) and the proposed TF, it was found that the proposed TF had ameliorated denoising performance.
[82]	*IEEE Sensors Journal*	2.512	Linear frequency modulated pulse radar	Ka band	Time-frequency spectrogram	The paper presents the way to differentiate the return of a micro-Doppler signature coming from a single walking person, two people walking, and a moving wheeled vehicle. From the time-frequency spectrograms, the paper reproduces a 3-D micro-Doppler feature vector. After comparison between the existing method of micro-Doppler extraction and the result obtained, higher

						classification accuracy with higher discriminative ability was achieved using this method. The paper mentioned that a knowledge gap remained in respect of the extraction of micro-Doppler features while in the presence of noise and when the target was not cooperative.
[83]	*IET Radar, Sonar and Navigation*	1.509	Passive radar	666 MHz	Joint time-frequency domain	The paper investigated extracting the micro-Doppler of a fast-rotating target. A tomography method has been found effective and feasible to image fast-rotating targets using passive radars. Experiment and simulation substantiated the statement of extracting micro-Doppler from narrowband continuous wave radar. To be able to get the data projection, a joint time-frequency has been used to process the micro-Doppler data.
[84]	*IEEE Transactions on Aerospace and Electronic Systems*	4.942	Multi-static radar	4 GHz	STFT	The sensitivity of human-activity recognition is low when the movements are not forward or backward in the line of sight of the radar antenna. Thus, the author proposed the use of a multi-static radar consisting of two bi-static micro-Doppler sensors to reduce the effect of low sensitivity of a monostatic radar. The classification of micro-Doppler signatures is enhanced when using multiple sensors rather than a monostatic radar. This is due to the different aspect angle formed by the signal and

						the target.
[85]	*IEEE Geoscience and Remote Sensing Letters*	2.761	Multi-static radar	2.4 GHz	Singular value decomposition	The paper presents multi-static radar and investigates a micro-Doppler spectrogram collected from three sets of human activities. At the most favourable aspect angle, the paper achieves high classification accuracy of above 98%. To reduce the unwanted effect brought about by the aspect angle, the paper proposed future research investigation in order to optimise the classification performance.
[86]	*IEEE Transactions on Geoscience and Remote Sensing*	4.942	Stepped frequency radar	10 GHz	STFT	The paper finds that transmitting the radar signal via diffraction in the wall corner decreases the detection of target returns. This phenomenon has been used to separate the transmitted and reflected signal. The paper subsequently processes the received signal using the STFT. The paper demonstrates that it is possible to detect breathing and the presence of a walking man behind a wall. The paper uses the return signal coming from a metallic sphere placed in the shadow region behind the corner, using the moving target indicator to test the extraction of the real time return signal.
[87]	*IET Radar, Sonar and Navigation*	1.509	Continuous-wave monostatic Doppler radar	6.5 GHz	STFT	The paper investigates the extraction of the micro-Doppler signature through the wall and in free space. The paper finds that it is possible to distinguish between

						different targets based on the micro-Doppler returns under certain circumstances. Furthermore, distinguishing between different human beings depends on the activities conducted. In addition, the authors find that two different targets can be separated only when they are travelling in the same direction and at different speeds. The paper identifies a shortcoming: the TWR affects the signal magnitude response of the Doppler spectrogram in terms of attenuation and fading. The Doppler spectrogram is affected to a limited degree by the distortion, so a signal can be detected in TWR.

APPENDIX B: IMAGE OF THE SIGNAL GENERATOR BOARD

The board used to generate the ramp signal of the radar as given in section 4.2.1, titled radar design, is expanded in this section.

From Figure B.1 to Figure B.7 the figures represent the different circuits on the printed circuit board (PCB). Figure B.1 presents the microcontroller and the different components required for its basic functionality.

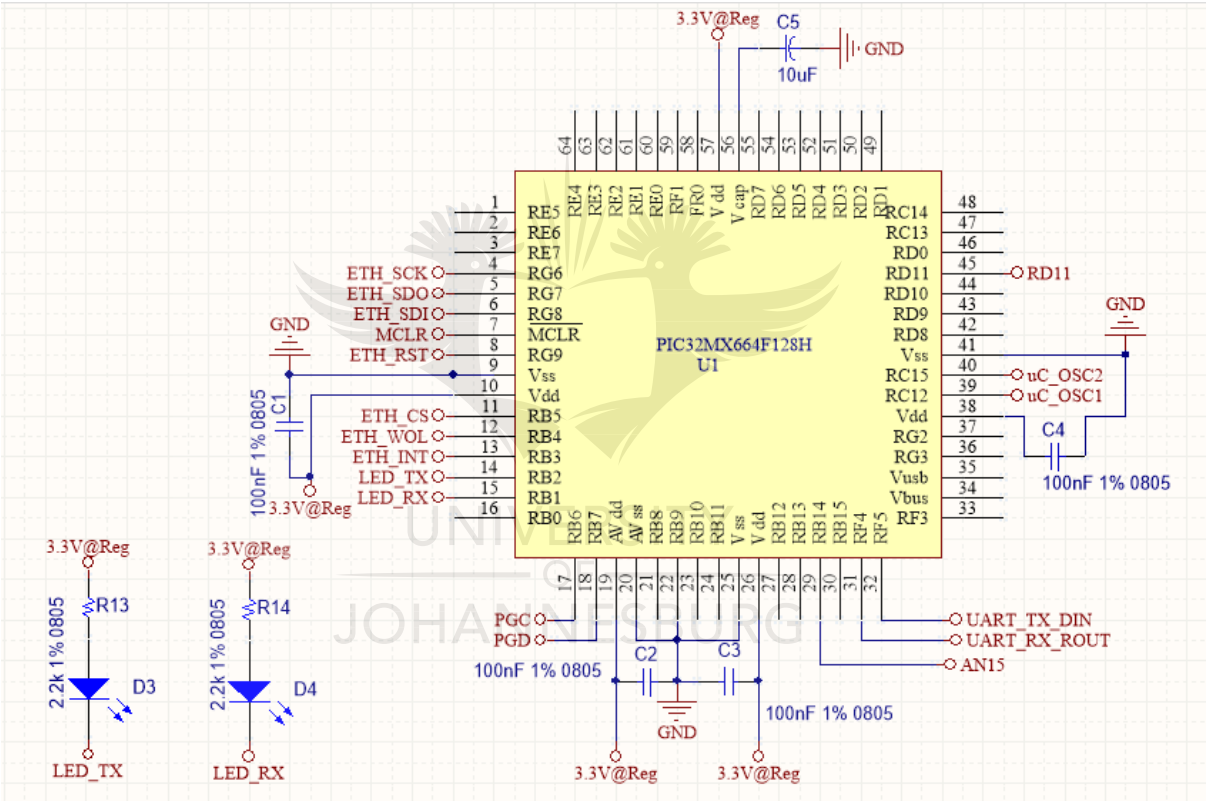

Figure B.1: Microcontroller PIC32MX664F128H.

Figure B.2 represents the Ethernet circuit. The ENC28J60 from Microchip is the integrated circuit used for the Ethernet connection.

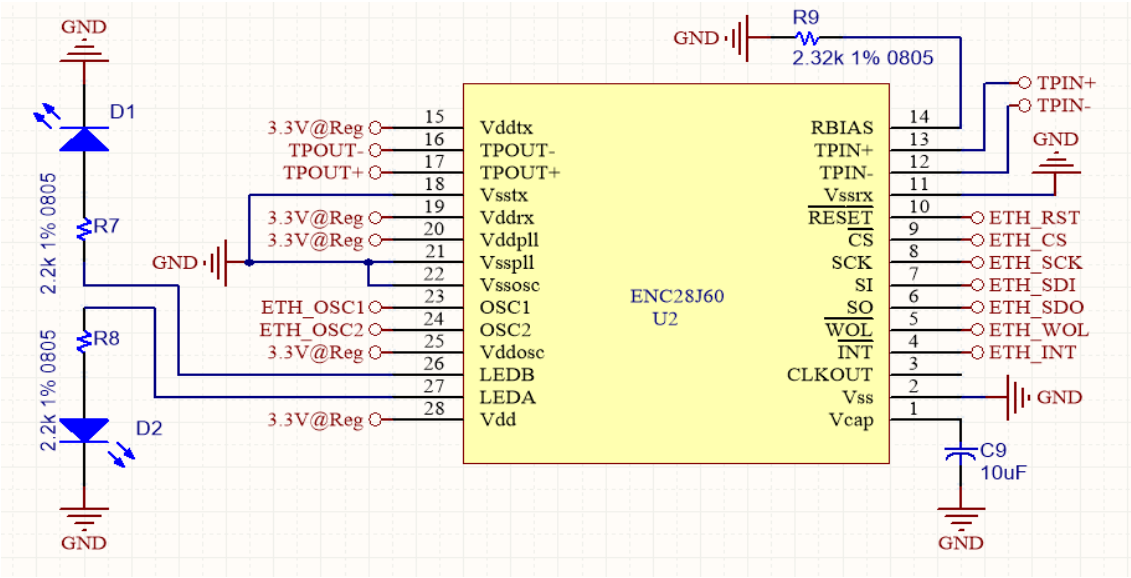

Figure B.2: ENC28J60 schematic.

The Ethernet connection has been placed on the board to allow the data to be sent and received from a laptop RJ45 connector.

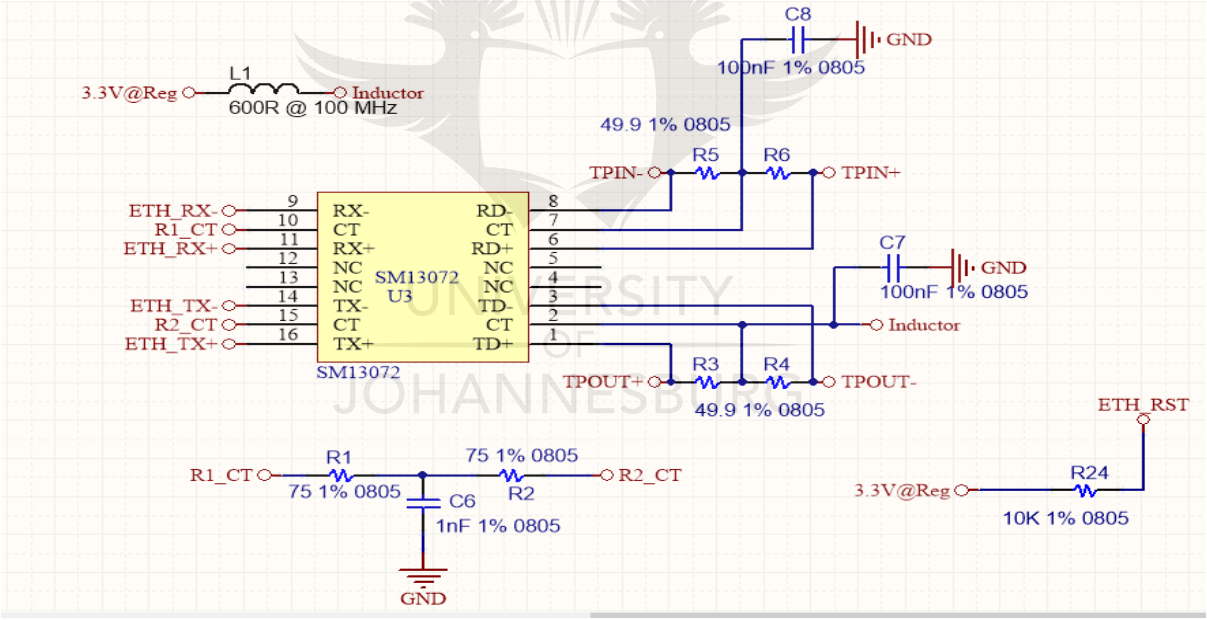

Figure B.3: Ethernet transformer.

Figure B.3 is the Ethernet transformer with its required component around the chip.

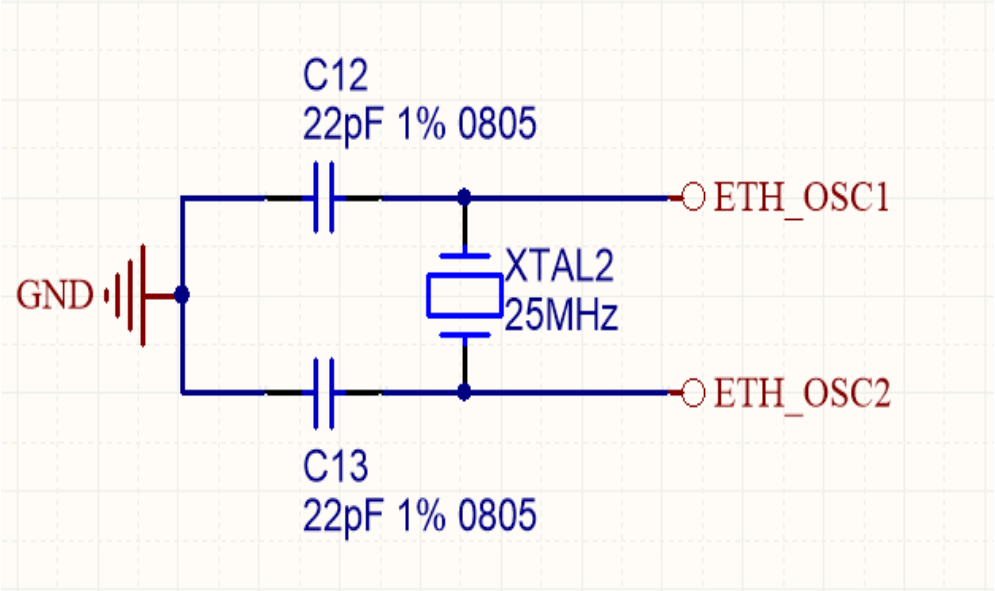

Figure B.4: Oscillator schematic for the ENC28J60.

Figure B.4 represents the oscillator circuit of the Ethernet chip. The oscillator provides the clock for the ENC28J60.

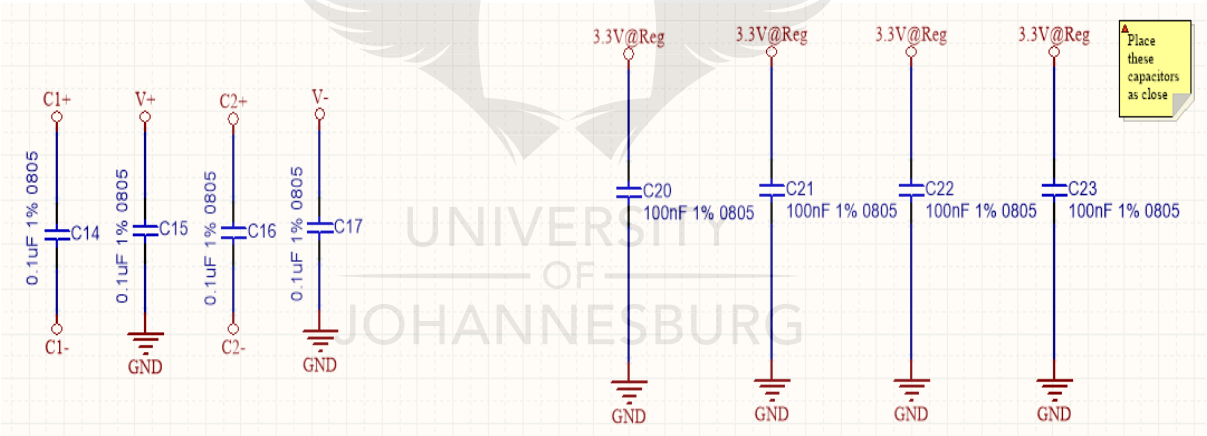

Figure B.5: Voltage regulator capacitor.

Figure B.5 presents different signal smoothing capacitors that are connected to the microcontroller.

Figure B.6 presents the ramp signal generator circuit. An operational amplifier with PNP transistor has been used in combination with the microcontroller to generate the ramp signal.

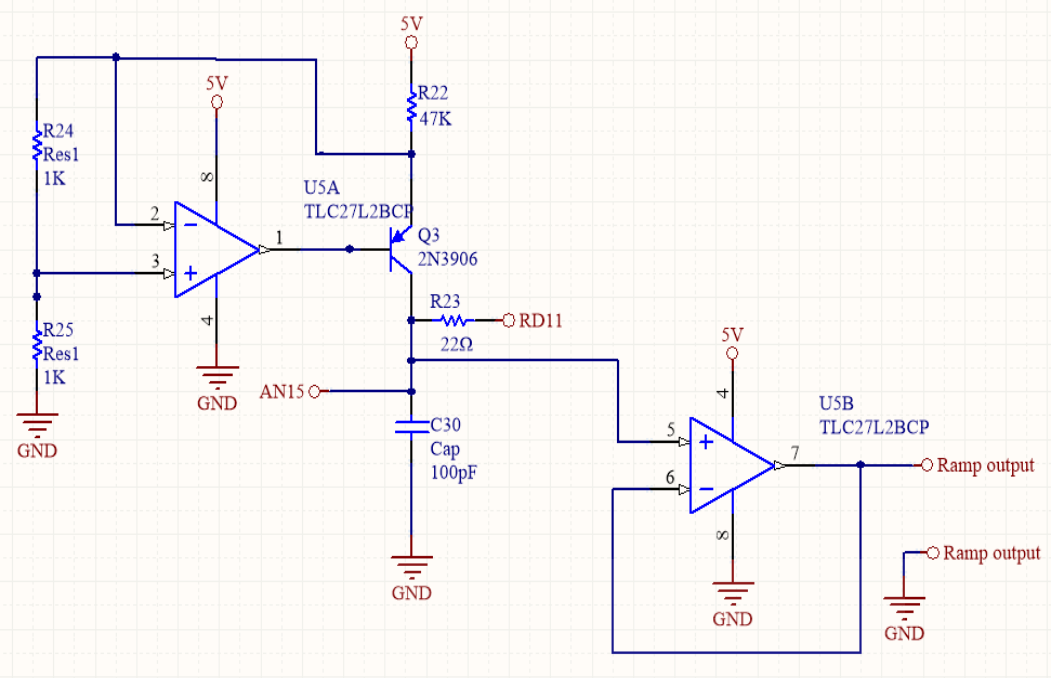

Figure B.6: Ramp signal generator circuit.

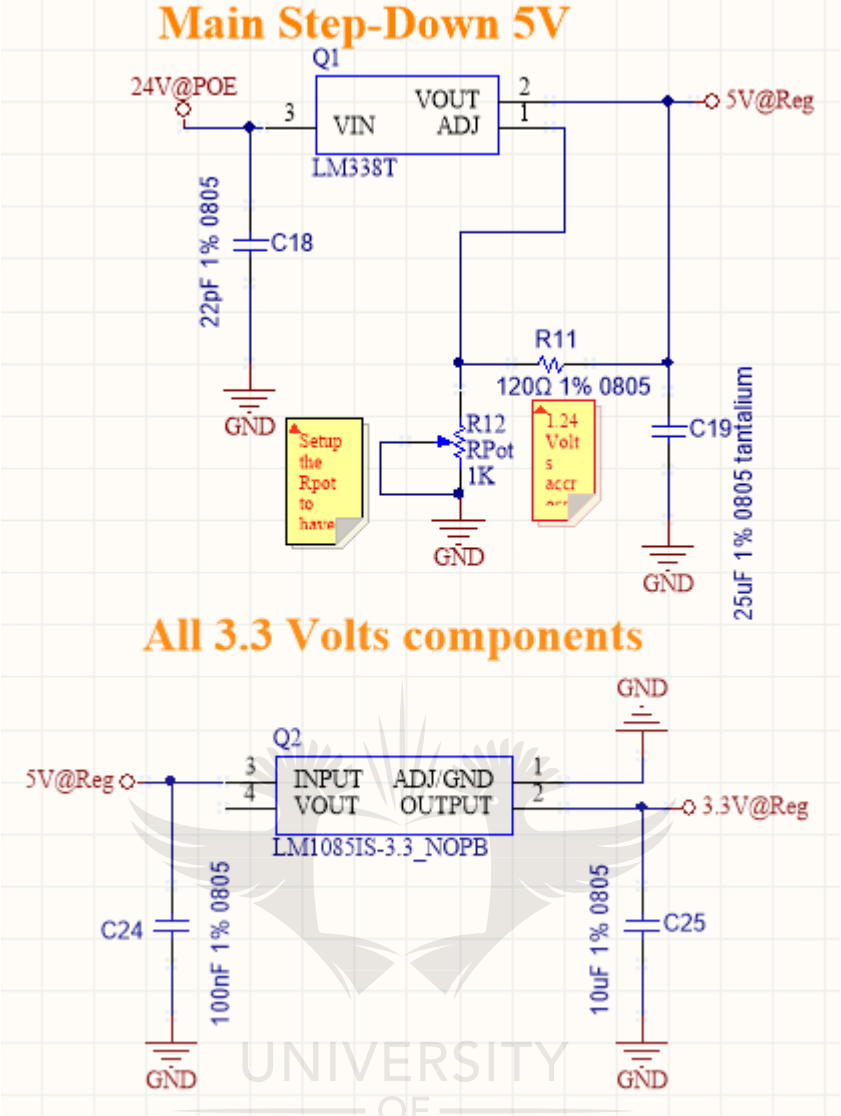

Figure B.7: Voltage regulator power supply circuits.

Figure B.7 represents the power supply circuits for the entire board. The board accepts an input voltage from 12 to 24 V. The input voltage is regulated, then yields 3.3 V and 5 V to supply different circuits on the board.

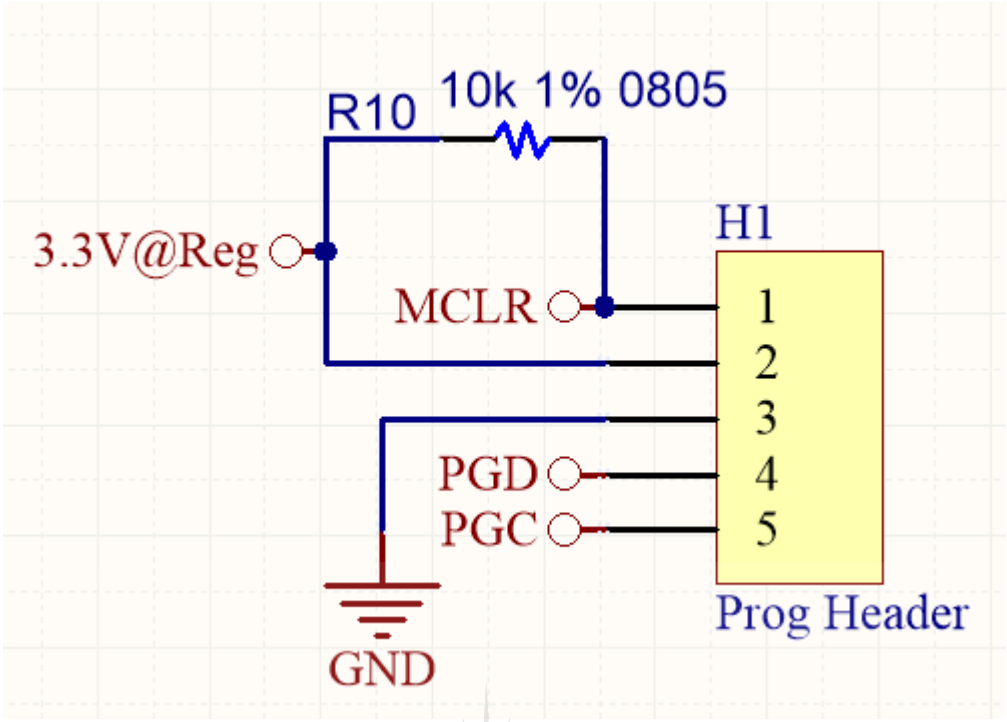

Figure B.8: Programming interface.

Figure B.8 presents the header where the microcontroller is programmed through the Pickit 3. The Pickit 3 is a programmer supplied by Microchip.

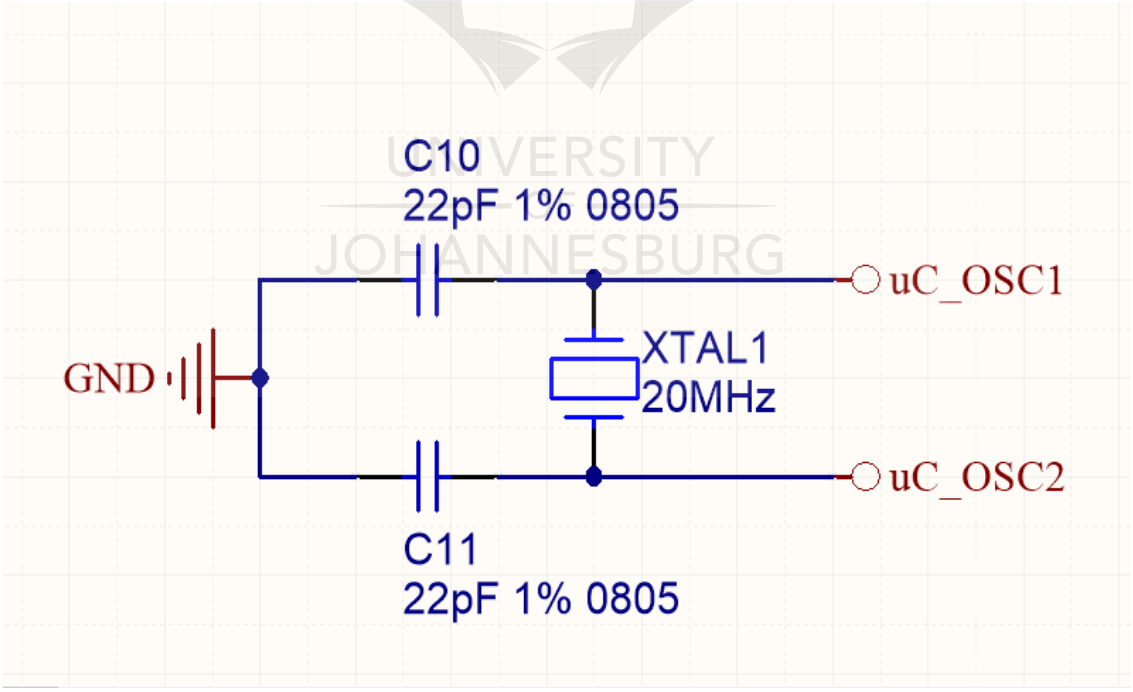

Figure B.9: Oscillator for microcontroller.

Figure B.9 presents the oscillator circuit to provide the clock signal to the microcontroller.

The circuit layout of each components is included in this appendix. Circuit layouts of Figures B.1 to B.9 are given in figures B.10 to B.11. Figures B.10 and B.11 present the PCB board as top layer and bottom layer respectively.

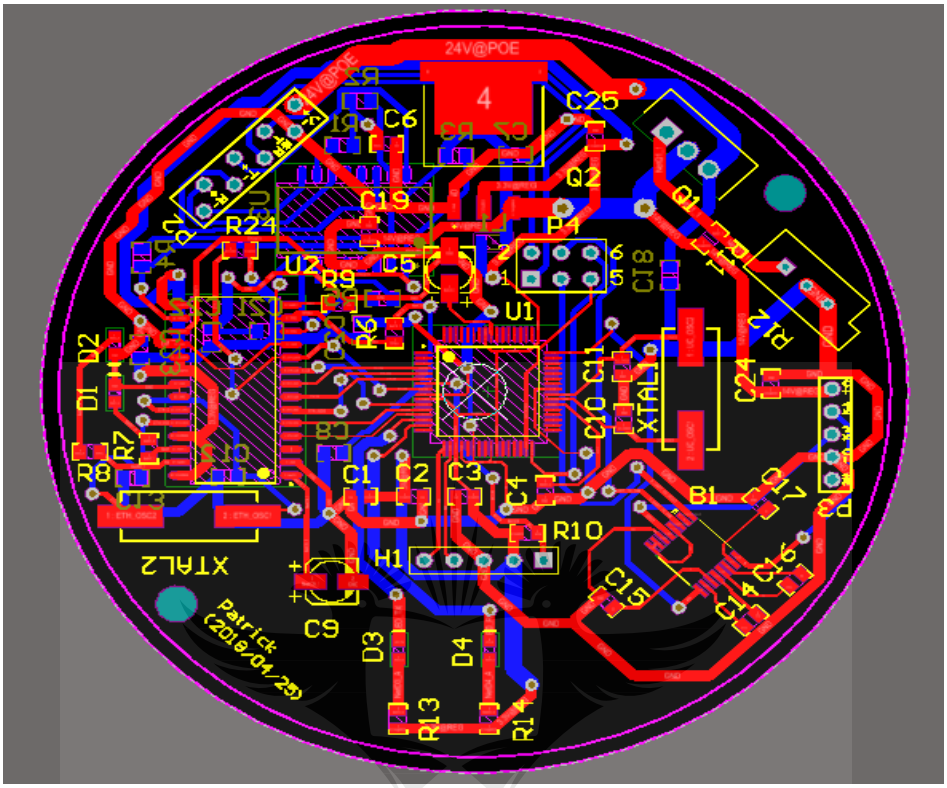

Figure B.10: Top layer view of the PCB.

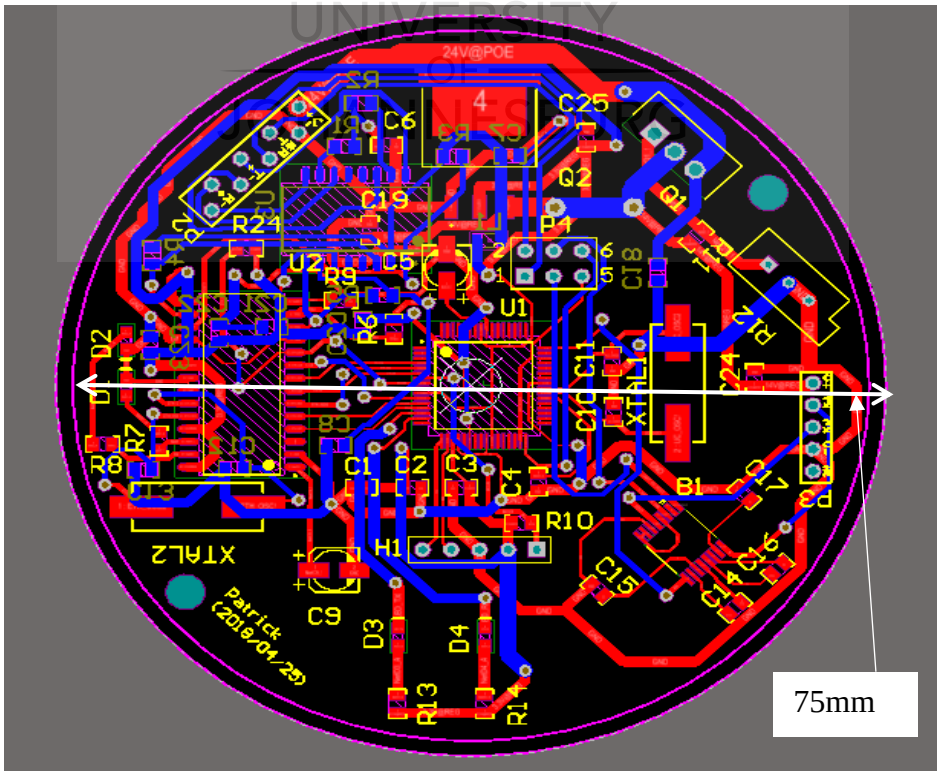

Figure B.11: Bottom view of the PCB.

The board is 75 mm in diameter. This board was designed to generate the sawtooth signal that is input to the radar. This part is the first stage of the FMCW radar. On the board PIC32MX695F512H is the processor.

Figure B.12 represents the two layers of the PCB.

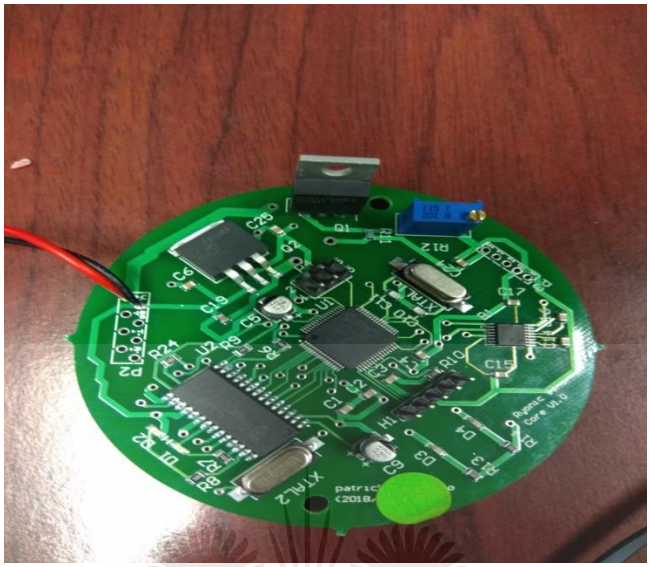

Figure B.12: Front of the board.

Figure A.13 shows the bottom of the board.

Figure B.13: Back of the board.

The MPLAB X IDE functions that were used to generate the ramp signal from the circuit board. Comments next to coded lines briefly describe the functionality of the lines/functions. The version of the MPLAB X IDE is 5.10 and the compiler used is XC32 V1.44.

```
//============================================================================
//============================================================================
// Author:      trikwabam@gmail.com (author of this thesis)
// Project:     FMCW radar signal generator
// Created:     27 July 2017
// Filename:    main.c
// Function:    The aim of this program is to generate a ramp signal for the
//              FMCW radar.
//============================================================================
//============================================================================



/* ************************************************************************** */
/* ************************************************************************** */
/* Section: Included Files                                                    */
/* ************************************************************************** */
/* ************************************************************************** */
/* This section lists the other files that are included in this file.
 */
#include <xc.h>
#include "config.h"
#include "delays.h"
#include "adc.h"

#define discharge_pin LATDbits.LATD11


/* end of the incluse section Files*/

//=============================== Globals variables=============================
int adc_voltage_measurement = 0;
int adc_voltage_upper = 0;
int adc_voltage_lower = 0;
int adc_sensor_3_measurement = 0;

int voltage_channel = 0XFF;
```

```
//============================== End of Globals variables=====================
/*begin of the main function */

int main() {

    SYSTEM_Initialize();                                          // Initialise
the uC
    initADC();                                                    // Initialise
the ADC
    Delay_ms(2000);                                               // Delay of
2000 millisecond
    discharge_pin = HIGH;                                         // Set up the
pin high
    while (1){
        adc_voltage_measurement = readADC(voltage_channel);       // Measure the
voltage on the AN15 pin
        if (adc_voltage_measurement> adc_voltage_upper)           // Check the
condition
        {
          discharge_pin = LOW;                                    //If the
condition is Ok bring the digital pin low
          while (adc_voltage_measurement> adc_voltage_lower)      // Continue
check
          {
           adc_voltage_measurement = readADC(voltage_channel);      //loop until
the capacitor is discharged
          }
          discharge_pin = HIGH;                                    // Bring back
pin D11 high
        }
    }


    return 0;
}

/* ******************************************************************************
 End of the main function
 */
```

```
//==============================================================================
// Author:      trikwabam@gmail.com (author of this thesis)
// Project:     FMCW radar signal generator
// Created:     27 July 2017
// Filename:    config.h
// Function:    Prepares functions for configuration.
//==============================================================================

#ifndef _CONFIG_H    /* Guard against multiple inclusion */
#define _CONFIG_H
#include <xc.h>
#include "pin_manager.h"
#include <stdint.h>
#include <stdbool.h>

#define _XTAL_FREQ  40000000

/**
 * @Param
    none
 * @Returns
    none
 * @Description
    Initializes the device to the default states configured in the
 *                  MCC GUI
 * @Example
    SYSTEM_Initialize(void);
 */
void SYSTEM_Initialize(void);

//void OSCILLATOR_Initialize(void);

    /* Provide C++ Compatibility */
#ifdef __cplusplus
}
#endif

#endif /* _EXAMPLE_FILE_NAME_H */

/* ************************************************************************** *
 End of File
 */
```

```
//==============================================================================
// Author:      trikwabam@gmail.com (author of this thesis)
// Project:     FMCW radar signal generator
// Created:     27 July 2017
// Filename:    config.h
// Function:    Prepares functions for PIN configuration.
//==============================================================================

#ifndef PIN_MANAGER_H
#define PIN_MANAGER_H

#define INPUT   1
#define OUTPUT  0

#define HIGH    1
#define LOW     0

#define ANALOG      1
#define DIGITAL     0

#define PULL_UP_ENABLED      1
#define PULL_UP_DISABLED     0



void PIN_MANAGER_Initialize (void);

/**
 * @Param
    none
 * @Returns
    none
 * @Description
    Interrupt on Change Handling routine
 * @Example
    PIN_MANAGER_IOC();
 */
void PIN_MANAGER_IOC(void);

#endif // PIN_MANAGER_H

 //End of File
```

```
//=============================================================================
// Author:      trikwabam@gmail.com (author of this thesis)
// Project:     FMCW radar signal generator
// Created:     27 July 2017
// Filename:    adc.h
// Function:    Prepares functions for adc.
//=============================================================================

#ifndef ADC_H
#define      ADC_H

#ifdef __cplusplus
extern "C" {
#endif

void initADC();
int readADC();

#ifdef __cplusplus
}
#endif

#endif /* ADC_H */

//=============================================================================
// Author:      trikwabam@gmail.com (author of this thesis)
// Project:     FMCW radar signal generator
// Created:     27 July 2017
// Filename:    delays.h
// Function:    Prepares functions for delays.
//=============================================================================

#ifndef DELAYS_H
#define      DELAYS_H

#ifdef __cplusplus
extern "C" {
#endif

    void Delay_ms(unsigned int n);
    void Delay_us(unsigned int n);

#ifdef __cplusplus
}
#endif

#endif /* DELAYS_H */
//=============================================================================
```

```
//============================================================================
// Author:      trikwabam@gmail.com (author of this thesis)
// Project:     FMCW radar signal generator
// Created:     27 July 2017
// Filename:    config.h
// Function:    Contains functions for configuration.
//============================================================================


// PIC32MX695F512H Configuration Bit Settings

// 'C' source line config statements

// DEVCFG3
// USERID = No Setting
#pragma config FSRSSEL = PRIORITY_7     // SRS Select (SRS Priority 7)
#pragma config FMIIEN = OFF             // Ethernet RMII/MII Enable (RMII
Enabled)
#pragma config FETHIO = OFF             // Ethernet I/O Pin Select (Alternate
Ethernet I/O)
#pragma config FUSBIDIO = OFF           // USB USID Selection (Controlled by Port
Function)
#pragma config FVBUSONIO = OFF          // USB VBUS ON Selection (Controlled by
Port Function)

// DEVCFG2
#pragma config FPLLIDIV = DIV_2         // PLL Input Divider (2x Divider)
#pragma config FPLLMUL = MUL_20         // PLL Multiplier (20x Multiplier)
#pragma config UPLLIDIV = DIV_2         // USB PLL Input Divider (2x Divider)
#pragma config UPLLEN = OFF             // USB PLL Enable (Disabled and Bypassed)
#pragma config FPLLODIV = DIV_2         // System PLL Output Clock Divider (PLL
Divide by 2)

// DEVCFG1
#pragma config FNOSC = PRIPLL           // Oscillator Selection Bits (Primary Osc
w/PLL (XT+,HS+,EC+PLL))
#pragma config FSOSCEN = OFF            // Secondary Oscillator Disable
(Disabled)
#pragma config IESO = OFF               // Internal/External Switch Over
(Disabled)
#pragma config POSCMOD = XT             // Primary Oscillator Configuration (XT
osc mode)
#pragma config OSCIOFNC = ON            // CLKO Output Signal Active on the OSCO
Pin (Enabled)
```

```
#pragma config FPBDIV = DIV_2           // Peripheral Clock Divisor (Pb_Clk is
Sys_Clk/2)
#pragma config FCKSM = CSDCMD           // Clock Switching and Monitor Selection
(Clock Switch Disable, FSCM Disabled)
#pragma config WDTPS = PS1048576        // Watchdog Timer Postscaler (1:1048576)
#pragma config FWDTEN = OFF             // Watchdog Timer Enable (WDT Disabled
(SWDTEN Bit Controls))

// DEVCFG0
#pragma config DEBUG = OFF              // Background Debugger Enable (Debugger
is disabled)
#pragma config ICESEL = ICS_PGx2        // ICE/ICD Comm Channel Select (ICE
EMUC2/EMUD2 pins shared with PGC2/PGD2)
#pragma config PWP = OFF                // Program Flash Write Protect (Disable)
#pragma config BWP = OFF                // Boot Flash Write Protect bit
(Protection Disabled)
#pragma config CP = OFF                 // Code Protect (Protection Disabled)

// #pragma config statements should precede project file includes.
// Use project enums instead of #define for ON and OFF.
#include "config.h"

void SYSTEM_Initialize(void)
{

    PIN_MANAGER_Initialize();

}



/**
 End of File
*/
```

```
//============================================================================
// Author:      trikwabam@gmail.com (author of this thesis)
// Project:     FMCW radar signal generator
// Created:     27 July 2017
// Filename:    config.h
// Function:    Contains functions for PIN configuration.
//============================================================================

#include <xc.h>
#include "pin_manager.h"

void PIN_MANAGER_Initialize(void)
{

    LATB = 0x0;
    LATC = 0x0;
    LATD = 0x0;
    LATE = 0x0;
    LATF = 0x0;
    LATG = 0x0;
    AD1PCFG= 0x8000;
    TRISB = 0x0;
    TRISC = 0x0;
    TRISD = 0x0;
    TRISE = 0x0;
    TRISF = 0x10;
    TRISG = 0x100;
}

void PIN_MANAGER_IOC(void)
{
}

/**
 End of File
*/
```

```
//==============================================================================
// Author:      trikwabam@gmail.com (author of this thesis)
// Project:     FMCW radar signal generator
// Created:     27 July 2017
// Filename:    adc.c
// Function:    Contains functions for adc.
//==============================================================================

#include "adc.h"
#include <xc.h>

//================================ initADC =====================================
void initADC()
{
    AD1CON1 = 0x00E0;                           // Automatic conversion, no
waiting for the DONE interrupt.
    AD1CSSL = 0;                                // No scanning of inputs.
    AD1CON2 = 0;                                // Mux A, Vdd/Vss as Vref+/-.
    AD1CON3 = 0x1FFF;                           // Tsamp = 32 x Tad     VERY
IMPORTANT NB NB!!! = 750 Hz sampling rate!!!!!!!!!
    AD1CON1bits.ADON = 1;                       // Switch on adc.
}
//==============================================================================
//================================ readADC =====================================
int readADC(int ch)
{
    AD1CHSbits.CH0SA = ch;                      // Selects AN of choice for
analog input.
    AD1CON1bits.SAMP = 1;                       // Start sampling process.
    while(!AD1CON1bits.DONE);                   // Wait for conversion.
    return ADC1BUF0;                            // Return the result.
}
//==============================================================================
```

```
//=============================================================================
// Author:      trikwabam@gmail.com (author of this thesis)
// Project:     FMCW radar signal generator
// Created:     27 July 2017
// Filename:    delays.c
// Function:    Contains functions for delays.
//=============================================================================

#include "delays.h"
#include <xc.h>

//============================== Definitions ==================================
#define SYSCLOCK 40000000L              // System clock @ 40 MHz
#define PBCLOCK 20000000L               // Peripheral clock @ 20 MHz
#define PBCLMS  20000L                  // Cycle for one millisecond.
#define PBCLUS  20L                     // Cycle for one microsecond.
//=============================================================================

//========================== Delay function in ms =============================
void Delay_ms(unsigned int n)
// Delays by n amount in milliseconds.
{
    T1CON = 0x8000;
    while(n--)
    {
        TMR1 = 0;
        while(TMR1 < PBCLMS);
    }
    T1CONCLR = 0x8000;
}

//========================== Delay function in us =============================
void Delay_us(unsigned int n)
// Delays by n amount in microseconds.
{
    T1CON = 0x8000;
    while(n--)
    {
        TMR1 = 0;
        while(TMR1 < PBCLUS);
    }
    T1CONCLR = 0x8000;
}
```

APPENDIX C: IMAGE OF THE PATCH ANTENNA

IMAGE OF THE PATCH ANTENNA

The antenna that was built is a patch antenna. Figures C.1 to C.3 present the patch antenna. Figure C.3 presents the patch antenna covered with a clear sheet of plastic to prevent humidity from reaching the metallic material. In the centre of the antenna one can see the feed point. The enclosure used comes from an old broken antenna.

A patch or microstrip antenna comprises a thin metallic patch on a dielectric substrate to radiate an EM wave. In multiple applications where size, weight, and performance are important constraints, it is always preferable to use an embedded low-profile microstrip antenna. As the radar has to be portable, a low-weight and non-cumbersome antenna is preferable rather than its counterparts such as a dish antenna.

Figure C.1 represents the top layer of the antenna design.

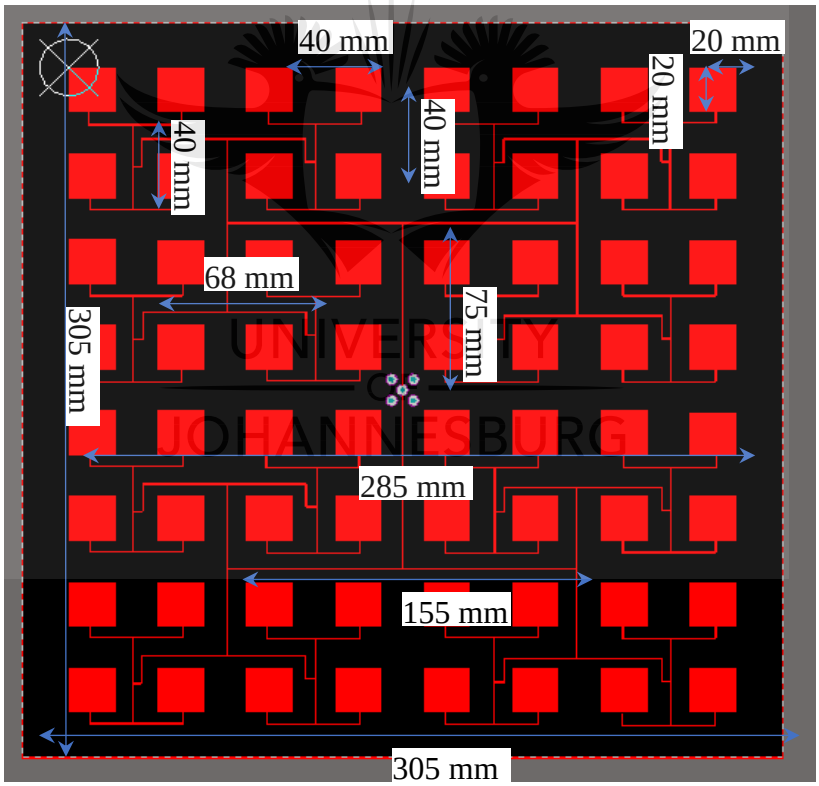

Figure C.1: Antenna design.

The dimensions of the antenna are 285 mm by 285 mm.

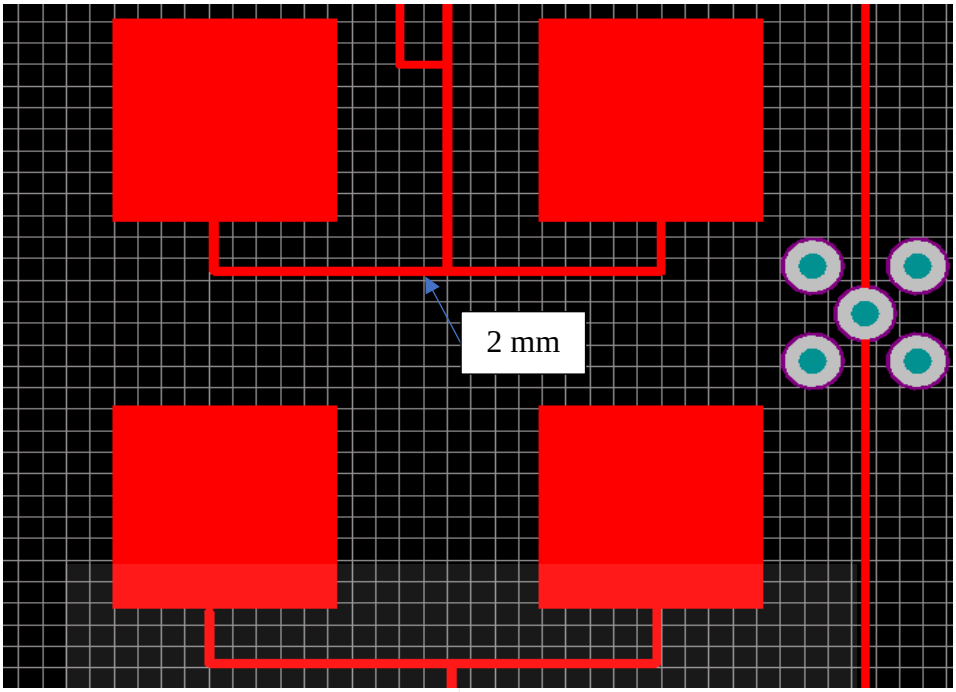

Figure C.2: Zoom-in view of the antenna.

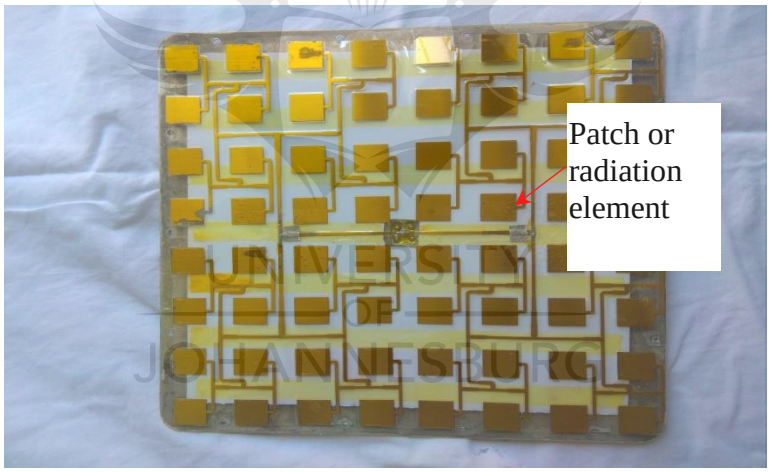

Figure C.3: Antenna front.

Figure C.4 presents the same antenna, where the substrate is visible underneath the patch.

The substrate electromagnetic property is an element that strongly influences the antenna size and performance. For this antenna design, the choice has been a substrate with a thickness of 3 mm, permittivity $\varepsilon_r = 9$ and substrate loss tangent of $tan\delta = 0.0009$.

To calculate the width of the patch, the following formula has been used:

$$W_e = \frac{c}{2f_0\sqrt{\frac{\varepsilon_r + 1}{2}}} \qquad \text{(B. 1)}$$

After calculating the width, the effective dielectric constant has to be computed. Therefore, based on the height and the width of the patch antenna, the dielectric constant can be found with the following formula:

$$\varepsilon_{eff} = \frac{\varepsilon_r + 1}{2} + \frac{\varepsilon_r - 1}{2}\left[1 + 12\frac{h}{W_e}\right]^{\frac{1}{2}} \quad \text{(B. 2)}$$

The calculation of the effective length is done using the following formula:

$$L_{eff} = \frac{c}{2f_0\sqrt{\varepsilon_{eff}}}. \quad \text{(B. 3)}$$

Afterward, the calculation of the length extension is found using the following formula:

$$\Delta L = 0.412h\frac{\left(\varepsilon_{eff} + 0.3\right)\left(\frac{W_e}{h} + 0.264\right)}{\left(\varepsilon_{eff} - 0.258\right)\left(\frac{W_e}{h} + 0.8\right)}. \quad \text{(B. 4)}$$

Having determined the effective length and the length extension, the actual length of the patch can be calculated as follows:

$$L = L_{eff} - 2\Delta L \quad \text{(B. 5)}$$

where the parameters from (B.1) to (B.5) are represented as follows:

c is the speed of light,

f_0 is the resonance frequency,

W_e is the width of the patch antenna,

L is the length of the patch,

h is the thickness, and

ε_r is the relative permittivity of the dielectric substrate.

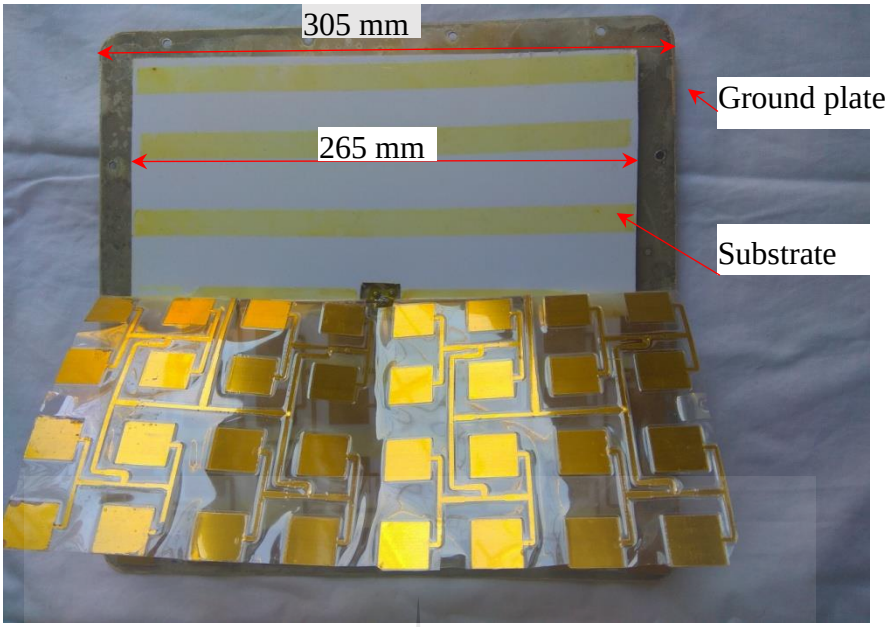

Figure C.4: Substrate.

Figure C.5 presents the enclosure of the antenna.

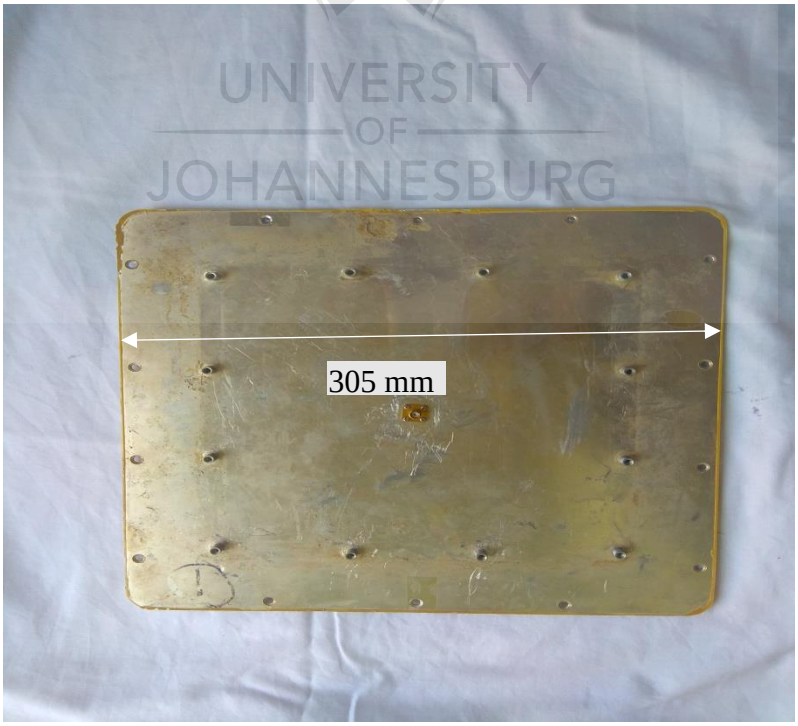

Figure C.5: Enclosure used.